Microscopy at the Frontiers of Science

Joint Meeting of SME and SPMicros

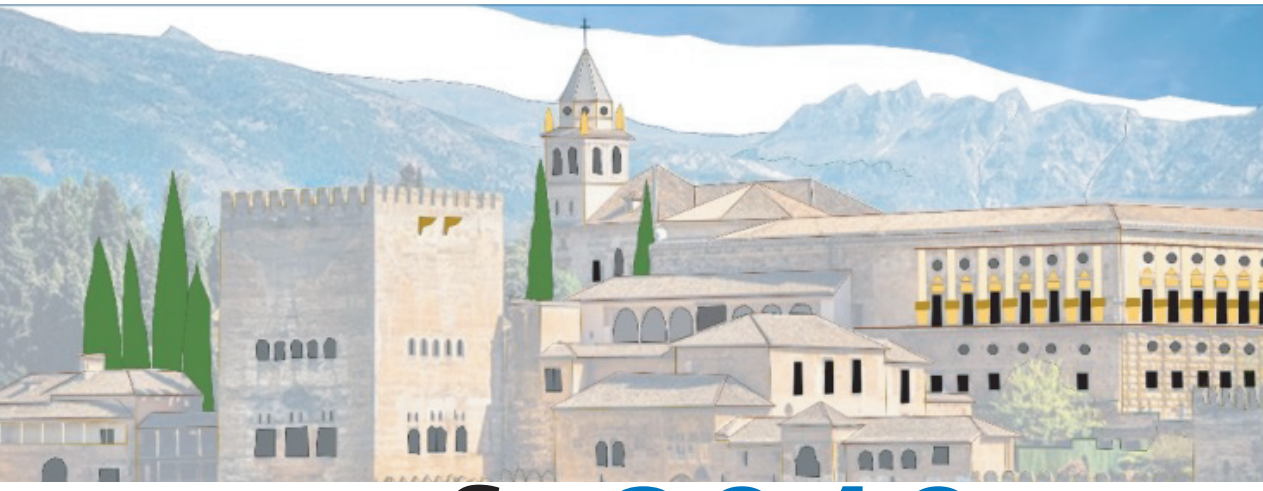

mfs2019

SME SOCIEDAD DE MICROSCOPÍA DE ESPAÑA

Sociedade Portuguesa de Microscopia SPMicros

Parque de las Ciencias - Granada, Spain
11-13 September 2019

Abstracts book

Microscopy at the Frontiers of Science

mfs2019

SME SOCIEDAD DE MICROSCOPÍA DE ESPAÑA

Sociedade Portuguesa de Microscopia SPMicros

Parque de las Ciencias
Granada, Spain
11-13 September 2019

Organizers:

CSIC Consejo Superior de Investigaciones Científicas

eez Estación Experimental del Zaidín

SME SOCIEDAD DE MICROSCOPÍA DE ESPAÑA

Sociedade Portuguesa de Microscopia SPMicros

CONGRESS WELCOME MESSAGE

Dear colleagues,

The organizers are very proud to welcome you to the “Parque de las Ciencias” in Granada, to celebrate a new joint meeting of SME and SPMicros, known as the Microscopy at the Frontiers of Science Congress Series (mfs2019). We believe that the Scientific Committee of the Congress has managed to define an appealing scientific program, offering microscopists and professionals from Spain, Portugal and beyond numerous opportunities to meet and interact in the framework of this growing community. The meeting includes lectures by keynote speakers, talks by invited and selected speakers and poster presentations.

Professional interactions previously assayed at other meetings in the form of technological advancements sessions have been scheduled again. The organizers also very much want to acknowledge the enthusiastic participation of numerous commercial companies, who bring to mfs2019 their latest innovations in advanced light and electron microscopy imaging, sample preparation, image analysis and many other aspects, presenting them in a broad commercial exhibition. They will also participate by leading flahs talks scheduled at the program of the meeting.

Of course, we will be dedicating a time slot to the SME general assembly, which will be held on Thursday 12th of September. There, we will debate our latest developments, news and future plans. We hope that the meeting will represent a great opportunity to exchange of idea, induce new developments and encourage collaborations between the participants. To promote such interactions, we have planned an intense social program, which takes advantage of the beauty and the facilities of the city.

Also, we want to sincerely thank the support of the staff of “Parque de las Ciencias” in the many different technical aspects of the organization of the meeting. We wish you a pleasant stay in the city and a fruitful exchange over the coming days.

The local organizing committee

- Juan de Dios Alché Ramírez. EEZ/CSIC. Granada, Spain
- Antonio J. Castro López. EEZ/CSIC. Granada, Spain
- José C. Jiménez López. EEZ/CSIC. Granada, Spain
- Francisco J. Huertas Puerta. IACT/CSIC-UGR. Granada, Spain
- Elena Lima Cabello. EEZ/CSIC. Granada, Spain
- David Porcel Muñoz. CIC/UGR. Granada, Spain
- Alicia Rodríguez Sánchez. EEZ/CSIC. Granada, Spain
- Adoración Zafra Álvarez, EEZ/CSIC. Granada, Spain

ORGANIZERS

Local Organizing Committee

- Juan de Dios Alché Ramírez. EEZ/CSIC. Granada, Spain
- Antonio Jesús Castro López. EEZ/CSIC. Granada, Spain
- José Carlos Jiménez López. EEZ/CSIC. Granada, Spain
- Francisco Javier Huertas Puerta. IACT/CSIC-UGR. Granada, Spain
- Elena Lima Cabello. EEZ/CSIC. Granada, Spain
- David Porcel Muñoz. CIC/UGR. Granada, Spain
- Alicia Rodríguez Sánchez. EEZ/CSIC. Granada, Spain
- Adoración Zafra Álvarez, EEZ/CSIC. Granada, Spain

Scientific Committee

- Juan de Dios Alché Ramírez. EEZ/CSIC. Granada, Spain.
- Jordi Arbiol. ICREA, ICN2, CSIC and BIST. Barcelona. Spain
- Ignacio Arechaga. IBBTEC. Cantabria. Santander. Spain
- Raúl Arenal. ARAID-INA. Zaragoza. Spain
- José R. Castón. CNB/CSIC. Madrid. Spain
- Pedro Coelho. University of Coimbra. Portugal
- Henrique Guirão. University of Coimbra. Portugal
- Francisco Javier García García. CNME/Complutense University. Madrid. Spain
- Francisca Peiró. LENS, MIND, IN2UB. University of Barcelona. Spain
- Ana Paula Piedade. University of Coimbra. Portugal
- Carmen San Martín. CNB/CSIC. Madrid. Spain
- Rúben Santos. University of Porto. Portugal
- Bruno Trindade. University of Coimbra. Portugal

INVITED SPEAKERS

Plenary lectures

- David Bhella. University of Glasgow. UK (Welcome lecture)
- José L. Carrascosa. CNB/CSIC. Madrid. Spain
- Joke Hadermann. University of Antwerp. Belgium
- Paul Midgley. University of Cambridge. UK

Keynote lectures

• Ernesto Arias-Palomo. CIB/CSIC. Madrid. Spain

• Álvaro Mayoral. ShanghaiTech University. China

• Gabriel Sánchez Santolino. ICMM-CSIC. Madrid. Spain

• Juan Manuel Losada. IHSM/CSIC/UMA. Malaga. Spain

• Ana Sánchez. University of Warwick. UK

• M. Rosario Fernández. CNB/CSIC. Madrid. Spain

• Erin Tranfield. Instituto Gulbenkian de Ciência. Oeiras. Portugal

TECHNICAL ORGANIZATION

mfs2019 Secretary

Phone: +34 958181600, ext. 215

E-mail: mfs2019@eez.csic.es

Technical Secretary

Enrique Martín and Sergio Martín

Arrayanes Viajes y Congresos

Avda. Madrid 3, 18012 Granada, Spain.

Phone: +34 958295250

E-mail: emartin@e-savia.net

During the conference the Technical Secretary will be located at the registration desk.

CONGRESS SCHEDULES

Wednesday 11th	8:30 – 18:30h
Thursday 12th	8:30 – 18:30h
Friday 13rd	8:30 – 14:00h

COMMERCIAL EXHIBITION SITEMAP

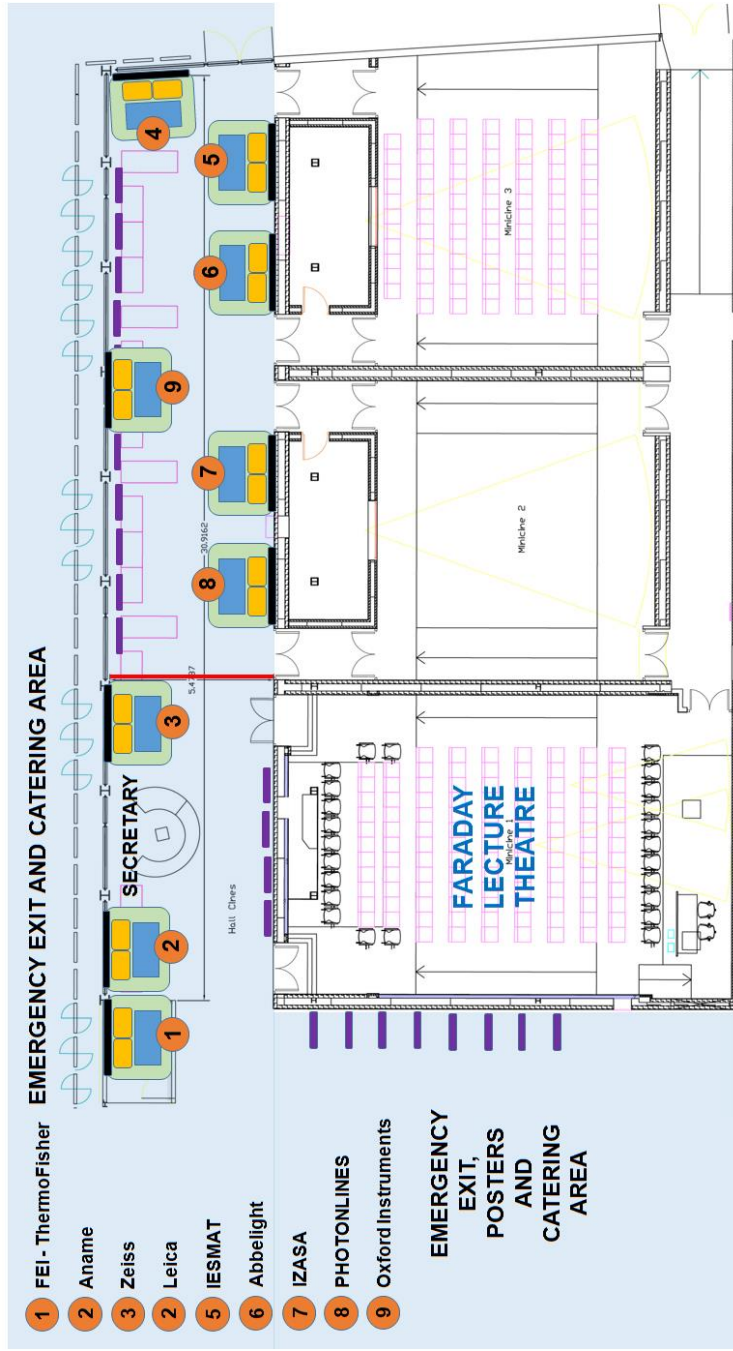

LECTURE ROOMS

FARADAY Lecture Theatre and Hall

GUTENBERG Lecture Theatre

SAGAN and CURIE Classrooms

TECHNICAL ORGANIZATION

mfs2019 Secretary

Phone: +34 958181600, ext. 215

E-mail: mfs2019@eez.csic.es

Technical Secretary

Enrique Martín and Sergio Martín

Arrayanes Viajes y Congresos

Avda. Madrid 3, 18012 Granada, Spain.

Phone: +34 958295250

E-mail: emartin@e-savia.net

During the conference the Technical Secretary will be located at the registration desk.

CONGRESS SCHEDULES

Wednesday 11th	8:30 – 18:30h
Thursday 12th	8:30 – 18:30h
Friday 13rd	8:30 – 14:00h

SOCIAL PROGRAMME

All days

- Coffee breaks will be provided on 11th and 12th (morning and afternoon) and 13rd (morning only) at the “Genil” terrace and gardens.
- Lunches will be provided on 11th and 12th at the “Genil” terrace and gardens.

“Via Lactea” Terrace

“Genil” Terrace

Wednesday 11th

- Refreshments at the “Via Láctea” terrace and gardens.

Thursday 12th

- Gala dinner at the “Carmen de los Mártires”. The "Carmen de los Mártires" is located in the heart of the Alhambra (see map). It is composed of a small palace and a romantic set of gardens of French and English styling. Dinner will take place from 20:00 to 22:00 h inside the palace or at the gardens depending on the weather. Buses will be provided from the Parque de las Ciencias to the place, and then back after the dinner.

“Carmen de los Mártires” palace (left) and gardens (right)

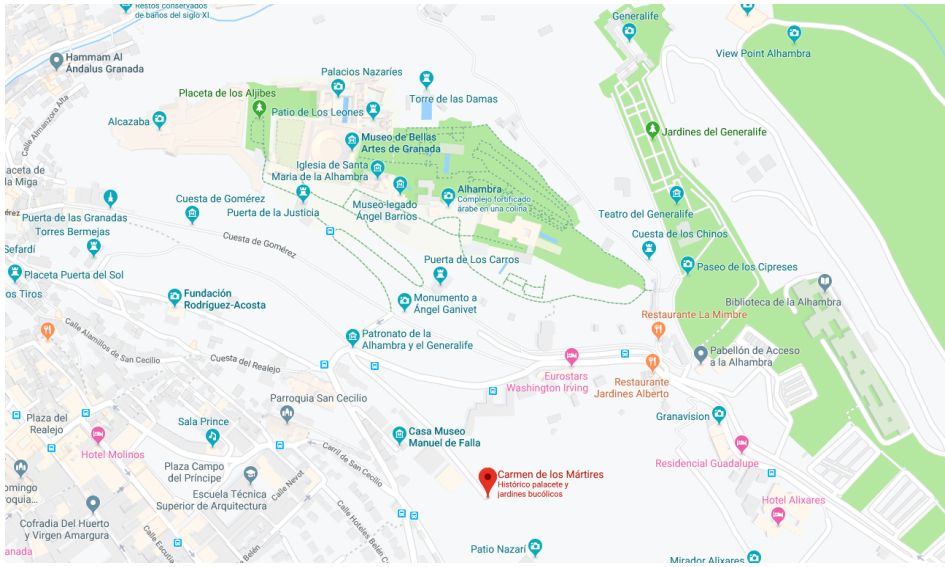

“Carmen de los Mártires” location

SOCIAL NETWORK

Share and follow everything that is happening at:

FACEBOOK: https://www.facebook.com/mfs2019
TWITTER: https://twitter.com/mfs2019
INSTAGRAM: https://instagram.com/mfs2019

SPECIAL ISSUE IN METHODS AND PROTOCOLS (MDPI)

Authors from MFS2019 are invited to submit an extended version of their work to a Special Issue published in the new open access journal Methods and Protocols (https://www.mdpi.com/journal/mps/special_issues/ambms). The Instructions for Authors are available at: http://www.mdpi.com/journal/mps/instructions. The deadline for submissions is 28th February 2020. All papers accepted for publication will be published in Open Access free of charge. Authors of selected papers are encouraged to prepare videoarticles to be published alongside textual manuscripts. Videoarticles are intended to be a step-by-step demonstration of new protocols/methods to ensure experiment reproducibility and to be potentially used for the training of young researchers. Further details on the preparation of videoarticles are available at the Instructions for Authors. For further details, please contact the Editorial Office of Methods and Protocols at mps@mdpi.com.

SCIENTIFIC PROGRAMME'S SCHEDULE

	Tuesday 10th Pre-congress workshop (Registered users)	Wednesday 11th		Thursday 12th		Friday 13th	
8:30	Registration	Registration					
8:45							
9:00	Welcome	Welcome		Plenary Lecture (Joke Hadermann)		Plenary Lecture (Paul Midgley)	
9:15	*Talk: Joerg Lindenau Carl Zeiss*	Plenary Lecture (Pepe Carrascosa)					
9:30							
9:45							
10:00	Coffee break			Posters, coffee, comercial exposition		Posters, coffee, comercial exposition	
10:15		Posters, coffee, commercial exposition					
10:30	"Hands on" demonstration *Carl Zeiss*			Session MS-3 Semiconductors -in situ-. Hybrid Nanostructures	Session LS-3 Plant/Animal Biology	Session MS-4 Functional Materials & Metals	Session LS-4 Biomedical Applications
10:45							
11:00		Session MS-1 Catalysis-Materials for Energy.	Session LS-1 Macromolecular Analysis				
11:15							
11:30							
11:45							
12:00							
12:15							
12:30	Buffet lunch						
12:45							
13:00		Buffet lunch and commercial exposition		Buffet lunch and commercial exposition		Closing remarks	
13:15							
13:30							
13:45							
14:00	*Talk: Jordi Recasens IZASA Scientific*						
14:15							
14:30	"Hands on" demonstration *IZASA Scientific*	Session MS-2 Oxides	Session LS-2 Microbial/ Virus Analysis	Session TD-2 Technical Developments in Life Sciences			
14:45							
15:00							
15:15							
15:30							
15:45							
16:00	*Talk: Jan De Weert. Leica Microsystems*			Posters, coffee, commercial exposition			
16:15	"Hands on" demonstration *Leica Microsystems*						
16:30							
16:45		Posters, coffee, commercial exposition		SME Best PhDs Award ceremony			
17:00	Coffee Break	Session TD-1 Technical Developments in Material Sciences		Best PhD Award Talk (LS)			
17:15	*Talks: ThermoFisher*						
17:30				Best PhD Award Talk (TD)			
17:45							
18:00		Flash company presentation. *Carl Zeiss*					
18:15		Flash company presentation. *ThermoFisher Scientific*		Best PhD Award Talk (MS)			
18:30	Welcome Lecture (David Bhella) * Open to WORKSHOP AND MFS2019 participants	Flash company presentation. *IZASA Scientific*		SME Assembly			
18:45							
19:00		Flash company presentation. *Leica Microsystems*					
19:15							
19:30	Welcome reception La Cabaña * Open to WORKSHOP AND MFS2019 participants	Posters and refreshments "Via Lactea" gardens					
19:45							
20:00							
20:15							
20:30				Gala buffet "Carmen de los Mártires"			

Curie Room

Sagan Room

Via Lactea Gardens

"Faraday" Lecture Theatre

Registration and Secretary, Main Hall

"La cabaña" Tapas Bar

"Cines Hall" and Gardens

"Gutenberg" Lecture Theatre

"Carmen de los Mártires"

SCIENTIFIC PROGRAMME

Tuesday, 10th September

18:00-19:00 Faraday lecture theatre. Welcome Lecture. David Bhella. *Scottish Centre for Macromolecular Imaging. Glasgow. UK*. "The Scottish Centre for Macromolecular Imaging - a national structural biology centre built around JEOL's CryoARM 300".
Chair: Carmen San Martín. *CNB-CSIC. Madrid. Spain*

19:00-21:00 La cabaña. Welcome Reception "Tapas" Granada's style

Wednesday, 11th September

8:30-9:00 Main Hall of Parque de las Ciencias. Registration

9:00-9:20 Faraday lecture theatre. Opening ceremony

- Jordi Arbiol. *President of the SME*
- Bruno Trindade. *President of the SPMicros*
- Luis Salvador. *Mayor of the city of Granada*
- Pilar Aranda. *Rector of the University of Granada*
- Matilde Barón. *Director of the EEZ-CSIC*
- Fco. Javier Huertas. *Director of the IACT-CSIC-UGR*

9:20-10:20 Faraday lecture theatre. Plenary Lecture. José L. Carrascosa. *CNB-CSIC. Madrid. Spain.* "Phage T7 viral tail machinery characterization: A model for DNA retention and ejection from the capsid".
Chair: Juan de Dios Alché. *EEZ-CSIC. Granada. Spain*

10:20-11:00 Hall cines and Gardens. Coffee break. Posters. Commercial exposition.

11:00-13:00 Faraday lecture theatre
Session MS-1: Catalysis-Materials for Energy
Chairs: Raúl Arenal / Gabriel Sánchez Santolino

-11:00-11:30 **Álvaro Mayoral. Invited Speaker.** Evolution of EM applied to nanoporous solids
-11:30-11:45 M.C. Spadaro. Cluster beam deposition for precise heterogenous catalysts
-11:45-12:00 R. Manzorro. Submonolayer ceria addition as a mechanism to stabilize Au nanoparticles: electron microscopy characterization
12:00-12:15 A.J.J. Benitez. Study of location of AuPd nanoparticles supported on ceria nanocubes by analytical electron tomography
12:15-12:30 J. Blanco-Portals. Doped cerium oxide mesoporous structure: a complete analytical TEM characterization based on MVA, clustering and X-EDS electron tomography
-12:30-12:45 J.M. Montes-Monroy. Preparation and characterization of NaBH4 modified CeO2/TiO2 nanostructured photocataysts
-12:45-13:00 C.M. Almeida Alves. Phase and compositional mapping of polycrystalline Li-ion NCM cathodes

11:00-13:00 Gutenberg lecture theatre
Session LS-1: Macromolecular Analysis Chairs: José Ruiz Castón / Jorge Cuéllar

-11:00-11:40 **Ernesto Arias-Palomo. Invited Speaker.** Unraveling bacterial DNA replication initiation using cryo-EM
-11:40-12:00 J. Cuéllar. Structural and functional analysis of the role of the chaperonin CCT in mTOR complex assembly
-12:00-12:20 M.T. Bueno-Carrasco. Structural characterization of human tyrosine hydroxylase
-12:20-12:40 J.P. López-Alonso. Mechanism of action of pyruvate carboxylase
-12:40-13:00 M. Lázaro. *De novo* structure determination of glutamate dehydrogenase

13:00-14:30 Hall cines and Gardens. Buffet lunch. Posters. Commercial exposition

14:30-16:30 Faraday lecture theatre
Session MS-2. Oxides
Chairs: Javier Garcia / Alvaro Mayoral

-14:30-15:00 **Ana Sánchez. Invited Speaker.** La0.7Sr0.3MnO3/PbTiO3 ferroelectric tunnel junctions: Domain configuration and interface characterization
-15:00-15:15 D. del Pozo. Study of magnetic iron oxide core/shell nanocubes using electron magnetic circular dichroism
-15:15-15:30 S. Hettler, STEM-EELS analysis of Fe3O4@CoFe2O4@Fe3O4 core - shell - shell nanoparticles
-15:30-15:45 C. D. Amos Understanding the cubic-to-tetragonal transition of Mn_3O_4 as a surface layer of $Li1\text{-}x[Mn_2]O_4$
-15:45-16:00 C. Coll. Verwey transition on iron oxide nanocubes elucidated by electron energy loss spectroscopy and density functional theory simulations
-16:00-16:15 M. López-Haro. Accurate determination of the oxygen stoichiometry in complex nanostructured oxides by combining STEM-HAADF tomography and STEM-XEDS quantification
-16:15-16:30 J.M. Muñoz-Ocaña. Optimization of STEM-HAADF electron tomography reconstructions by smart parameters selection in compressed-sensing based algorithms

14:30-16:30 Gutenberg lecture theatre
Session LS-2 Microbial/Virus Analysis
Chairs: Ignacio Arechaga / Jose Ruiz Castón

-14:30-14:45 R. Cuesta. Structural studies of filamentous plant viruses by cryoEM
-14:45-15:00 C. Allende. Near-atomic resolution cryo-EM structure of *Brevibacterium linens* encapsulin
- 15:00-15:15 I. Arechaga. Bacterial conjugation directly observed by optical microscopy
-15:15-15:30 M. Pérez Ruiz. Understanding the mechanism of phage T7 DNA delivery to the bacterial cytoplasm
-15:30-15:45 D. Gil-Cantero. Cryo-EM for the study of genome and viral polymerase within the capsid of dsRNA viruses
-15:45-16:00 G.N. Condezo. Structure of a polinton-like virus, the missing link between bacteriophage and eukaryotic viruses of the PRD1-like lineage
-16:00-16:15 C. San Martin. Structural surprises in reptilian adenoviruses

16:30-17:00 Hall cines and Gardens. Coffee break. Posters. Commercial exposition

17:00-18:00 Faraday lecture theatre
Session TD-1: Technical Developments in Material Sciences. Chair: Juan J. Calvino

-17:00-17:20 S. Plana-Ruiz. Fast and automated diffraction tomography: how to acquire 3D electron diffraction in a systematic and accurate way
-17:20-17:40 M. López-Haro Quantitative evaluation of the accuracy of compressed sensing electron tomography reconstructions using material-realistic 3D-phantoms
-17:40-18:00 S. Trasobares. Scanning Transmission Electron Microscopy as a tool to optimise and characterise encapsulated agrochemicals in fully-organic reservoirs

18:00-19:00 Faraday lecture theatre. Flash company presentations

-18:00-18:15 Connecting imaging modalities of all kind – Zeiss correlative microscopy workflows. Joerg Lindenau. *Carl Zeiss*
-18:15-18:30 Advances in 3D Image Processing Automation in Amira-Avizo Software. Sarawuth Wantha. *ThermoFisher*
-18:30-18:45 Intelligent illumination for super resolution in living cells. Jordi Recasens. *IZASA Scientific*
-18:45-19:00 Array tomography with Leica's new ultramicrotome ARTOS 3D. Jan De Weert. *Leica Microsystems*
- 19:00-19:15 Flash company presentation. Hitachi. Soto Nakatsuru. *IESMAT.*

19:15- Via lactea Gardens. Refreshments

Thursday, 12th September

9:00-10:00 Faraday lecture theatre. Plenary Lecture. Joke Hadermann. *University of Antwerp. Belgium. "*Electron diffraction tomography for atomic structure determination, ex and in situ".

Chair: Raúl Arenal. *ARAID Researcher. University of Zaragoza. Zaragoza. Spain*

10:00-10:30 Hall cines and Gardens. Coffee break. Posters. Commercial exposition.

10:30-13:00 Faraday lecture theatre. Session MS-3. Semiconductors – In-situ –Hybrid Nanostructures Chairs: Francesca Peiró / Ana Sánchez

- 10:30-10:45 N. Fernández-Delgado. Estructural characterization of small colloidal CdSe-ZnS core-shell QDs through HAADF-STEM
- 10:45-11:00 S. Martí-Sánchez. Morphology driven electronic band modulation in semiconductor core-shell nanowires
- 11:00-11:15. N. Ruiz-Marín. Formation of agglomerations in high-density multilayer InAs/GaAs quantum dot structures: the role of Sb in the capping layer
- 11:15-11:30 V. Braza. Sb and N incorporation interplay in GaAsSbN/GaAs epilayers
- 11:30-11:45 S. Flores. Comparative analyses of the In exchange in the InAs/GaAs system during the capping process with GaAs(Sb) at different growth rates
- 11:45-12:00 B. Ballesteros. Synthesis and electron microscopy of tubular van der Waals heterostructures
- 12:00-12:15 R. Arenal. Detailed atomic structure analyses of N-doped nanodiamonds
- 12:15-12:30 J. Pablo-Navarro. In situ real-time annealing of 3D ferromagnetic nanowires fabricated by focused electron beam induced deposition
- 12:30-12:45 M. Rosado. High spatial resolution, low voltage and ultrafast energy dispersive x-ray spectroscopy on a scanning electron microscope

10:30-13:00 Gutenberg lecture theatre
Session LS-3 Plant/Animal Biology
Chairs: Antonio Jesús Castro / José Carlos Jiménez-López

- 10:30-11:00. **J.M. Losada. Invited Speaker.** Bringing light onto hidden complex interactions: microscopy as a tool to study sexual reproduction in trees
- 11:00-11:20 A.L. Sousa. It is not easy being green - Electron microscopy techniques for the study of moss.
- 11:20-11:40 R.P. Louro. Ultrastructural analysis of carotenoid storage cells in aril of *Bixa orellana* L.
- 11:40-12:00 J.D. Alché. Developmental analysis of glutathione reductase localization in the olive (*Olea europaea* L.) seed tissues
- 12:00-12:20 M. M'rani-Alaoui. Localization of seed storage proteins (SSPs) in seeds of agricultural/nutritional interest
- 12:20-12:40 R. Nisa. What´s a protein like you doing in a place like this? Localization of a bacterial group II intron encoded protein in Arabidopsis thaliana protoplasts
- 12:40-13:00 A.J. Castro. Live-cell imaging of storage lipid dynamics in pollen tubes

13:00-14:30 Hall cines and Gardens. Buffet lunch. Posters. Commercial exposition.

14:30-16:00 Faraday lecture theatre
Session TD-2. Technical Developments in Life Sciences. Chair: José Mª Valpuesta

-14:30-14:45 S. Bonucci. Negative-staining: a simple technique with modern applications in biological research
-14:45-15:00 M. Zuzarte. Applications and challenges of SEM in Biomedicine
-15:00-15:30 R. Melero. The Instruct Image Processing Center (I2PC): support to structural biologists
-15:30-16:00 J.D. Alché. Microscopical detection of ROS and RNS in plant samples by using chromogenic and fluorescent probes

-15:30-16:00 J.D. Alché. Microscopical detection of ROS and RNS in plant samples by using chromogenic and fluorescent probes

16:00-16:30 Hall cines and Gardens. Coffee break. Posters. Commercial exposition.

16:30-18:30 Faraday lecture theatre. SME Best Ph.D. Awards. Chairs: Jordi Arbiol and Carmen San Martín.

- 16:30-17:10 (Ph.D. award in Biological Sciences. To be announced)
- 17:10-17:50 (Ph.D. award in Technological Advances. To be announced)
- 17:50-18:30 (Ph.D. award in Material Sciences. To be announced)

18:30-19:30 Faraday lecture theatre. SME General Assembly

20:00-23:30 Carmen de los Mártires. Gala Buffet

Friday, 13th September

9:00-10:00 Faraday lecture theatre. Plenary Lecture. Paul Midgley. *University of Cambridge. U.K.* "Low-dose scanning electron diffraction of 'soft' materials – application to polymers and pharmaceuticals".

Chair: Jordi Arbiol.

10:00-10:30 Hall cines and Gardens. Coffee break. Posters. Commercial exposition.

10:30-13:00 Faraday lecture theatre
Session MS-4. Functional Materials & Metals
Chairs: Jordi Arbiol / Kimberly Dick-Thelander

-10:30-11:00 **Gabriel Sánchez Santolino. Invited Speaker.** Direct visualization of electric and magnetic field structures in materials using differential phase contrast STEM
-11:00-11:15 O. Emadinia. Microstructural characterization of Ti6Al4V/Al2O3 joints produced using Ag-Cu sputtered coated Ti foil.
-11:15-11:30 L. Lajaunie. Atomic structure and optoelectronic properties of inorganic nanotubes
-11:45-12:00 C.E. Castillo. Chemical discrimination of single atom species in a heterobinuclear Au(III)-Pd(II) complex with an Hexa-aza macrocycle by advanced electron microscopy
-12:00-12:15 L.M. Valencia. Effect of the annealing temperature on the growth and properties of (Au)-NiOx films for electrochemical applications
-12:15-12:30 P.C. Ryan. Arsenic speciation in trioctahedral clays: insights from a serpentine synthesis study
-12:30-12:45 M. de la Mata. (S)TEM characterization of plasmonic UV nanoparticles
-12:45-13:00 C.E. Carlton. In-situ aberration-corrected TEM nanoindentation of silver nanoparticles

0:30-13:00 Gutenberg lecture theatre
Session LS-4 Biomedical Applications
Chairs: Juan de Dios Alché / Erin Tranfield

- 10:30-11:00 **Erin M. Tranfield. Invited Speaker.** The art of selecting and applying electron microscopy techniques to understanding biomedical research questions
-11:00-11:20 G. Ciasca. Searching for mechanical biomarkers of pathologies: some applications of atomic force microscopy to tissue and cell mechanics
- 11:20-11:40 M. Lopes-da-Silva. Using CLEM to unravel intracellular membrane trafficking defects
- 11:40-12:00 E. Lima-Cabello. Imaging induced anti-inflammatory response in human cell cultures and *ex vitro* blood cultures
- 12:00-12:20 A.J. Castro. Live cell imaging of soybean BBI proteins internalization in HT29 colorectal cancer cell
- 12:20-12:50 **Rosario M. Fernández. Invited Speaker.** Exploring neuronal subcellular architecture in the mouse brain

13:00-13:30 Faraday theatre. Closing remarks

POSTER COMMUNICATIONS. MATERIAL SCIENCES

MS-P1. A. Ruiz, A. Nuñez, A. Vargas, J.F. Almagro. Characterization of brittle phases in EN 1.4462, 1.4482 and 1.4410 duplex stainless steels in heat treatments

MS-P2. S. Xu, J. Pons, R. Santamarta, I. Karaman, R.D. Noebe. Strain glass state in Ni-rich Ni-Ti-Zr shape memory alloys

MS-P3. A. Ibarra, R. Córdoba, D. Mailly, J.M. De Teresa. Characterization of 3D superconducting WC nanotubes fabricated by a novel focused ion-beam induced deposition direct-write method

MS-P4. T. Zhang, K. Wan, J. Luo, Ch. Zhou, X. Lu, B.W. Mao, X. Zhang, J. Fransaer, J. Arbiol. Hierarchical porous Ni3S4 with enriched high-valence Ni sites as a robust eectrocatalyst for efficient oxygen evolution reaction

MS-P5. K. Barragán Sanz, S. Irsen. The Rocking Phase Plate – another step towards improved stability

MS-P6. M. Navarro M, L. Paseta, C. Echaide, J. Benito, I. Gascón, J. Coronas, C. Téllez. TEM characterization of nanocomposite polymer membranes with MOF fillers for nanofiltration

MS-P7. Ch. Koch, Y. Liu, S. Martí-Sánchez, P. Krogstrup, J. Arbiol. Study of epitaxy in proximity coupled semiconductor -ferromagnetic insulator - superconductor heterostructures for mejorana-based topological quantum computing

MS-P8. J. García-Fernández, M. García-Carrión, A. Torres-Pardo, R. Martínez-Casado, J. Ramírez-Castellanos, E. Nogales, B. Méndez, J.M. González-Calbet. Study of structural variations in the homologous series NaxGa4+xTin-4-xO2n-2 by electron microscopy techniques: influence on its luminescent properties

MS-P9. S. Hettler, D. Valenzuela, R. Arenal. Transmission electron microscopy investigation of graphene oxide flakes

MS-P10. M. Botifoll, S. Martí-Sánchez, E. Yücelen, Ph. Caroff, J. Arbiol. Comparative characterization of selective-area growth and vapour-liquid-solid III-V semiconductor-superconductor nanowire networks for topological quantum computing

MS-P11. X. Han, T. Zhang, Y. Zuo, Y. Liu, K. Sivula, A. Cabot, J. Arbiol. The characterization of the process of electrochemical oxidation of Cu2S into CuO nanowires by using transmission electron microscopy

MS-P12. M.L. Ruiz-González, R. Cortés-Gil, K. Sigcho Villacís, A. Azor Lafarga, J. Alonso, J.M. González-Calbet. Atomically resolved La-Mn-O nanomanganites

MS-P13. A. Ibarra, M. Ciria, M. G. Proiettia, E.C. Corredor, D. Coffey, A. Begué, C. de la Fuente, J.I. Arnaudas. Crystal structure and local ordering in epitaxial Fe1 00−xGax/MgO (001) films

MS-P14. J. Grzonka J, M. Claro, S. Sadewasser, P.J. Ferreira. Atomic structure of defects in GaSe/InSe heterostructure

POSTER COMMUNICATIONS. LIFE SCIENCES

LS-P1. J.C. Jiménez-López. Cytoskeletal scaffolding proteins as modulators of the functional responses of thylakoid membranes

LS-P2. E. Lima-Cabello, A.M. Rodríguez-Pöhnlein, F. Molina-Borrego, J.D. Alché, J.C. Jimenez-Lopez. Functional association between storage proteins mobilization and redox metabolism signaling in narrow-leafed lupin (*Lupinus angustifolius*) cotyledons driving seed germination and seedling development

LS-P3. D. Porcel. How three enzymes play during the long famine in terrestrial snails

LS-P4. C. Capel, R. Micol-Ponce, M. García-Alcázar, F.J. Yuste-Lisbona, B. Pineda, J. Capel, V. Moreno, R. Lozano. *VIPP1* develops a crucial function in the maintenance of chloroplast membrane integrity and survival of tomato plants

LS-P5. S. Hafidh, E. Lima-Cabello, J.D. Alché. Establishing TCTP1 secretion patway using TEM immunocytochemistry

LS-P6. A. Kućko, E. Wilmowicz, T. Przywieczerski, J.D. Alché. ABA and ET involvement in the nodule-specific response on drought in yellow lupine

LS-P7. E. Wilmowicz, A. Kućko, K. Panek, S. Burchardt, J.D. Alché. The EPIP peptide as a crucial component of phytohormonal-dependent pathway regulating flower shedding in yellow lupine

SCIENTIFIC PROGRAMME
ABSTRACTS
- PLENARY LECTURES -

The Scottish Centre for Macromolecular Imaging - a national structural biology centre built around JEOL's CryoARM 300

David Bhella

Scottish Centre for Macromolecular Imaging, MRC - University of Glasgow Centre for Virus Research, Sir Michael Stoker Building, Garscube Campus, 464 Bearsden Road, Glasgow, G61 1QH. Scotland, United Kingdom
E-mail for correspondence: david.bhella@glasgow.ac.uk

Keywords: capsid, cryo-EM, protein structure, single-particle analysis, tomography, virion, virus

As my talk will follow the ADVANCED MICROSCOPY IMAGING AND IMAGE ANALYSIS workshop, it will be delivered in two parts:

The Scottish Centre for Macromolecular Imaging

Cryo-transmission electron microscopy has undergone a technological revolution in recent years. It is now possible to achieve structural data on macromolecular assemblies such as proteins and nucleoprotein complexes at atomic and near-atomic resolutions. This has led to widespread interest in adopting the technology and significant investment in high-performance cryo-microscopes to serve structural biology communities. The Scottish Centre for Macromolecular Imaging (SCMI) was established by a consortium of Scottish Universities to provide access to cutting-edge cryo-EM resources for Scottish structural biologists. SCMI will provide high-quality training and support to new users as they learn to become proficient cryo-EM practitioners. It is envisaged that SCMI will form the hub for a network of like-minded investigators allowing knowledge sharing and support.

Cryo-EM instrumentation is most widely bought from two market-dominant companies - Thermo-Fisher (formerly FEI/Phillips) and Gatan. An important dimension of the SCMI project was our decision to purchase new to market instruments - The JEOL CryoARM 300 automated 300 keV cryo-microscope, and a Direct Electron DE64 detector. In my talk, I will introduce SCMI and discuss our reasons for selecting these new tools over the market-dominant Thermo-Fisher Titan Krios and Gatan K3

detector. I will discuss some of the challenges of being early-adopters and explain our current status. Finally, I shall present some data from the CryoARM 300/DE64.

Breaking the shackles of symmetry in structural studies of icosahedral viruses

Since the earliest days of transmission electron microscopy researchers have used TEMs to study the structures of viruses. These large and often highly symmetric macromolecular assemblies were among the first targets for three-dimensional image reconstruction following the invention of cryo-EM. In particular, helical phage tails and icosahedral capsids and virions allowed structural detail to be discerned from comparatively few particle images owing to the presence of many regularly arrayed proteins in each image. Until very recently, a major limitation of structural analyses that exploit symmetrical averaging was the loss of asymmetric features that can be critical for our full understanding of virus biology. Improvements in the quality of image data from cryo-EM combined with advances in image processing methods now allow us to investigate the structures of small asymmetric components and deviations from symmetry in large icosahedral viruses, yielding surprising insights into virus biology. Here I will present some recent data from my lab describing asymmetric features in the large DNA containing herpesviruses and smaller RNA containing caliciviruses, that play critical roles in the infectious processes of these important pathogens.

References

1.- Bhella D. (2019). *Biophys. Rev*. doi: 10.1007/s12551-019-00571-w.
2.- Conley MJ *et al.* (2019). *Nature* 565: 377
3.- McElwee M et al. (2018). *PLoS Biol.* 16: e2006191

Phage T7 viral tail machinery characterization: A model for DNA retention and ejection from the capsid

José L. Carrascosa

Centro Nacional de Biotecnología, Consejo Superior de Investigaciones Científicas (CNB-CSIC). Darwin 3, Campus Cantoblanco. 28049 Madrid, Spain
E-mail for correspondence: jlcarras@cnb.csic.es

Keywords: cryo-electron microscopy, DNA ejection, three-dimensional reconstruction, tail assembly, virus structure

The transfer of DNA from viral particles into bacteria is a complex process which involves several key steps. In tailed dsDNA viruses, the most abundant virus group, the onset of the infective process requires recognition of the receptors in the target cell by the virus, attachment of the virus to the cell wall, the formation of a conduit to allow ordered DNA transfer, the actual DNA translocation, and the incorporation of the whole DNA genome into the bacteria to start the successful replicative process. Most tailed dsDNA phages incorporate the DNA through a unique portal vertex into a preformed icosahedral capsid[1], where it is coiled to reach quasi-crystalline densities with the help of small molecules and viral proteins which build a proteinaceous core. To secure this DNA inside the shell under the constraints of a high torsional stress and extensive electrostatic repulsions, the tail components incorporate to the capsid by the adaptor to get the final mature phage with the DNA secured inside[2].

The tail complex plays a critical role both for securely retaining the DNA inside the viral capsid and, also, for allowing its translocation inside the target bacteria during infection[3]. To get an insight on how these functions are carried out by this machinery, we have studied the tail of phage T7[4]. The T7 tail machinery is composed of four proteins: the connector (gp8), the adaptor (gp11), the nozzle (gp12) and the fibers (gp17). We have solved the structure of the fiber-less tail by Cryo-Electron Microscopy at ~3.3 Å resolution, which has allowed to completely trace the three structural protein amino acid chains (1.5 MDa). The tail complex shows a tubular conical shape of 293 Å long and 175 Å wide, organized in two 12-fold rings (gp8 and gp11) and a 6-fold nozzle (gp12). The structure presented two invaginations: the first, between the

connector and the adaptor, serves for capsid docking; and the second, between the adaptor and the nozzle, creates the interaction surface with the fibers.

A most important feature is that the tail inner channel is closed at the hexameric nozzle by four different loops (building hexameric valves) that could retain the DNA inside the capsid in the mature phage. This internal channel is mainly negatively charged, which has been suggested to be essential to avoid DNA staking during ejection.

Comparison of the structure of the connector in the tail complex with those derived from x-ray diffraction from isolated connectors[4], reveals that there are three related conformations: two alone and one in complex within the tail. These different conformations, together with the structure of the tail, allow the proposal of a mechanism for DNA retention and ejection from the capsid at different stages of viral assembly.

References

1.- Cuervo A, Carrascosa JL. (2012). *Curr. Opin. Biotechnol.* 23: 529
2.- Cuervo A *et al*. (2013). *J. Biol. Chem.* 288: 26290
3.- González-García VA *et al.* (2015). *J. Biol. Chem.* 290: 10038
4.- Cuervo A *et al*. *Nat. Commun.* (in press)

Electron diffraction tomography for atomic structure determination, *ex* and *in situ*

Karakulina OM[1], Batuk M[1], Hendrickx M[1], Abakumov AM[1,2], **Joke Hadermann**[1,*]

1. EMAT, Department of Physics, University of Antwerp, Groenenborgerlaan 171, 2020 Antwerp, Belgium
2. Centre for Energy Science and Technology, Skoltech, Skolkovo Institute of Science and Technology, Bolshoj Blvd. 30, bld. 1, Moscow, Russia 121205
*Author for correspondence: joke.hadermann@uantwerpen.be

Keywords: electron diffraction tomography, *in situ*, electrochemical cell, gas cell, Li-ion

Quantitative electron diffraction in the form of electron diffraction tomography has been used for about a decade now to solve and refine structures of different types of compounds. It is based on reconstructing the three dimensional reciprocal space with minimal dynamic diffraction effects, to allow using the intensities for direct structure solution and even precise and accurate refinement of the coordinates. This gives access to the refinement of many compounds that are out of reach for single crystal X-ray or neutron diffraction, for example to study cycled lithium ion battery cathode materials, where large crystal sizes (as required for X-rays and neutrons) have too long Li diffusion paths to allow proper charging and discharging of the electrode material. Electron diffraction tomography single crystal experiments can then solve and refine the complete crystal structures, even including the sites and occupancies of the lithium atoms.

Initially, we performed this type of experiments using data from ex situ experiments, but recently we have been able to also refine structures from in situ data obtained using an electrochemical cell or a gas environment cell. This allows performing single crystal electron diffraction experiments also on submicron scale materials in realistic environments instead of the high vacuum of the microscope, and eventually should allow to follow the structure evolution upon reactions such as oxidation and reduction.

In this talk, I will not only show the exciting possibilities of in situ electron diffraction tomography, but also highlight the problems that still need to be overcome before this can become an established technique.

References

1.- Karakulina OM *et al.* (2016) *Chem. Mater.* 28: 7578
2.- Fedotov SS *et al.* (2016) *JSSC* 242: 70

3.- Mikhailova D *et al*. (2016) *Inorg. Chem*. 55: 7079
4.- Drozhzhin OA. (2016). *Electrochim. Acta* 191: 149
5.- Fedotov SS. (2016). *Chem. Mater.* 28: 411
6.- Karakulina OM *et al*. (2018). *Nano Letters* 18: 6286

Low-dose scanning electron diffraction of 'soft' materials – application to polymers and pharmaceuticals

Paul A Midgley[*], Johnstone DN

Department of Materials Science and Metallurgy, University of Cambridge, 27 Charles Babbage Road, Cambridge, CB3 0FS, UK
*E-mail for correspondence: pam33@cam.ac.uk

Keywords: electron diffraction, electron crystallography, pharmaceutical materials, polymers, semi-crystalline materials

Over the past decade or so, there have been some remarkable advances in electron microscopy including the advent of aberration correctors and monochromators. However, just as important has been the rise in the speed and efficiency of electron microscope cameras and detectors, coupled with an increase in associated computational power for image and spectral processing, and for handling large data sets in general. This has been an important factor in the increase of interest in crystallographic mapping, or 'crystal cartography', using the (scanning) transmission electron microscope, (S)TEM. This has led also to a convergence of interest between the imaging and diffraction communities, both of whom are now acquiring large 4-dimensional data sets composed of diffraction patterns acquired at every real space pixel within a scan of a region of interest.

For high resolution image reconstruction, electron ptychography methods has been adopted, in which a highly coherent convergent probe is used to form CBED patterns with disc overlaps encoding relative phase changes between diffracted discs. For crystallographic mapping at the nanoscale, a near diffraction-limited (almost parallel) beam is used to form 'spot' patterns which extend out in reciprocal space (with a resolution beyond $1Å^{-1}$) but are formed using real space probes ca. 3-5nm in diameter; this type of mapping is often called 'scanning electron diffraction', or SED[1]. A series of patterns recorded by SED may be used to determine relative changes to the pattern geometry across the region of interest and those changes used to determine crystal phase, orientation and strain.

In this presentation we will show how SED may be used to provide nanoscale crystallographic information not readily obtained using other techniques and, in

particular, focus on how fast, low-dose acquisition of SED patterns allows for the study of highly beam-sensitive 'soft' materials[2], such as polymeric[3,4] and pharmaceutical crystals[1]. In particular, using this method I will focus on nano-structures that have been elucidated in 'semi-crystalline' polyethylene[5,6], see for example Figure 1, and on pharmaceutical crystals that can show remarkable defects and ordered structures.

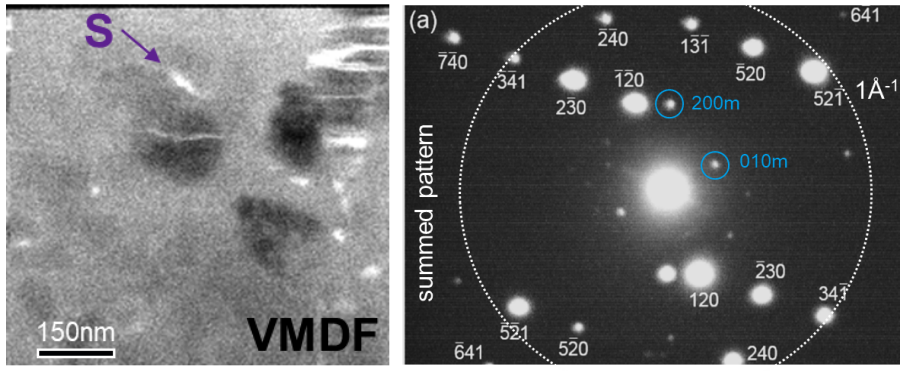

Figure 1. Characterization of shish-kebab polyethylene[7]. Left, virtual multiple dark-field image showing a lamella ('kebab') in the top right hand part of the image connected to a semi-crystalline shish, arrowed with an 'S'. Right, summed diffraction pattern from individual patterns recorded down the lamella axis of the kebab structure. Indexing is to an orthorhombic cell, except for those in blue which correspond to the monoclinic variant. The dotted circle indicates 1Å^{-1} resolution.

References

1.- Johnstone DN, Midgley PA. (2017). Microsc. Microanal. 23: 1192
2.- Egerton RF. (2013). Ultramicroscopy 127: 100
3.- Drummy LF, Kübel C. (2010). Polym. Rev. 50: 231
4.- Panov O *et al*. (2016). Micron 88: 30
5.- Keller A. (1979). Faraday Discuss. 68: 145
6.- Bevis MJ, Allan PS. (1974). Stress-induced martensitic transformations and twinning in organic molecular crystals, in: Surface and defect properties of solids, Roberts MW, Thomas JM (Eds.), The Royal Society of Chemistry, vol. 3, pp. 93-131
7.- Somani RH *et al*. (2005). Polymer 46: 8587

SCIENTIFIC PROGRAMME
ABSTRACTS
- ORAL PRESENTATIONS -

SESSION MS-1. INVITED SPEAKER

Evolution of EM applied to nanoporous solids

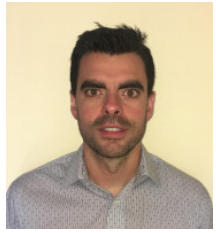

Álvaro Mayoral

Center for High-resolution Electron Microscopy (CħEM), School of Physical Science and Technology, ShanghaiTech University, 393 Middle Huaxia Road, Pudong, Shanghai, 201210, China
E-mail for correspondence: amayoral@shanghaitech.edu.cn

Keywords: beam damage, catalysis, porous solids, radiolysis, zeolite

Zeolites are porous aluminosilicates formed by tetrahedra sharing oxygens (figure 1a) with important industrial applications in different fields such as petrochemical catalysts, washing powders or even food industry. Characterization of these materials is carried out by several methods with the intention of gaining information at atomic level. In this sense, Transmission Electron Microscopy (TEM) can provide unique information as it combines the possibility of obtaining direct images of the materials together with diffraction information as well as spectroscopic data, all of it from nanocrystals as small as few tens of nanometers. Despite the enormous importance that TEM is having in the development of the current materials, its application to the area of zeolites and related porous materials is extraordinarily difficult due to the low stability of these solids under the electron beam[1]. In the current presentation, the results obtained by means of Cs-corrected STEM imaging obtained from various porous solids will be shown[2]; in order to assist to solve new structures, characterize structural defects not accessible by other methods (figure 1b) or helping to evaluate the ion exchange capabilities of the porous frameworks[3].

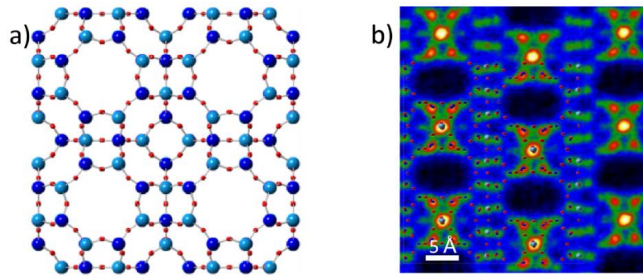

Figure 1. a) Schematic representation of a zeolite framework. b) Atomic resolution image of ETS-10 with the model superimposed.

References

1.- Diaz I, Mayoral A. (2011). *Micron* 42: 512
2.- Mayoral A *et al*. (2016). *Angew. Chem.* 55: 16127

Acknowledgements

We acknowledge to The Centre for High-resolution Electron Microscopy (ChEM), supported by SPST of ShanghaiTech University under contract No. EM02161943; and the National Natural Science Foundation of China NFSC-21850410448 and NSFC-21835002.

Cluster beam deposition for precise heterogeneous catalysts

Spadaro M C[1,2,*], Martinez L[3], Rongsheng C[2], Niu Y[2], Huttel Y[3], Palmer R[2], Arbiol J[1,4]

1. Catalan Institute of Nanoscience and Nanotechnology (ICN2), CSIC and BIST, Campus UAB, Bellaterra, 08193 Barcelona, Catalonia, Spain
2. College of Engineering, Swansea University, Bay Campus, Fabian Way, Swansea SA1 8EN, UK
3. Instituto de Ciencia de Materiales de Madrid, Consejo Superior de Investigationes Cientifica (CSIC), Campus de Cantoblanco, 28049 Madrid, Spain
4. ICREA, Pg Lluis Companys 23, 08010 Bercelona, Catalonia, Spain
*Author for correspondence: mariachiara.spadaro@icn2.cat

Keywords: cluster, heterogeneous catalysis, STEM-EDX

One of the most critical challenges in heterogeneous catalysis is the improvement and control of the atomic efficiency which can both reduce the cost of the catalysts and improve their performance. Cluster beam deposition (CBD) is a solvent-free technique that offers high degree of flexibility on cluster's size and composition, which results the most promising technique in this scenario.

To correctly address these challenges, cluster analysis must be complemented with novel and advanced characterization techniques, such as transmission electron microscopy (TEM). By acquiring high resolution (HR) TEM and scanning (S) TEM images it is possible to determine clusters structure, exposed planes or edges/steps; as well as their chemical composition by acquiring EELS or EDX maps in STEM mode.

Recently, a number of efforts have been devoted in enhancing the structure control of the produced clusters as well as their scale up to the industrial level. We describe here the new generation of magnetron based CBD source, the Multiple Ions Cluster Source (MICS)[1], where the single magnetron is replaced with three independent magnetrons allowing the production of a wide range of nanoalloy clusters starting from pure targets. The advantage of this source is the possibility to grow a wide range of samples via the controlled sputtering of pure targets, controlling both their structure (alloys, core@shell and shell@core) and composition by changing the mutual magnetron positions as well as their sputtering rate. But the beam current from CBD sources is typically limited to the 0.1 – 1 nA, corresponding to only $\sim \mu g/h$ of deposited material. In order to use this novel system in real applications it is necessary to scale-up the deposition rate up to $\sim mg/hour$ or even $\sim g/hour$ rates. This challenge is nowadays being addressed though the recently invented Matrix Assembly Cluster Source (MACS)[2] to generate clusters with high rate. It is based on a completely new concept for cluster production, an Ar^+ ion sputters a pre-condensed Ar-M matrix (where M is the metal) producing a collision cascade and consequent cluster formation.

Here we will present our recent results dedicated to optimise the electrochemical response of both metallic and transition metal dichalcogenides nanostructures produce by the above cluster beam source. Our study is complemented with atomic resolved electron microscopy characterisation.

References
1. - Martínez L. *et al.* (2017). *Nanoscale* 9(19): 6463
2. - Palmer RE *et al.* (2016). *Rev. Sci. Instr.* 87: 046103

Acknowledgments
This project has received funding the EU H2020 project CritCat (project ID: 686053). MCS has received funding from the European Union's Horizon 2020 research and innovation programme under the Marie Sklodowska-Curie grant agreement No 754510 (PROBIST). ICN2 acknowledge funding from Generalitat de Catalunya 2017 SGR 327 and the Spanish MINECO project ENE2017-85087-C3. ICN2 is supported by the Severo Ochoa program from Spanish MINECO (Grant No. SEV-2017-0706) and is funded by the CERCA Programme-Generalitat de Catalunya.

Submonolayer ceria addition as a mechanism to stabilize Au nanoparticles: Electron microscopy characterization

Manzorro R[1,2,*], Celín WE[1], Montes Monroy JM[1,2], Pérez-Omil JA[1,2], Calvino JJ[1,2], Trasobares S[1,2]

1. Departamento de Ciencia de los Materiales e Ingeniería Metalúrgica y Química Inorgánica, Facultad de Ciencias, Universidad de Cádiz, Campus Río San Pedro, Puerto Real, 11510 Cádiz, Spain
2. IMEYMAT. Instituto de Microscopía Electrónica y Materiales, Universidad de Cádiz, Spain
*Author for correspondence: ramon.manzorro@uca.es

Keywords: advanced electron microscopy, Au nanoparticles, catalysis, Ceria monolayers, DFT calculations

Since the pioneering work of Haruta, Au nanoparticles below 5 nm deposited over different oxides are commonly used in the CO oxidation reaction, a key process in the purification of H_2 produced via steam or methane reforming. However, this noble metal, due to its relatively low melting point, suffers from significant sintering at moderate temperatures, just above 400^{o}C. This low resistance against sintering has limited up to now the application of supported gold catalysts to low temperature reactions.

Among all the strategies explored to stabilize Au nanoparticles, the addition of low amounts of ceria on the catalysts surface by Incipient Wetness Impregnation stands out as the simplest, most straightforward and effective method to modify supported gold catalysts, as recently reported for CeO_2/Au/TiO_2[1] and CeO_2/Au/YSZ[2] systems.

Both catalysts have a better performance in terms of activity and stability in the CO oxidation reaction than the starting Au/TiO_2 or Au/YSZ catalysts.

Advanced STEM characterization has proven essential to rationalize this effect. Thus, Figure 1 (top) shows the X-EDS map corresponding to the ceria-modified catalysts. In the case of CeO_2/Au/TiO_2, CeO_2 crystals (displayed in green) are observed, most of them in contact with Au nanoparticles. In CeO_2/Au/YSZ, a highly dispersed CeO_2 phase nanostructured as an ultrathin surface layer (displayed in blue) has been detected.

Further electron microscopy studies, in combination with DFT calculations and image simulations have provided more details of the ceria layer as well as their interaction with Au in the YSZ based catalyst. Thus, atomically resolved EELS-STEM evidence the presence of a coherent one-atom ceria layer after a harsh thermal treatment. The comparison of experimental and simulated HAADF images, Figure 1 (bottom), confirms a perfect structural match between ceria and the YSZ support, which involves a contraction of the ceria lattice parameter. On its hand, DFT calculations have pointed out that there is a very small energy barrier for the YSZ system to accommodate the ceria phase in the form of a supported bidimensional layer without

interrupting the crystal structure of the bulk, as well as a good agreement with the CeO_2 lattice parameter observed experimentally, matching that of YSZ.

In summary, aberration corrected, electron microscopy techniques are a requirement to unveil the subtleties of such unique nanostructures, which connect the differences in the CeO_2 dispersion to the structural relationships existing between the supported phase and the support.

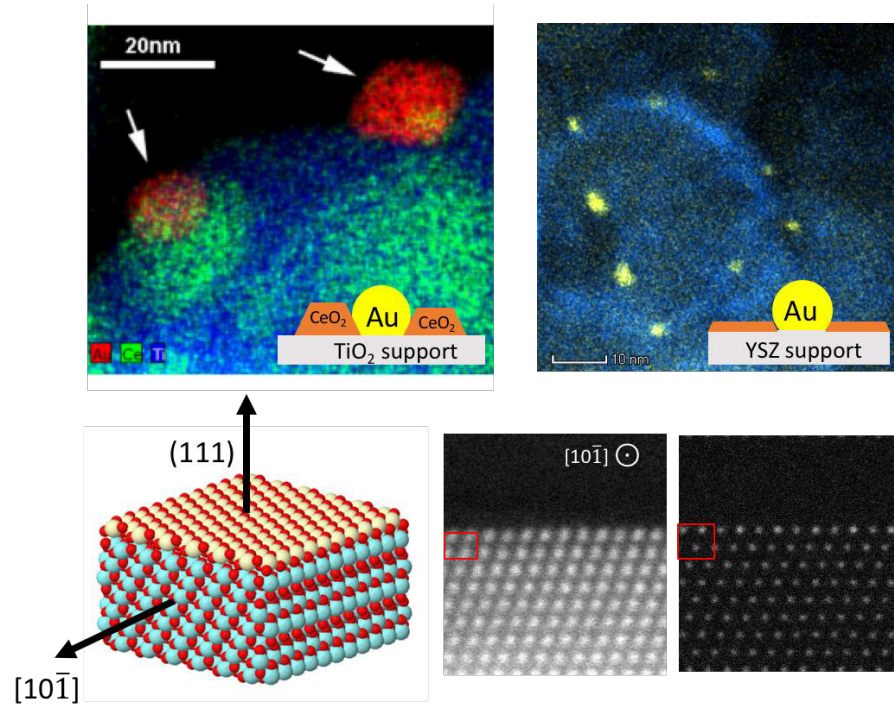

Figure 1. X-EDS maps corresponding to the CeO_2/Au/TiO_2 and CeO_2/Au/YSZ catalysts (Upper images). Atomic model, experimental and simulated images describing the ceria dispersion on the ceria-modified Au/YSZ sample (Bottom images)

References

1.- del Río E *et al*. (2016). *Appl. Catalysis B: Environment.* 197: 86
2.- Manzorro R *et al*. (2019). *ACS Catalysis* 9 (6): 5157

Acknowledgements

This project has received funding from the European Union's Horizon 2020 research and innovation programme under Grant 823717−ESTEEM3. Financial support from Junta de Andalucía (FQM334), MINECO/FEDER (Projects MAT2017-87579- R, MAT2016-81720-REDC) is also acknowledged. STEM studies were performed at SC-ICYT DME-UCA.

Study of location of AuPd nanoparticles supported on ceria nanocubes by analytical electron tomography

Benítez AJJ, Calvino JJ, López-Haro M*, Hungría AB

Departamento de Ciencias de los Materiales e Ingeniera Metalúrgica y Química Inorgánica, Facultad de Ciencias, Universidad de Cádiz, Campus de Puerto Real, 11510 Puerto Real (Cádiz), Spain
*Author for correspondence: miguel.lopezharo@uca.es

Keywords: ceria, gold, palladium, nanostructured – catalysts, tomography, X-EDS

Gold nanoparticles supported on ceria with controlled morphology have become a very interesting material to better understand the catalytic activity in reactions of major technological interest, *e.g.* CO oxidation or CO preferential oxidation (CO-PROX). In the particular case of CeO_2 nanocubes (NC), it is well known that the crystallography surfaces are mostly dominated by {100} facets, although {110} and {111} planes are also found at truncated edges and corners respectively.

In the literature, many authors assume that the gold nanoparticles are located at {100} crystallographic faces representing roughly 90% of the surface of the cubes[4]. Note that, this evidence is inferred by the analysis of 2D TEM images. However, a recent work carried out in our laboratory using HAADF-STEM tomography has demonstrated that gold nanoparticles supported on ceria NC are principally located on the edges and the corners of the nanocrystals, *e.i.* at {110} and {111} crystallographic faces, Figure 1(right)[1]. On the contrary, new experiments also carried out in our group on Pd nanoparticles supported on ceria NC have shown a clearly different disposition of the nanoparticles, being homogeneously distributed, interacting mostly with the dominant {100} facets of NCs, Figure 1b.

As shown in the literature, Au and Pd tend to form bimetallic particles, which exhibit synergistic behaviour for various reactions. Therefore, it seems a good approach to prepare bimetallic Au-Pd catalysts in order to drive the location of gold to the dominant {100} facets of the NCs.

3D characterization of bimetallic Au-Pd catalysts supported on heavy oxides, like CeO_2 NC, is a very challenging task. Note that, *i)* a very small difference between the atomic number (Z) of metal and support (Z_{Pd}=46, Z_{Au}=79, Z_{Ce}=58) complicates both the detection and discrimination of the chemical nature of the small particles; *ii)* Signal-noise-ratio is very low, even using the new 4 quadrant windowless X-EDS detectors.! This makes that both, acquisition of the tilt series and reconstruction algorithms have to be carefully optimized to improve the visualization and identification of the nanoparticles, as is shown in Figure 2.

In this work, we have study the location of Au-Pd nanoparticles supported on CeO_2 nanocubes by analytical electron tomography using FEI TITAN^3 THEMIS 60-300

operated at 200kV at SC-ICYT of Cádiz University. Data collection were obtained by tilting the specimen about a single axis perpendicular to the electron beam. Series of projections were acquired manually between -70º and +70° each 10º. In particular, for each tilt angle EDS spectrum imaging and HAADF image were recorded simultaneously using Super-X detector. The images series were aligned using Inspect3D and TomoJ and reconstructed using the ASTRA Toolbox implemented in Matlab[3]. In the particular case of CS, Total Variation Minimization (TVM) was carried by using the TVAL3 solver[2].

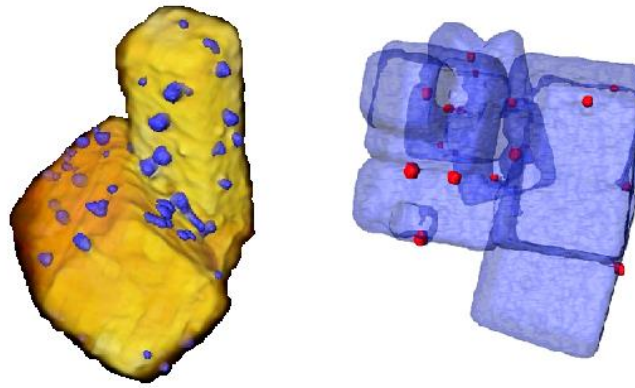

Figure 1. Tomography images of different NP over CeO_2–NC. (Left) Pd/CeO_2 (right) Au/CeO_2.

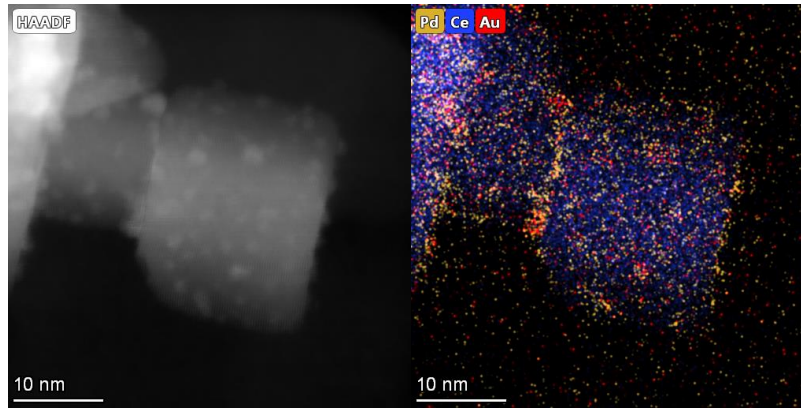

Figure 2. HAADF of $Au\text{-}Pd/CeO_2$ (left) and X-EDS of $Au\text{-}Pd/CeO_2$ (right).

References

1.- Tinoco M *et al*. (2015). *ACS Catalysis* 4: 3504
2.- López-Haro M *et al*. (2018). *Part. Part. Sys. Char.* 35: 1700343
3.- Olmos CM *et al*. (2016). *Catalysis Letters* 146: 144
4.- Ha H *et al*. (2018). *ACS Catalysis* 8: 11419

Doped cerium oxide mesoporous structure: a complete analytical TEM characterization based on MVA, clustering and X-EDS electron tomography

Blanco-Portals J[1,2,*], Baiutti F[3], Anelli S[3], Torrell M[3], López-Haro M[4], Estradé S[1,2], Tarancón A[3,5], Calvino JJ[4] and Peiró F[1,2]

1. LENS-MIND, Departament d'Enginyeria Electrònica i Biomèdica, Universitat de Barcelona, 08028 Barcelona, Spain
2. Institute of Nanoscience and Nanotechnology (IN2UB), Universitat de Barcelona, 08028 Barcelona, Spain
3. Catalonia Institute for Energy Research (IREC), Department of Advanced Materials for Energy, 1 Jardins de les Dones de Negre, Barcelona 08930, Spain
4. Dep. de Ciencia de los Materiales e Ingeniería Metalúrgica y Química Inorgánica Facultad Ciencias Universidad de Cádiz. Campus Rio San Pedro, 11510 Puerto Real, Cádiz, Spain
5. ICREA, 23 Passeig Lluís Companys, Barcelona 08010, Spain
*Author for correspondence: jblanco@el.ub.edu

Keywords: CeO_2, clustering, EELS, electron tomography, mesoporous, TVM, X-EDS

Cerium Oxide (CeO_2) doped with different composites, mainly transition metals and rare earths, has been routinely proposed as a solid electrolyte in solid state oxide fuel cells. Variations of the electrical behaviour are bounded to the distribution of dopants and, thus, a precise analytical characterization of the spatial morphology and elemental distribution becomes mandatory to understand variations on the devices performance.

We present the characterization of a CeO_2 mesoporous structure, doped with gadolinium (Gd) and praseodymium (Pr) at different ratios. The analysis of the corona regions of the structure at large magnifications was carried out by conventional *multivariate analysis* techniques (MVA) and *k-means clustering algorithms,* recently demonstrated as a valid routine for *electron energy loss spectroscopy* (EELS) data treatment[1].

Due to the interconnected double-gyroid geometry of the mesoporous CeO_2, analysis based on projection spectrum images would lead to artefacts on the dopant segregation study of the inner regions of the mesoporous structure. Hence, X-EDS analytical electron tomography experiments were conducted. To reduce the electron dose on the sample, only a few projections were acquired and, thus, robust algorithms in case of under-sampling for the reconstruction were required, such as the *total variation minimization* (TVM)[2].

Segregation of dopants (Pr and Gd) and changes in the oxidation state of Ce towards grain boundaries were resolved in the analysis of the EELS spectrum images, and further confirmed by the analytical electron tomography experiments.

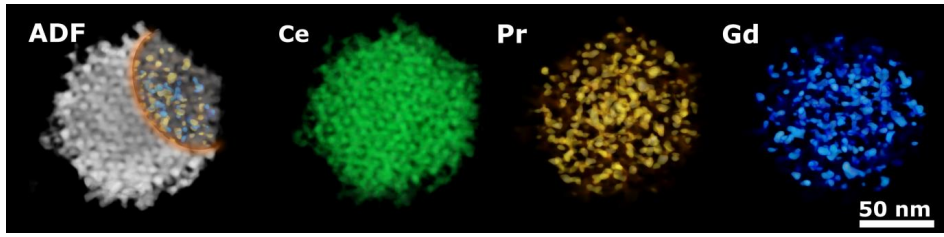

Figure 1. X-EDS electron tomography volume renderings. From left to right, ADF morphological volume rendering (gray), Ce signal volume rendering (green), Pr volume rendering (yellow) and Gd volume rendering (blue).

References

1.- Torruella P *et al*. (2018). Ultramicroscopy 185: 42
2.- López-Haro M *et al*. (2018). *Part. Part. Syst. Char.* 35 (3): 1700343

Preparation and characterization of NaBH4 modified CeO2/TiO2 nanostructured photocatalysts

Montes-Monroy JM*, Manzorro R, Trasobares S, López-Haro M, Calvino JJ, Pérez-Omil JA

Dpto. Ciencia de los Materiales e Ingeniería Metalúrgica y Química Inorgánica, Universidad de Cádiz, Avda. República Saharaui s/n, 11510 Puerto Real, Cádiz, Spain
*Author for correspondence: josemanuel.montes@uca.es

Keywords: band-gap, CeO_2, HREM, photocatalysis, STEM, TiO2

In this communication, we present an in-depth characterization of photocatalytic systems with potential applications in the sustainable production of energy, trying to establish a relationship between the structure of the material and its chemical behaviour. These systems have been studied using combination of advanced TEM/STEM techniques.

Materials based on titanium oxide have been tested in many photocatalytic processes related to environmental protection[1]. Breakage of the water molecule generates hydrogen that can be used as a primary fuel or as a reagent in the production of methanol. Numerous formulations have been proposed in order to improve the photocatalytic behaviour of titanium oxide by controlling both the band gap and the recombination rate of the electron-hole pairs generated by photons[2,3].

In this work, commercial titanium oxides (P25 and pure anatase) have been modified with cerium oxide (equivalent to 0.25 monolayers) and sodium borohydride. Its photocatalytic activity has been measured through the degradation of methylene blue under simulated sunlight. The influence of the synthesis method on the structure of the cerium oxide deposited onto the support has been studied using both structural and analytical techniques. Figure 1 gathers EDX elemental maps, recorded in a Titan3 Themis 60-300 microscope, showing the distribution of CeO2 onto the P25 support. Note that ceria is highly dispersed over the surface of the titania crystallites, in the form of nanometer sized structures.

Further analysis by structural techniques (HAADF and HREM), in combination with structural modelling techniques (Rhodius program) and image simulation (TEM-SIM software) reveals that CeO2 grows epitaxially on the surface of anatase crystallites, as illustrated in Figure 2. Finally, the CeO2/TiO2 samples were modified by a treatment with sodium borohydride, via reaction both in solid state and in solution. All samples treated with sodium borohydride were found to be more photocatalytically active than the reference sample TiO2 P25. The influence of the Boron / Titanium ratio on the structure of the resulting material and its degree of crystallinity was also studied. Moreover, the analysis of both the fine structure of the EELS Ti-L2,3 signal and the

Low Loss range (band gap) was performed to characterize in detail the electronic structure of the resulting materials. These studies have been complemented with macroscopic data, like X-ray diffraction, XPS spectroscopy and band gap measurements by Diffuse Reflectance Spectroscopy. The whole set of data obtained has allowed us establishing structure-function correlations in these materials, which will be used to improve the formulation of these systems, with large potential as photocatalysts.

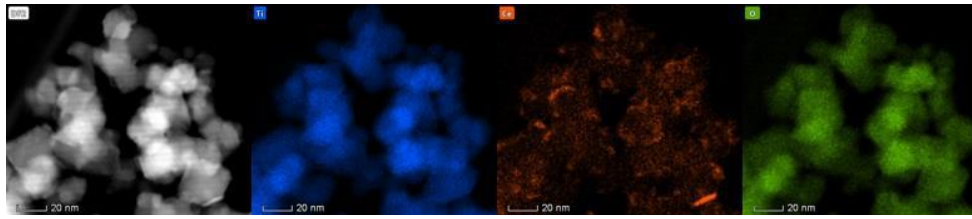

Figure 1. STEM-HAADF image of a CeO_2/P25 sample and EDS maps for Ti, Ce and O.

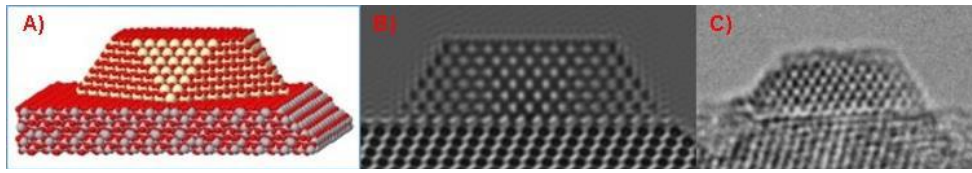

Figure 2. A) Model of a CeO_2 nanoparticle supported on a TiO_2 anatase surface. B) Simulation of the model. C) Real HREM image of the CeO_2/anatase sample.

References
1.- Gupta SM, Tripathi M. (2011). *Chinese Sci. Bull.* 56: 1639
2.- Ariyanti D *et al*. (2017). *Mater. Chem. Phys.* 199: 571
3.- Magesh G *et al*. (2009). *Indian J. Chem. - Sect. A Inorganic, Phys. Theor. Anal. Chem.* 48: 480

Acknowledgements
Financial support from MINECO/FEDER (MAT2017-87579 and MAT2016-81118-P) is acknowledged. JMMM acknowledges support from FPI Grants Program. Electron Microscopy data were acquired at DMe SC-ICYT UCA.

Phase and compositional mapping of polycrystalline Li-ion NCM cathodes

Almeida Alves CF[1], Xie Q[2], Manthiram A[2], Ferreira PJ[1,2,3;*]

1. INL - International Iberian Nanotechnology Laboratory, Av. Mestre José Veiga s/n, 4715-330 Braga, Portugal
2. Materials Science and Engineering Program, University of Texas at Austin, Austin, Texas 78712, USA
3. Mechanical Engineering Department and IDMEC, Instituto Superior Técnico, University of Lisbon, Av. Rovisco Pais, 1049-001 Lisboa, Portugal
*Author for correspondence: paulo.ferreira.at@inl.int

Keywords:

LiNixCoyMnzO2 (NCM), one of the most common cathode battery materials, exhibits a specific capacity and operating voltage comparable to LiCoO2, while being less toxic. These layered materials exhibit some degree of cation disorder and thus Ni exchanges with Li in the lithium layer, which disrupts the Li+ pathways, decreases the Li mobility, and degrades the cycling performance. For practical applications, the cathode particles used for the fabrication of batteries are porous micrometer polycrystalline particles, where the primary micron size particles possess a very complex microstructure, in particular an agglomeration of many nano sized particles, porosity, as well as chemical and phase heterogeneity.

In this regard, the aim of this work is to fundamentally understand the changes in phase and chemical distribution as a function of Ni content in polycrystalline NCM cathode materials. In particular, the chemical composition and structure were investigated by FIB-SEM, double-corrected TEM-STEM, and EDS/EELS mapping. Slice-and-view analysis revealed a geode-like morphology. Furthermore, STEM-EDS results revealed differences in structure, which are concomitant with variations in chemical composition across the particle, in particular segregation of Mn, which is dependent on the Ni content.

SESSION MS-2. INVITED SPEAKER

$La_{0.7}Sr_{0.3}MnO_3/PbTiO_3$ ferroelectric tunnel junctions: Domain configuration and interface characterization

Ana M. Sánchez[1,*], Peters JPP[1], Bristowe N[2], Apachitei G[1], Alexe M[1]

1. Department of Physics, University of Warwick, Coventry CV4 7AL, United Kingdom
2. School of Physical Sciences, University of Kent, Canterbury, United Kingdom
*Author for correspondence: a.m.sanchez@warwick.ac.uk

Keywords: annular bright field, ferroelectrics, interface, STEM, octahedral tilting

The development of spherical aberration correctors for electromagnetic lenses established a major improvement in the new generation of electron microscopes. The growing desire to control materials at an atomic level requires the capability to image and analyse material with atomic resolution. This work focuses on the application of state of the art electron microscopy to ferroelectric oxide materials.

Using aberration-corrected scanning transmission electron microscopy (STEM), we analysed in detail the domain structure of $PbTiO_3$/(La,Sr)MnO_3 ferroelectric capacitors with ultra-thin active layers. Annular Bright Field (ABF) imaging was used to visualise the both heavy and light elements, measuring the relative displacement and dipole distribution unit cell by unit cell. For a given system with a set lattice strain, the depolarization field becomes large – approaching the polarisation of the ferroelectric – at small film thicknesses (a few unit cells). The polarisation maps of different $PbTiO_3$ thin films revealed a clear influence or the asymmetric screening of the depolarizing field on the equilibrium domain pattern. The dipole distribution reveals the evolution from conventional 180° Kittel type domains to flux closure and vortex type domain configurations with reduced film thickness. Additionally, effects such as polarisation and octahedral tilt suppression can be observed local to the interface. We show how the different polarisation orientations interact with the LSMO at the interface. This provides insight into how such devices may be designed and tuned to achieve the desired performance.

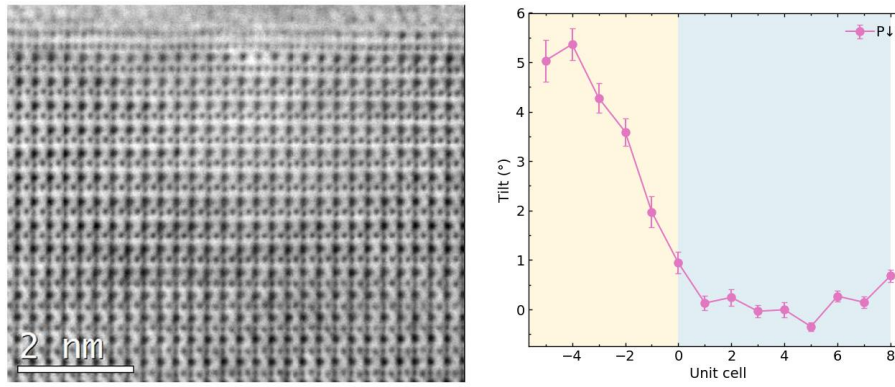

Figure 1. **(a)** ABF-STEM image of the LSMO/PTO interface **(b)** Out of plane octahedral tilt profile.

References
1.- Pantel D *et al*. (2012). *Nat. Mater.* 11: 289
2.- Stengel M *et al*. (2009). *Nat. Mater.* 8: 392
3.- Peters JJP *et al*. (2016). *Nat. Commun.* 7: 13484

Acknowledgements
EPSRC grants EP/P031544/1.

Study of magnetic iron oxide core/shell nanocubes using electron magnetic circular dichroism

del Pozo D[1,2,*], Estradé S[1,2,*], Varela M[3], Estrader M[4], López-Ortega A[4], Nogués J[4], Peiró F[1,2,*]

1. LENS-MIND, Departament d'Enginyeria Electrònica i Biomèdica, Universitat de Barcelona, 08028, Barcelona, Spain
2. Institut de Nanociència i Nanotecnologia (IN2UB), Universitat de Barcelona, Diagonal 645, 08028, Barcelona, Spain
3. Departamento de Física de Materiales, Facultad de Ciencias Físicas, UCM, 28040, Madrid, Spain
4. Institut Català de Nanociència i Nanotecnologia (ICN2), UAB Campus, 08193 Bellaterra, Barcelona, Spain

*Author for correspondence: dpozo@el.ub.edu / sestrade@ub.edu / francesca.peiro@ub.edu

Keywords: core/shell nanoparticles, EMCD, iron oxide, magnetism, magnetite, nanocubes

Electron magnetic circular dichroism (EMCD) is a technique, proposed in 2003[1] and experimentally demonstrated in 2006[2], which is analogous to the X-ray magnetic circular dichroism technique (XMCD) and it is based on electron energy loss spectroscopy (EELS). In the considered EMCD experiments, the dichroic signal from the magnetic material is obtained by getting a two-beam condition with two different positions for the detector, chiral plus and minus.

The EMCD main benefit in comparison with XMCD is the high spatial resolution at which the magnetic information of the sample is obtained. As in the case of XMCD, it is possible to quantitatively extract the orbital to spin magnetic moment ratio mL/mS. In our case, the EMCD technique is used to study magnetic nanocubes with a core/shell structure, formed by an iron II oxide core (FeO), 25 nm thick, covered by a magnetite shell (Fe_3O_4) of about 5 nm. This structure is observed in the Figure 1, where spectra of a spectrum image are classified using clustering algorithms, identifying the iron oxidation states.

The EMCD experiments are carried out in an aberration corrected S/TEM with a cold field gun at low temperature, 77 K. The two-beam condition is satisfied using the transmitted beam and g = (002). In the Fe3O4/FeO nanocubes it is imperative to probe the dichroic signal from the core and shell regions separately, to characterize the magnetic properties of the magnetite shell. EEL spectra are obtained with a 0.25eV lateral resolution and classified using clustering algorithms. Once both contributions are separated, the dichroic signal from both core and shell are obtained. As no net dichroic signal is expected from the FeO region, the core region data can be used as a sanity check measure. The spin magnetic moment ratio mL/mS is calculated for the magnetic shell. The dichroic signal obtained from these iron oxide nanocubes is presented in the Figure 2. Showing the EEL spectra for the iron L3 and L2 edges, and the resulting dichroic signal.

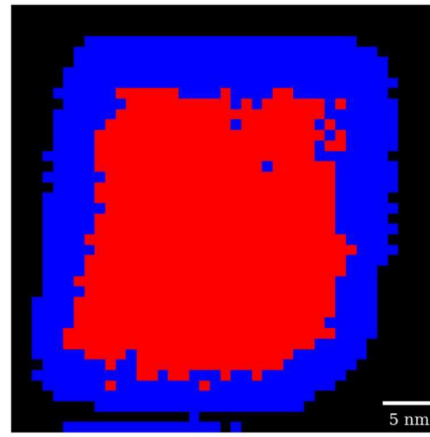

Figure 1. Colour map of an iron oxide nanocube resulting from the clustering analysis. The core is presented in red and the shell in blue.

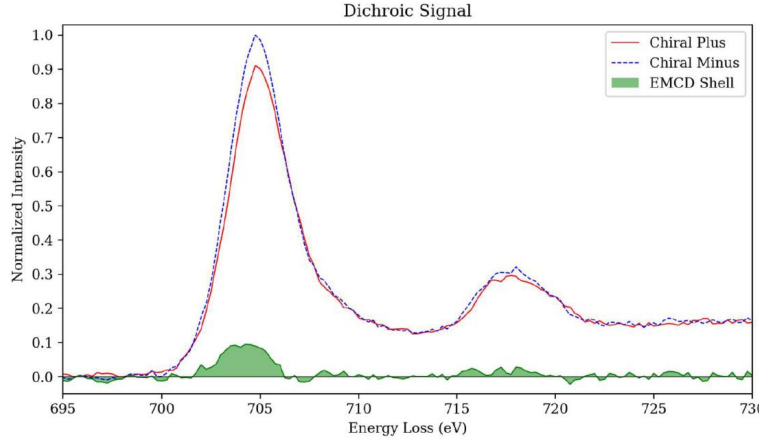

Figure 2. EEL spectra showing the iron white lines from the nanocube shell. Each spectrum is acquired with the detector aperture in two different positions, chiral plus and chiral minus. In solid green, difference between both EEL spectra.

References

1.- Hébert C, Schattschneider P. (2003). *Ultramicroscopy* 96 (3-4): 463
2.- Schattschneider P *et al*. (2006). *Nature* 441 (7092): 486

STEM-EELS analysis of Fe3O4@CoFe2O4@Fe3O4 core-shell-shell nanoparticles

Hettler S[1,*], Sartori K[2,3], Pichon B[2,3], Arenal R[1,4,5]

1. Laboratorio de Microscopías Avanzadas, Instituto de Nanociencia de Aragón, Universidad de Zaragoza, Zaragoza, Spain
2. CNRS-IPCMS, Université de Strasbourg, UMR 7504, 67000 Strasbourg, France
3. IMPMC, Sorbonne Université, 75005 Paris, France
4. ARAID Foundation, Zaragoza, Spain
5. Instituto de Ciencias de Materiales de Aragón, CSIC-Univ. Zaragoza, 50009 Zaragoza, Spain

*Author for correspondence: hettler@unizar.es

Keywords: EELS, iron and cobalt oxide, nanoparticles, STEM

Scanning transmission electron microscopy (STEM) in combination with electron energy-loss spectroscopy (EELS) is well suited to reveal the detailed chemical composition of nanomaterials[1]. Here we present the experimental results on a series of Fe3-δO4@CoFe2O4@Fe3-δO4 core@shell@shell (CSS) nanoparticles (NPs) with promising magnetic properties[2,3]. The NPs were investigated in a probe-corrected FEI Titan low-base with a high-brightness field-emission gun operated at 80 kV. Figure 1 shows three HAADF-STEM images of (a) Fe3-δO4 C-NP, (b) Fe3-δO4/CoFe2O4 CS-NP and (c) Fe3-δO4/ CoFe2O4 /Fe3-δO4 CSS-NP. The NPs appear single-crystalline with a round (C) or slightly facetted (CS,CSS) shape and an average size of 8, 10 and 13 nm (C,CS,CSS respectively). The homogeneous contrast of the atomic columns allows no conclusion on the presence of a shell and suggests an in-phase incorporation of Co in the Fe3O4 matrix.

Figure 2a shows an example EELS spectrum (PCA-filtered and extracted from a spectrum image) acquired in the centre of a CS-NP revealing the prominent peaks of O-K and Fe-L edges as well as a small peak corresponding to the Co-L edge. Using the three edges, the local quantitative composition of the NPs has been deduced. The composition across a CS-NP is depicted in Figure 2b and reveals the slightly increasing Co concentration from 3.5% in the center to 5% at the edge of the NP. A spectrum image of a CSS-NP reveals the very homogeneous distribution of Fe (green), O (red) and Co (blue) (Fig. 3b). A comparison of the O-K edge of the C-NPs with a Fe3O4 bulk reference[4] (black and red line in Fig. 3a, respectively) proves the intended spinel structure of the NPs. The presence of Co in the NP leads to a shift of intensity from the first peak of the O K-edge at 531 eV to the following minimum at 533 eV as shown by exemplary spectra from CS and CSS-NPs. Further investigation revealed that the Fe-L3 edge at an energy loss of 710 eV shows a slight red shift if Co is incorporated in the lattice. The dimension of the shell in case of the CS-NP was determined to 2-4 nm. In summary, the structure and composition of these complex NPs has been determined. The results indicate the presence of an increasing Co

content in a shell. The findings are crucial for better understanding of the outstanding magnetic properties of such nanostructures[5-6].

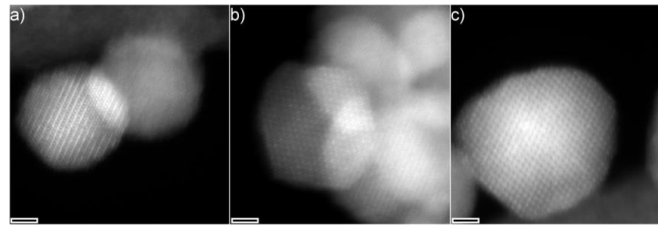

Figure 1. STEM-HAADF images of Fe3-δO4@CoFe2O4@Fe3-δO4 NP series. (a) C, (b) CS and (c) CSS**.** The NPs appear single-crystalline. Scale bars are 2 nm.

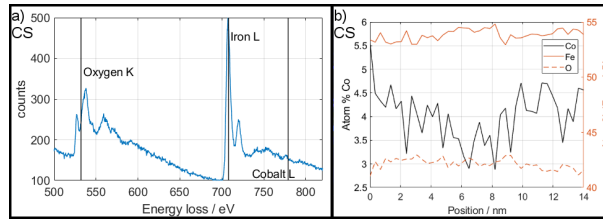

Figure 2. (a) Example Spectrum from CS-NP showing prominent O-K and Fe L as well as weak Co L-edges and (b) Distribution of Fe (solid red), O (dashed red) and Co (black) across a CS NP.

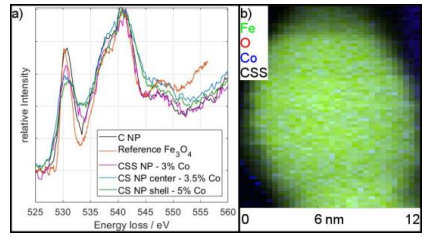

Figure 3. STEM-EELS analysis of the NP series. (a) comparison of Oxygen K-edge for C NP (black), center of CS (blue), shell of CS (green), CSS (magenta) with Fe3O4 bulk-reference (red) [4]. (b) Spectrum image of CSS NP.

References

1.- Advanced TEM: Applications to nanomaterials, Francis L, Mayoral A, Arenal R (Eds.), Springer, 2015
2.- Liu X *et al*. (2015). *Chem. Mater.* 27(11): 4073
3.- Sartori K *et al*. (2019). *J. Am. Chem. Soc.* (in press), DOI: 10.1021/jacs.9b03965
4.- Gloter A, Chen A. (2008). EELS database; https://eelsdb.eu/spectra/iron-oxide-magnetite-2/
5.- Krycka KL *et al*. (2013). *J. Appl. Phys.* 113 (17): 17B531
6.- Nogues J *et al*. (2005). *Phys. Rep*. 422 (3): 65

Acknoledgements

Research supported by the Spanish MINECO (MAT2016-79776-P, AEI/FEDER, EU), Government of Aragon through project DGA E13_17R (FEDER, EU), European Union H2020 programs “ESTEEM3” (823717), Flag-ERA GATES (JTC 2017), French Agence Nationale de la Recherche (ANR-11-LABX-0058-NIE) and SOLEIL synchrotron / Laboratoire Léon Brilluoin fellowship.

Understanding the cubic-to-tetragonal transition of Mn_3O_4 as a surface layer of $Li_{1-x}[Mn_2]O_4$

Amos CD[1], Pardo V[2], Goodenough JB[3], Ferreira PJ[1,3,4,*]

1. International Iberian Nanotechnology Laboratory (INL), Advanced Electron Microscopy Imaging and Spectroscopy (AEMIS), Av. Mestre José Veiga, 4715-330 Braga, Portugal
2. Universidade de Santiago de Compostela, Applied Physics Department, Rúa de José María Suárez Núñez, s/n, 15705 La Coruña, Spain
3. The University of Texas at Austin, Materials Science and Engineering, 1 University Station C2201, 78712 Austin, Texas, USA
4. Instituto Superior Técnico, Universidade de Lisboa, Instituto de Engenharia Mecânica (IDMEC), Av. Rovisco Pais 1, 1049-001 Lisboa, Portugal
*Author for correspondence: paulo.ferreira@inl.int

Keywords: batteries, EELS, HAADF STEM, LMO, TEM

$Li[Mn_2]O_4$ (LMO) is a well-known cathode material for Li-ion batteries, but it is plagued with cyclability problems associated with the loss of Mn^{2+} to the organic liquid electrolyte during electrochemical cycling. The surface disproportionation of Mn ($2Mn^{3+} \rightarrow Mn^{2+} + Mn^{4+}$) creates Mn^{2+} and leads to a stabilization of the surface of $Li[Mn_2]O_4$ through a surface reconstruction that creates a thin surface layer of Mn_3O_4 and a Li-rich subsurface layer of $Li_{1+x}[Mn_2]O_4$.[1] We have applied chemical treatments (aqueous acid treatment, a non-aqueous chemical delithiation, and an oxygen plasma treatment) to $Li[Mn_2]O_4$ and find that Mn_3O_4 is a robust surface phase in the $Li_{1-x}[Mn_2]O_4$ system regardless of the widely varying mechanisms of the treatments or the amount of Li, Mn, and O that is removed from $Li[Mn_2]O_4$. We use aberration-corrected scanning transmission electron microscopy (STEM) to identify that the native surface Mn_3O_4 phase is cubic whereas thicker Mn_3O_4 layers undergo a cooperative Jahn-Teller distortion to tetragonal symmetry. We utilize full-potential density functional theory (DFT) calculations to atomistically understand the transition from cubic to tetragonal symmetry. These insights help to understand why Mn_3O_4 is such a robust surface layer in the $Li[Mn_2]O_4$ system, whether this surface layer is potentially beneficial or detrimental for Li-ion batteries, and avenues to remove or modify the surface layers to give better electrochemical performance.

References

1.- Amos CD *et al.* (2016). *Nano Lett.* 16: 2899

Verwey transition on iron oxide nanocubes elucidated by electron energy loss spectroscopy and density functional theory simulations

Coll C[1,2,*], López-Conesa L[1,2,3,*], Muro-Cruces J[4], Roca AG, Trushkina Y[5], Salazar-Álvarez G[5], Fernández-Pacheco R[6], Magén C[6,7,8], Estradé S[1,2], Peiró F[1,2], Nogués J[4,9]

1. Laboratory of Electron Nanoscopies (LENS-MIND), Departament of Electronics and Biomedical Engineering, Universitat de Barcelona, 08028 Barcelona, Spain
2. Institute of Nanoscience and Nanotechnology, Universitat de Barcelona (IN2UB), 08028 Barcelona, Spain
3. Centres Científics i Tecnològics de la Universitat de Barcelona (CCiT-UB), 08028 Barcelona, Spain
4. Catalan Institute of Nanoscience and Nanotechnology (ICN2), CSIC and BIST, Campus UAB, Bellaterra, 08193 Barcelona, Spain
5. Department of Materials and Environmental Chemistry, Stockholm University, 106 91 Stockholm, Sweden
6. Laboratorio de Microscopías Avanzadas, Insituto de Nanociencia de Aragón (LMA-INA), 50018 Zaragoza, Spain
7. Departamento de Física de la Materia Condensada, Universidad de Zaragoza, 50018 Zaragoza, Spain
8. Fundación ARAID, 50018 Zaragoza, Spain
9. ICREA, Pg. Lluís Companys 23, 08010 Barcelona, Spain

*Author for correspondence: ccoll@el.ub.edu / llopez@el.ub.edu

Keywords: DFT simulations, EELS, TEM, Verwey transition

In the last decades, the Verwey transition, i.e., the phase transition that takes place in magnetite (Fe3O4) at low temperature, has been an unsettled discussion topic in condensed matter physics[1]. At room temperature (RT) magnetite is a half-metal with a cubic structure (Fd3□m), but at temperatures around 125 K it changes to an insulator with a monoclinic phase. However, the exact crystalline arrangement of the insulating phase is still an open question, where currently the proposed candidate phases are sthe Cc, C2/c and P2/c structures[2-4].

In the present work, the structure of the low temperature magnetite for single 25 nm nanocubes has been assessed combining experimental imagining and spectroscopy approaches in the Transmission Electron Microscope (TEM) and Density Functional Theory (DFT) calculations. The experiment was carried out in a liquid nitrogen cryo-holder allowing to acquire the data both at 100K (low temperature, LT) and at RT. The DFT calculations of the iron electron energy loss spectroscopy (EELS) edge of the RT phase and the potential LT phases were performed using WIEN2k package[5-6].

For HT, both the high resolution TEM and the EELS experimental data are in good agreement with the Fd3□m structure, as expected. However, for the low T phase, the high resolution TEM images do not yield a univocal result. Interestingly, DFT calculations suggest that a difference in the Fe L3 edge energy loss near edge structure (ELNES) can be used to distinguish between the diverse candidate phases. The LT experimental EELS data will be compared with the DFT results obtained from the different monoclinic candidates to elucidate the LT phase of magnetite in these nanocubes.

References

1.- Verwey EJW. (1939). *Nature* 144 (3642): 327
2.- Walz F. (2002). *J. Phys. Condens. Matter* 14 (12): R285
3.- García J, Subías G. (2004). *J. Phys. Condens. Matter* 16 (7): R145
4.- Senn MS *et al*. (2011). *Nature* 481 (7380): 173
5.- Hébert C. (2007). *Micron* 38 (1): 12
6.- Schwarz K *et al*. (2002). *Comput. Phys. Commun.* 147 (1-2): 71

Accurate determination of the oxygen stoichiometry in complex nanostructured oxides by combining STEM-HAADF tomography and STEM-XEDS quantification

M. López-Haro[1*], I. Gómez Recio[2], H. Pan[1], J.J. Delgado[1], M.L. Ruiz-González[2], J.M. González-Calbet[2], J.J. Calvino[1,*]

1. Departamento de Ciencia de los Materiales e Ingeniería Metalúrgica y Química Inorgánica, Universidad de Cádiz, Campus Rio San Pedro, 11510-Puerto Real, Cádiz, Spain
2. Departamento de Química Inorgánica, Universidad Complutense de Madrid, Ciudad Universitaria s/n, 28040 Madrid, Spain
*Author for correspondence: jose.calvino@uca.es / miguel.lopezharo@uca.es

Keywords: chronospectroscopy, light elements quantification, nano-oxides, STEM-EDX, STEM-HAADF tomography, Z-factors

The detailed description of the oxygen sublattice is key to rationalize the macroscopic performance of complex multimetallic nano-oxides. Determining with high accuracy the oxygen stoichiometry, at the nanometre and sub-nanometre levels, is a quite challenging task not only because of the light-element nature of O but also due to the influence of beam damage effects.

By combining different high-quality signals available in an aberration-corrected microscope, a new method has been devised to carry out such determination at low voltages, to minimize beam damage. The approach involves accurate measurements of local thickness values from STEM-HAADF electron tomography series reconstructed and segmented using advanced algorithms (TVM 3D)[1], and the quantification of time series of STEEM-EDX experiments using the so-called z-factor method (Figure 1)[2].

Using this new methodology, the oxygen content of K-Mn hollandite oxide nanorods was determined as a function of exposure time to the electron beam. From the kinetic analysis of the corresponding O-content vs time plots (Figure 2), the stoichiometry of the starting, non-damaged, oxide was determined as $K_{0.13}MnO_{1.94}$. Noteworthy, this formula was very close to those determined by macroscopic techniques, like neutron diffraction ($K_{0.13}MnO_{1.97}$) or Temperature Programmed Reduction in hydrogen ($K_{0.13}MnO_{1.93}$). This last result provides support to the experimental approach.

The developed methodology is quite general and can be applied whenever low voltage capabilities, a high efficiency XEDS detector system which allows fast acquisition of XEDS maps with appropriate S/N ratios and HAADF-STEM electron tomography capabilities are available. The detailed quantitative analysis of the XEDS-maps by the z-factor method opens the route to accurate chemical analysis at subnanometer level on this so complex type of nanostructured materials.

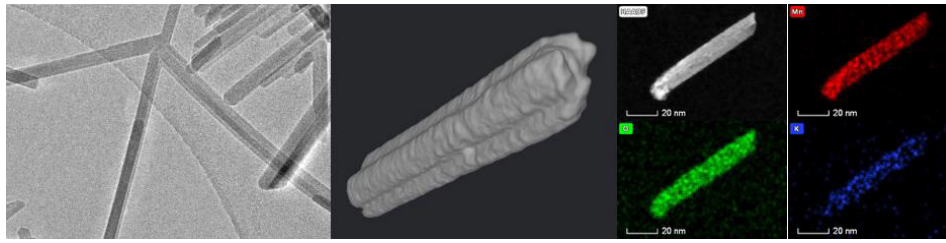

Figure 1.- (left) 2D BF-TEM image showing the nanorod type $K_{0.12}MnO_x$ hollandite particles; (middle) 3D rendered view of the STEM-HAADF tomography reconstruction; (right) STEM-HAADF and corresponding Mn, O and K EDX raw maps.

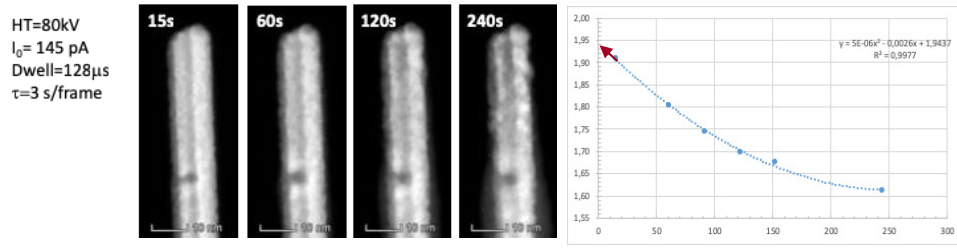

Figure 2.- (left) STEM-HAADF images of the hollandite nanorods after increasing exposure to the e-beam. Damage is directly observed; (right) O/Mn ratio vs exposure time plot. Extrapolating to "virtual" 0 time the fitted curve (plotted) provides the estimate of the O/Mn ratio of the non-damaged oxide.

References

1.- Watanabe M *et al*. (1996). *Ultramicroscopy* 65: 187

2.- Midgley PA, Bals S. (2009). Electron Tomography, in "Handbook of Nanoscopy", G. Van Tendeloo, D. Van Dyck, S.J. Pennycook (Eds.), Wiley-VCH, vol. 1, chapter 7, pp 253-280, ISBN: 978-3-527-31706-6

Acknowledgements

This work has received financial support from MINECO/FEDER (MAT2017- 87579-R, MAT2016-81118-P and MAT2016-81720-REDC). STEM data were acquired at DME-UCA (SC-ICYT).

Optimization of STEM-HAADF electron tomography reconstructions by smart parameters selection in compressed-sensing based algorithms

Muñoz JM[1,*], Bouziane A[2], Sakina F[3], Baker RT[3], Hungría AB[2], Calvino JJ[2], Rodríguez-Chía AM[1], López-Haro M[2,*]

1. Departamento de Estadística e Investigación Operativa, Facultad de Ciencias, Universidad de Cádiz, Campus Rio San Pedro, 11510 Puerto Real, Cádiz, Spain
2. Departamento de Ciencia de los Materiales e Ingeniería Metalúrgica y Química Inorgánica, Facultad de Ciencias, Universidad de Cádiz, Campus Rio San Pedro, 11510 Puerto Real, Cádiz, Spain
3. EaStChem School of Chemistry, University of St Andrews, St Andrews, Fife, KY16 9ST, United Kingdom
*Author for correspondence: juanmanuel.munoz@uca.es / miguel.lopezharo@uca.es

Keywords: compressed-sensing, nanomaterials, optimization, parameters selection, STEM-HAADF electron tomography

3D structural analysis of nanostructured materials by means of Electron Tomography is currently a well-stablished approach, which provides meaningful information out of reach for conventional 2D TEM/STEM analysis[1]. Most recent efforts in the field concentrate on improvements to reduce the amount of required information (tilt range, number of projections or sampled image points) while still improving the quality of the reconstructed volumes. At this respect, new methods based on Compressed-Sensing (CS) and exploiting the minimization of the Total Variation (TVM) of the whole set of images in the tilt series, have proven as quite efficient at this respect[2].

The implementation of CS-TVM algorithms, as e.g. in TVAL3, involves the use of a-priori user-fixed parameters, which provide a balance between the level of image detail and the match between the experimental and reconstructed sinograms[3]. Particularly, the model used in TVAL3 can be written as follows:

$$\min_{x,y_i} \sum_i (\|y_i\|_2 + \frac{\beta}{2}\|D_i x - y_i\|_2^2 - v_i^T(D_i x - y_i)) + \frac{\mu}{2}\|Ax - b\|_2^2 - \lambda(Ax - b),$$

where **x** is the image we reconstruct, **b** is the sinogram of **x**, and $\mathbf{D_i}$ calculates the gradient of **x** at pixel **i**. TVAL3 method adds new variables $\boldsymbol{y_i}$ to avoid non-differenciability difficulties when the l_2 norm derivative is calculated to obtain an optimal value of **x.** Therefore, $\boldsymbol{y_i}$ variables are related to the variable **x** by means of the constraints $y_i = D_i x$. Finally, v_i and $\boldsymbol{\lambda}$ are Lagrangian penalty parameters which are updated in the lagrangian iterations usually through a gradient method and μ and β are square penalty parameters that should be fixed in advance. Note that the results of the reconstruction will depend on the values chosen for β and μ parameters, which are routinely estimated on the basis of previous experience or, instead, following recommendations in the literature.

Although CS-TVM reconstructions very often provide much better results than other alternatives (e.g. SIRT or WBP), the manual selection of parameters does not guarantee that the algorithm provides an optimum output. To overcome this limitation, we have devised and developed a smart procedure that automatically searches for the optimum combination of parameters, within reasonable execution times.

This novel approach was tested on two different problems of interest in catalysis. The first, Figures 1(a-b), relates to the characterization of Au nanoparticles supported on CeO_2 nanocubes. The automatically determined parameter values provides in this case reconstructed volumes, Figure 1(b), which are much more efficiently segmented into Au (yellow) and CeO_2 (red) components, as well as CeO_2 crystallites with better defined, not so rough, surfaces, in better agreement with 2D TEM/STEM observations. The second sample, consisting of a C-based membrane with an ordered array of nanopores, was more challenging. In this case the reconstruction obtained using routine parameters, Figure 1(c), losses most of the pore details which, on the contrary are finely captured in the optimized reconstruction, Figure 1(d). Moreover, the segmentation of the reconstructed volume allowed us quantifying the pore volume of the system. The value estimated from the optimum TVAL3 reconstruction (0.55 cc/g) was quite close to the experimental one, determined by physisorption techniques. Likewise, the pore size distribution computed from the 3D reconstructions matched very closely that determined at macroscopic level. The developed methodology is quite general and can be applied to a variety of samples, including those containing nanopores, which fall out of reach for “conventional” TVM approaches.

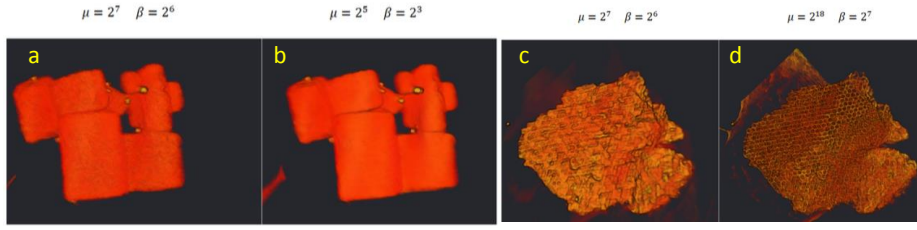

Figure 1.- 3D Rendered volumes obtained from a Au/CeO_2 nanocatalyst sample using TVAL3 with fixed (a) and after automatic optimization of μ and β values (b). The same comparison for a reconstruction of a nanoporous carbon membrane sample is shown in (c-d). The μ and β values are shown at the top.

References

1.- Midgley PA, Dunin-Borkowski RE. (2009). *Nature Mat.* 8 (4): 271
2.- López-Haro M *et al*. (2018). *Part. Part. Syst. Char.* 35 (3): 1700343
3.- Li C *et al.* (2013). *Comput. Optim. Appl.* 56: 507

Acknowledgements

This work has received financial support from MINECO/FEDER (MAT2017- 87579-R, MAT2016-82252-R, MTM2016-74983-C2-2-R). ET data were acquired at DME-UCA (SC-ICYT)

Structural characterization of small colloidal CdSe-ZnS core-shell QDs through HAADF-STEM

Fernández-Delgado N[1*], Herrera M[1], Pizarro J[2], Galindo P[2], Molina SI[1]

1. Department of Material Science, Metallurgical Engineering and Inorganic Chemistry, IMEYMAT, Faculty of Science, University of Cadiz, 11510 Puerto Real, Cadiz, Spain
2. Department of Computer Engineering, School of Engineering, University of Cadiz, 11510 Puerto Real, Cadiz, Spain
*Author for correspondence: natalia.fernandezdelgado@uca.es

Keywords: colloidal QDs, HAADF-STEM, intensity analysis, semiconductor, strain analysis

Environmentally friendly and renewable energy sources are currently the focus of research due to the continuous reduction in the reserve of fossil fuel and the negative impact of using non-renewable fuels to the environment. In particular, solar energy has gained a lot of importance in the past years due to its increase in competitiveness compared to other energy sources together with a gradual increase of carbon prizes[1,2]. In the photovoltaic field, colloidal CdSe/ZnS core-shell QDs are gaining interest due to properties such as QD confinement or tuneable band gap. The ZnS shell has as the main function to passivate the defects at the surface of the CdSe QDs[3], which has a remarkable importance due to their high impact in the functional properties. In order to progress in the development of these core-shell QDs, understanding the structural characteristics of the shell for specific synthesis conditions is essential as they have a strong influence in the adequate passivation of the surface defects at the CdSe core[4]. Despite the importance of obtaining direct information from the ZnS shell, most of the studies found in literature are related to indirect measurements like photoluminescence (PL) or quantum yield (QY)[5,6]. In this sense, *High Angle Annular Dark Field-Scanning Electron Microscopy* (HAADF-STEM) technique is a powerful tool for the analysis of the structural properties of advanced materials with high spatial resolution. This technique allows imaging with compositional information because the intensity of the image is related to the average Z1.7-2 of the material. According to the difference in average Z between the CdSe core (Zav. = 82) and the ZnS shell (Zav. = 46), both materials are expected to be distinguishable by HAADF-STEM technique.

In this communication, we have analysed by HAADF-STEM the structural properties of CdSe-ZnS core-shell QDs with a nominal shell thickness of only 2 MLs (0.62 nm). We have found that the analysis of these CdSe-ZnS core-shell QDs is extremely challenging due to the reduced nominal thickness of the shell and to the instability of the QDs under the electron beam. Fig. 1 a) shows a HAADF-STEM image of a CdSe-ZnS core-shell QD, where a clear reduction of the intensity can be observed at the edge of the QD. This is more clearly observable in the HAADF-STEM intensity profile

shown in Fig. 1 b), obtained from the region marked with an arrow in Fig. 1 a). It should be mentioned that the intensity of the HAADF-STEM images is related to the composition of the material analysed, but the thickness of the material also has a strong effect on it. In our particular case, both Z and thickness vary simultaneously along the QD, making the analysis of the intensity not straightforward. Because of this, we are developing two methodologies to analyse the HAADF-STEM images more precisely. The first one works with the intensity variations of the image, and has the objective to distinguish the intensity fluctuations coming from the spherical shape of the QD and from the different compositions due to the existence of the shell. The second methodology works with the variation in the position of the atomic columns instead. In particular, the PPA software has been used to distinguish the atomic displacements between the core and the shell due to the lattice mismatch between both materials (12%). Our results show that both methodologies are able to prove the existence of the shell in CdSe-ZnS QDs.

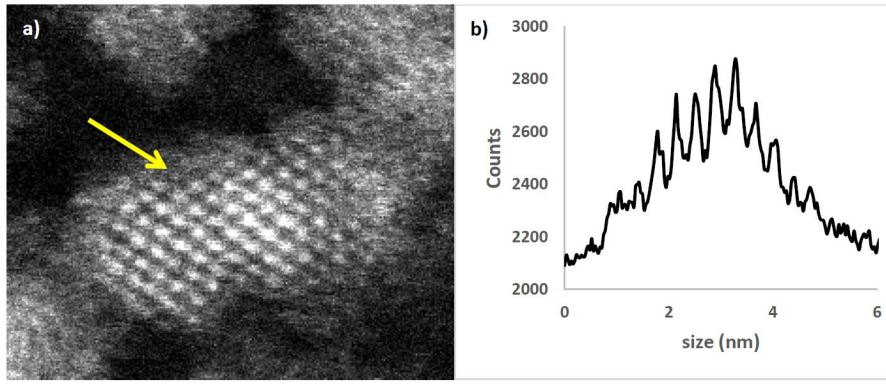

Figure 1. a) HAADF-STEM image of a CdSe-ZnS core-shell QD with a nominal shell thickness of 2 MLs; b) Intensity profile taken along the line marked by the yellow arrow in the image in a).

References
1.- Best R, Burke PJ. (2018). *Energy Policy* 118: 404-417
2.- Rekinger M *et al*. (2019). *Sol. Power Eur.* 1-32. www.solarpowereurope.org
3.- Krivenkov V *et al*. (2018). *J. Phys. Chem. C*. 122: 15761-15771
4.- Vinayakan R *et al*. (2007). *J. Phys. Chem. C.* 111: 10146-10149
5.- Chern M *et al*. (2017). *Nanoscale* 9: 16446-16458
6.- Owen JS *et al*. (2010). *J. Am. Chem. Soc.* 132: 18206-18213

Acknowlegments
National project TEC2017-86102-C2-2-R. INNANOMAT group TEP-946. Co-funding from UE. DME-SC-ICyT-UCA.

Morphology driven electronic band modulation in semiconductor core-shell nanowires

Martí-Sánchez S[1], Botifoll M[1], Oksenberg E[2], Joselevich E[2], Arbiol J[1,3]

1. Catalan Institute of Nanoscience and Nanotechnology (ICN2), CSIC and The Barcelona Institute of Science and Technology (BIST), Campus UAB, Bellaterra, 08193 Barcelona, Catalonia, Spain
2. Department of Materials and Interfaces and Chemical Research Support, Weizmann Institute of Science, Rehovt, 76100, Israel
3. ICREA, Passeig Lluís Companys 23, 08010 Barcelona, Catalonia, Spain
*Author for correspondence: sara.marti@icn2.cat

Keywords: core-shell, electronic structure, morphology, semiconductor, nanowires, strain

The improvements in VLS growth of semiconductor heterostructured nanowires towards more efficient (opto)electronic devices have allowed tailoring their properties for excellent performances. Particularly, epitaxial strain plays a key role inducing variations in carrier mobility or energy band gap, so predicting its effects at the atomic scale is essential, especially when dealing with horizontally grown arrays of nanowires as the material-substrate interface area gets highly enlarged.

In this work, we studied strain and interfaces of guided grown horizontal arrays of ZnSe@ZnTe core-shell nanowires grown into different substrates, being outstanding candidates for high performance photodetectors[1]. The core morphology, when increasing its curvature, is responsible of a complex strain minimization phenomenon which implies mirror plane bending, dividing the shell into two sections. Due to the polar nature of II-VI compounds, oppositely oriented internal electric fields are created due to the plane bending, affecting the system's electronic band alignment.

We inquire into the origin of plane bending and demonstrate how core morphologies are responsible of different device performances by calculating the band structure in different situations.

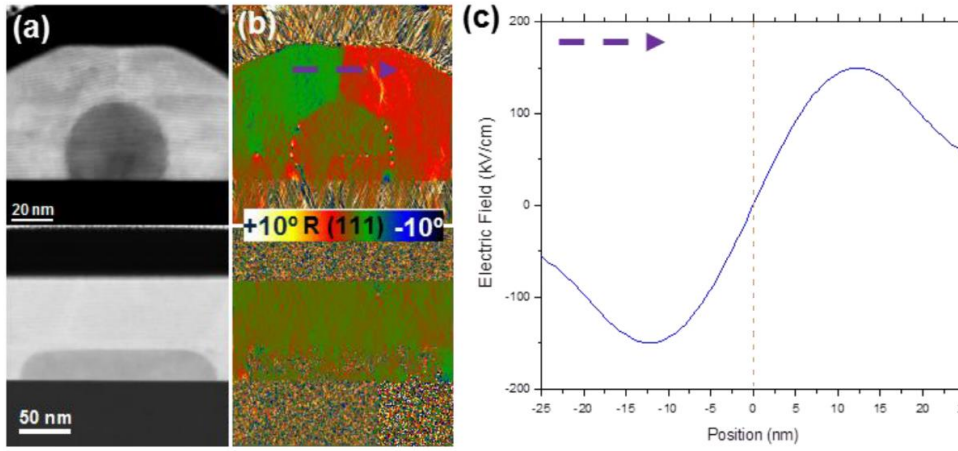

Figure 1. (a) HAADF-STEM micrographs of cylindrical and planar cored nanowires. (b) Rotation maps of (111) planes obtained through GPA for both situations (c) Dipole induced horizontal component of electric field calculated across the line marked in (b) for a cylindrical cored nanowire. An Ex-field direction switch is taking place at the domain boundary.

References

1.- Oksenberg E *et al*. (2017). *ACS Nano* 11: 6155

Formation of agglomerations in high-density multilayer InAs/GaAs quantum dot structures: the role of Sb in the capping layer

Ruiz-Marín N[1], Reyes DF[1,*], Braza V[1], Flores S[1], Gonzalo A[2], Ulloa JM[2], Ben T[1], González D[1]

1. University Research Institute on Electron Microscopy and Materials, (IMEYMAT), Universidad de Cádiz, 11510 Puerto Real, Cádiz, Spain
2. Institute for Systems based on Optoelectronics and Microtechnology (ISOM), Universidad Politécnica de Madrid, Ciudad Universitaria s/n, 28040 Madrid, Spain
*Author for correspondence: daniel.fernandez@uca.es

Keywords: III-V semiconductors, capping layers, intermediate band solar cells, quantum dots, transmission electron microscopy (TEM)

Vertically aligned (VA) InAs/GaAs quantum dots (QDs) structures with very thin spacers present an intermediate band generated by the electronic coupling that could provide numerous advantages for implementing the concept of intermediate based solar cells (IBSCs)[1]. However, the use of very small spacing layers between InAs QD layers results in poorer optical properties[2] due to the formation extended defects or even of different kind of agglomerations[3]. A possible solution is the incorporation of GaAsSb as capping layer (CL) on top of InAs QD layer since Sb acts as surfactant reducing In/Ga exchange of the QDs[4]. Furthermore, for a Sb content above 16%, the band alignment becomes type II with the holes localized outside the QD in the CL improving the carrier lifetime, which makes it very attractive to envisage the IBSC concept.

In this work, we analyze the mechanism of the formation of these agglomerations in closely stacked InAs/GaAs MQD and the effect of incorporate Sb into the CLs by up-to-date (scanning) transmission electron microscopy ((S)TEM) related-techniques. The analysis by energy dispersive X-Ray spectroscopy (EDX) mappings revealed the presence of different agglomerations in the InAs/GaAs sample (Figure 1(a,b)) with a higher In contents (Figure 1(c)). Moreover, the configuration of these agglomerations hinders the formation of a regular distribution of VA QDs, where only the first layer of InAs has a regular density of QDs and there is almost no presence of QDs in the upper layers of regions between the agglomerations. Based on our results, the agglomerations may be described between two different extreme types that are closely related to different QD configurations at the first layer. The first, called *conical-like (1)*, is related to the presence of 2 coalesced QDs in the first layer. The second one, presents a *volcano-like* shape *(4)* due to the collapse of the upper layers with a higher accumulation of In.!It is proposed that the origin of this type of agglomeration is suggested due to the formation of a quantum ring in the first layer. On the contrast, the use of GaAsSb as capping layer showed an almost complete removal of these

agglomerations with a high density of VA QD as could be observed in Figure 1(d). In fact, Sb accumulates over the QDs (Figure 1(e)) avoiding the migration of In adatoms and, therefore, the formation of In-rich agglomerations.

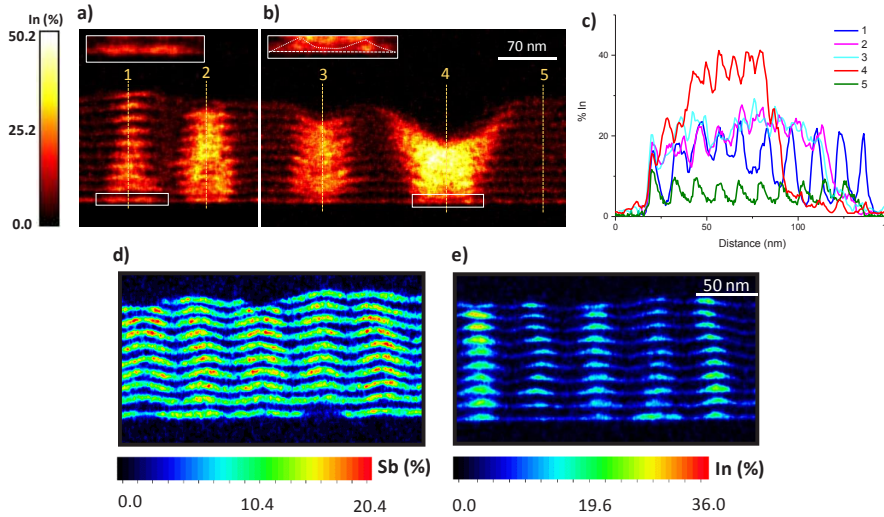

Figure 2. For InAs/GaAs sample (a,b) In mappings using EDX for different agglomerated-areas, from the conical shape (1) to the volcano shape (4) and intermediate situations (2, 3). (c) Plot of the In profiles along the growth direction for each agglomeration together to the one without agglomerations (5). For InAs/GaAsSb sample (d) In and (e) Sb mappings using EDX. EDX analyses were performed using ChemiSTEM technology in a double aberration corrected FEI Titan3 Cubed Themis operated at 200 kV.

References

1.- Luque A *et al*. (2013). *Appl. Phys. Lett.* 103: 123901
2.- Park CY *et al*. (2008). *Semicond. Sci. Technol.* 23: 085026
3.- Ng J, Missous M. (2006). *Microelectronics J.* 37: 1446
4.- Utrilla AD *et al*. (2013). *Appl. Phys. Lett.* 103: 111114

Sb and N incorporation interplay in GaAsSbN/GaAs epilayers

Braza V[1,*], Reyes DF[1], Gonzalo A[2], Ruiz N[1], Flores S[1], Utrilla AD[2], Ben T[1], Ulloa JM[2], González D[1]

1. Instituto de investigación de microscopia electrónica y materiales (IMEYMAT), Universidad de Cádiz, 11510 Puerto Real, Cádiz, Spain
2. Institute for Systems based on Optoelectronics and Microtechnology (ISOM), Universidad Politécnica de Madrid, Ciudad Universitaria s/n, 28040 Madrid, Spain
*Author for correspondence: veronica.braza@uca.es

Keywords: DBAC model, dilute nitride semiconductor, GaAsSbN, structural and optical characterization

Dilute nitride alloy systems lattice matched to GaAs are currently being extensively investigated for solar cell and photodetector applications[1,2]. Among dilute nitrides, the GaAsSbN alloy has been attracting a great attention due to the Sb surfactant effect, the possibility of an independent tuning of the electron and hole confinements, and a large range of reticular parameters that permits lattice matching to GaAs. Certainly, in comparison to the InGaAsN system, it is necessary less Sb and N contents to reach longer wavelengths, reducing the global strain in the system and the non-radiative defects associated to N diluted alloys. In the photovoltaic field, its incorporation acting as a lattice-matched sub-cell in the 1-1.2 eV energy range in multi-junction solar cells is attracting huge attention[3,4]. However, the homogeneity and composition control in GaAsSbN materials present important challenges, since there are three elements competing for the group V positions, which could produce different problems such as segregation, clustering or phase separation. These facts cause a decrease in the quality of the GaAsSbN layers, complicating the ultimate goal of obtaining high efficiency devices.!

The present work analyses the optical and compositional characteristic of a set of dilute nitride GaAsSbN alloys in the 1.0–1.16 eV energy range and lattice matched to GaAs[5]. First, taken advantage of the temperature gradient in the MBE wafer holder, we have analysed the impact of temperature on the incorporation of Sb and N species. The results from X-ray diffraction (XRD) and energy-dispersive X-ray spectroscopies (EDS) show an opposite rate of incorporation between N and Sb as we move away from the centre of the wafer (figure 1). A competitive behaviour between Sb and N in order to occupy the group-V position is observed due to the growth rate and the substrate temperature. Second, the optical properties obtained by photoluminescence, before and after annealing, are discussed in the framework of the double-band anti-crossing model. After reviewing the literature, we have found that two different sets of N energy parameters are needed to describe the optical behaviour in GaAsSbN layers depending on the growth conditions. The variation of

the incorporation of Sb and N for the different growth parameters and its effects on the PL spectra are discussed.

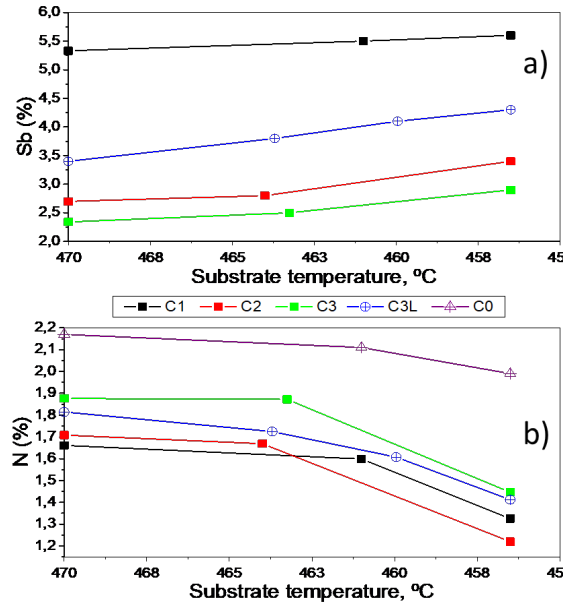

Figure 1. Plots of the average composition of a) Sb and b) N versus estimated growth substrate temperature for the studied samples.

References

1.- Erol A. (2008). Dilute III-V Nitride Semiconductors and Material Systems, vol, 105, A Erol (Ed.), Springer (Berlin, Heidelberg)
2.- O'Reilly EP *et al*. (2009). *Semicond. Sci. Technol.* 24: 033001
3.- Miyashita N *et al*. (2018). *Sol. Energy Mater. Sol. Cells* 185: 359
4.- Gonzalo A *et al*. (2019). *Sol. Energy Mater. Sol. Cells* 200: 109949
5.- Braza V *et al*. (2017). *Nanoscale Res. Lett.* 12: 356

Comparative analyses of the In exchange in the InAs /GaAs QD system during the capping process with GaAs(Sb) at different growth rates

Flores S[1,*], Braza V[1], Reyes DF[1], Stanojević L[2], Gonzalo A[2], Ruiz N[1], Ben T[1], Ulloa JM[2], González D[1]

1. University Research Institute on Electron Microscopy & Materials, (IMEYMAT), Universidad de Cádiz, 11510 Puerto Real, Cádiz, Spain
2. Institute for Systems based on Optoelectronics and Microtechnology (ISOM), Universidad Politécnica de Madrid, Ciudad Universitaria s/n, 28040 Madrid, Spain
*Author for correspondence: sara.flores@uca.es

Keywords: III-V semiconductors, capping layers, morphological and compositional distribution, quantum dots, transmission electron microscopy (TEM)

InAs/GaAs QDs grown via the Stranski–Krastanov mode have received considerable attention due to their promising properties in different fields such as solar cells, lasers, detectors, etc. However, the structural properties not only of the QDs, but also of the wetting layer (WL) are strongly affected by the nature and growth conditions of the capping layer (CL)[1]. On one hand, the QD decomposition could be greatly reduced when CLs of GaAsSb are used instead of GaAs[2]. On the other hand, the GaAs capping rate also allows kinetically controlling the QD dissolution process[3] and thus the thickness and content of the WL. However, the precise analysis of the QD/WL system after the capping process in these systems is complicated, as it requires dealing with a large number of data to provide consistent and reliable results.

In this work, we statistically compare the features of samples of 10 InAs QD layers after using CLs of GaAs at different growth rates or a GaAsSb alloy. The chemical characterization of the WL together with the measurement of the morphology of several dozens of buried InAs QDs by (S)TEM related techniques allows us to analyse statistically the QD decomposition obtained under both capping processes.

Assuming that buried QDs adopted a well-defined lenticular shape[4], the statistics of the QD volume are shown in Figure 1a) as box charts, together with the corresponding histograms. The average volumes of the buried QDs follow a clear dependence on the GaAs CL growth rate, where the slower the growth rate, the greater the decomposition of the QDs. Notably, the average QD volume increases greatly in the case of capping with GaAsSb. On the other hand, elemental energy dispersive X-Ray (EDX) analyses allows us to measure the In/Ga interchange between the QDs and the WL and point to an impoverishing of In of the WL regarding the QDs as the growth rate increases[5], though it seems that the presence of Sb intensifies it more efficiently (Figure 1b). However, taking into account the average volume of the QDs and assuming an identical QD density, the most enriched QDs are those grown using GaAs CL at 1.5

ML/s, (Figure 1c). The different mechanisms of QD dissolution that operate during the capping process under both growth conditions are discussed.

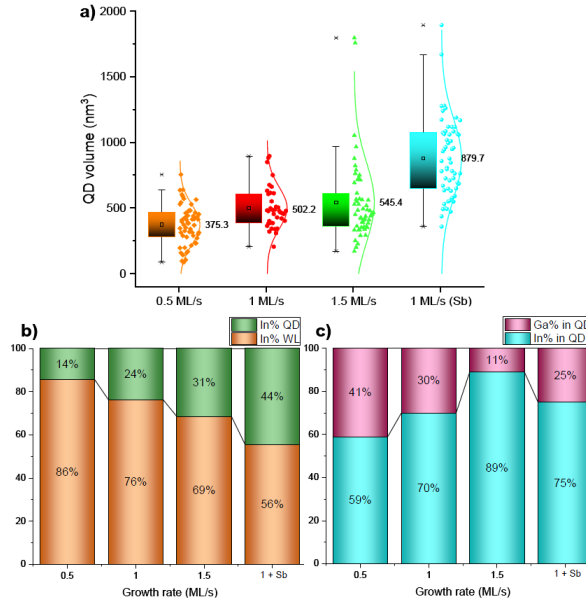

Figure 1. a) QD volume distribution of each sample displayed as a combined histogram and box representation.Normalised to percent stacked bar graph b) showing the In distribution in the QD/WLsystem and c) the averaged In content inside the QDs. (EDXanalyseswere performed using ChemiSTEM technology in a double aberration corrected FEI Titan3 Cubed Themis operated at 200 kV).59%70%89%75%41%30%11%25%0.511.52020406080100Growth rate (ML/s) Ga% in QD In% in QD1 + Sb86%76%69%56%14%24%31%44%0.511.52020406080100Growth rate (ML/s) In% QD In% WL1 + Sb375.3502.2545.4879.70.5 ML/s1 ML/s1.5 ML/s1 ML/s (Sb)0500100015002000QD volume (nm3)a)c)b)

References

1.- Gonzalez D *et al.* (2016). *Sol. Energy Mater. Sol. Cells* 145: 154
2.- Ulloa JM *et al.* (2017). *J. Appl. Phys.* 101: 081707
3.- Utrilla AD *et al.* (2018). *Appl. Surf. Sci.* 444: 260
4.- González D *et al.* (2016). *Nanotechnology* 27: 125703
5.- Gonzalez D *et al.* (2017). *Nanotechnology* 28: 425702

Synthesis and electron microscopy of tubular van der Waals heterostructures

Ballesteros B*

Catalan Institute of Nanoscience and Nanotechnology (ICN2), CSIC and The Barcelona Institute of Science and Technology (BIST); Campus UAB, Bellaterra 08193, Barcelona, Spain
*Author for correspondence: belen.ballesteros@icn2.cat

Keywords: 2D materials, heterostructures, metal halides, laser, single-walled inorganic nanotubes

Single-layered van der Waals heterostructures have attracted a great interest for both fundamental research and advanced applications.!Theoretically any layered inorganic material could roll up into a cylinder, forming inorganic nanotubes that will combine the characteristics of both 2D and 1D materials[1].

Here we present our latest results on the synthesis and electron microscopy characterisation of novel single-crystalline cylindrical van der Waals heterostructures using carbon nanotubes as templates. We have explored two synthesis approaches: melt filling[2,3] and a laser-assisted methodology[4]. The former has proven to be a highly versatile strategy, but requires the use of high temperatures for prolonged periods of time and results in a large fraction of other nanostructures in the interior of the carbon nanotubes. On the other hand, a highly selective growth of single-crystalline inorganic nanotubes has been achieved by the laser assisted approach. In addition to the high selectivity, this strategy has the advantages of being ultrafast, energy efficient and easily scalable.

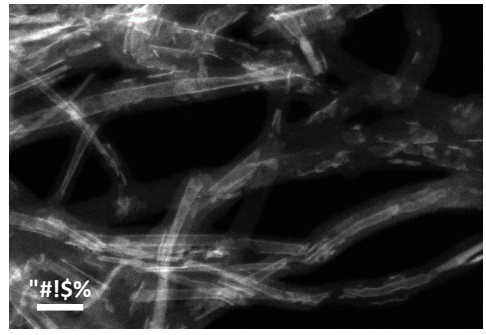

Figure 1. HAADF-STEM images of PbI_2@MWCNTs prepared by laser irradiation.

References
1.- Goldberger J *et al*. (2006). *Acc. Chem. Res.* 39: 239
2.- Cabana L *et al.* (2014). *Adv. Mater.* 26: 2016
3.- Sandoval S *et al*. (2017) *Carbon* 123: 129
4.- Sandoval S *et al.* (2018). *ACS Nano* 12: 6648

Detailed atomic structure analyses of N-doped nanodiamonds

Arenal R[1,2,3,*], Hage F[4], Ramasse Q[4], Gruen DM[5]

1. Laboratorio de Microscopías Avanzadas, Instituto de Nanociencia de Aragón, Universidad de Zaragoza, Zaragoza, Spain
2. ARAID Foundation, Zaragoza, Spain
3. Instituto de Ciencias de Materiales Aragon, CSIC-U. Zaragoza, 50009 Zaragoza, Spain
4. SuperSTEM Laboratory, Daresbury WA4 4AD, UK
5. Materials Science Division, Argonne National Laboratory, Illinois 60439, USA

*Author for correspondence: arenal@unizar.es

Keywords: nanodiamonds, STEM, EELS

Ultrananocrystalline diamond (UNCD) film is a crystalline diamond film consisting of 3-5 nm randomly oriented diamond crystallites surrounded by 0.2-0.3 nm wide grain. These films possess exemplary mechanical, electronic and optical properties[1,2]. Under normal process conditions, these UNCD films are highly electrically insulating, but they can become highly conducting when Ar is substituted in the synthesis gas with some N_2 [1,5]. In this contribution, we have revisited, using aberration corrected microscopes and combining HR(S)TEM and EELS, the structure and local composition of these n-type UNCD films[3-5].

n-type UNCD films are composed of elongated diamond nanocrystals (called nanowires (NWs)[3]), see Figure 1. The formation of these NWs is initiated when the N_2 content in the gas phase reaches about 10% in volume. From these studies, we concluded that the insulator-metal transition of these films is strongly correlated with the formation of these diamond NWs. Indeed, these NWs are enveloped by a sp^2-based carbon layer that seems to provide the conductive path for electrons[3-5]. Thus, here we will present the atomic structure studies and local EELS analyses developed on these complex films, see Figure 2[5]. These results show where the nitrogen is located into these nanostructures and provide insights into their atomic configuration. These aspects provide very important information about the role played by nitrogen in the formation of such nano-objects.

In summary, these studies elucidate crucial questions concerning the local composition (atomic configuration) of these materials. This detailed knowledge is essential for better understanding the outstanding properties of such materials as well as for shedding light on their growth mechanism.

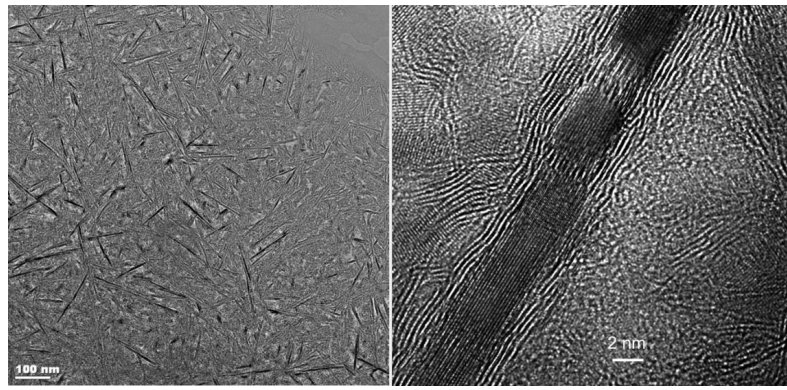

Figure 1. TEM images of N-doped UNCD materials: (left) low-magnification micrograph displaying diamond filaments; (right) HRTEM image showing a diamond nanocrystal covered by a sp^2 C sheath.

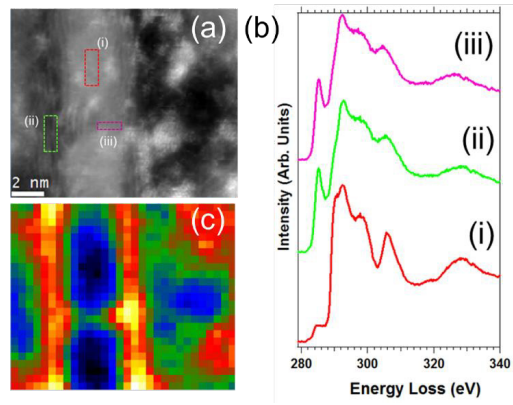

Figure 2. EELS analyses on N-doped UNCD materials: (a) STEM-EELS spectrum-image (SPIM) recorded on a nanodiamond nanostructure. (b) Three different areas have been selected from this SPIM and representative EEL spectra (C-K edge) from these regions are displayed. They correspond to: (i) middle of a NW, where sp^3 C can be detected with a small contribution of sp^2 bonded carbon from the surface of the NW; (ii) edge of the NW corresponding to sp^2 bounded C material; (iii) In one area between two diamond crystals forming the core of the NW, which is also mainly composed by sp^2 bonded carbon. (c) Map displaying the spatial distribution of sp^2 bonded carbon, obtained from the analysis of the π^* peak in the C-K edge.

References

1.- Shenderova OA, Gruen DM. (2012). UNCD: synthesis, properties & applications. William Andrew
2.- Arenal R, Review paper, to be submitted.
3.- Arenal R *et al*. (2007). *Phys. Rev.* B 75: 195431
4.- Arenal R *et al*. (2009). *Appl. Phys. Lett.* 94: 111905
5.- Arenal R *et al* (unpublished data)

Acknowledgments

Research supported by the Spanish MINECO (MAT2016-79776-P, AEI/FEDER, EU), Government of Aragon through project DGA E13_17R (FEDER, EU) and European Union H2020 programs "ESTEEM3" (823717) and Flag-ERA GATES (JTC 2017).

In situ real-time annealing of 3D ferromagnetic nanowires fabricated by focused electron beam induced deposition

Pablo-Navarro, J[1,2,*], Winkler R[3], Haberfehlner G[4], Plank H[3,4,5], Magén C[1,2,6], de Teresa JM[1,2,6]

1. Laboratorio de Microscopías Avanzadas (LMA) - Instituto de Nanociencia de Aragón (INA), Universidad de Zaragoza; Mariano Esquillor s/n, 50018 Zaragoza, Spain
2. Instituto de Ciencia de Materiales de Aragón (ICMA), Universidad de Zaragoza-CSIC; Pedro Cerbuna 12, 50009 Zaragoza, Spain
3. Christian Doppler Laboratory DEFINE, Institute of Electron Microscopy and Nanoanalysis, Graz University of Technology; Steyrergasse 17, 8010 Graz, Austria
4. Institute of Electron Microscopy and Nanoanalysis, Graz University of Technology; Steyrergasse 17, 8010 Graz, Austria
5. Graz Centre for Electron Microscopy, Steyrergasse 17, 8010 Graz, Austria
6. Departamento de Física de la Materia Condensada, Universidad de Zaragoza, 50009 Zaragoza, Spain

*Author for correspondence: javpablo@unizar.es

Keywords: composition purification, ferromagnetic nanowires, focused electron beam induced deposition, three-dimensional nanostructures, transmission electron microscopy

The fabrication of three-dimensional (3D) magnetic nanostructures is currently a central topic in nanomagnetism [1]. Ferromagnetic nanowires (NWs) are potential candidates for magnetic data storage, logic and sensing, and Focused Electron Beam Induced Deposition (FEBID) could play a crucial role in the fabrication of these architectures [2].

Most purification procedures performed by annealing experiments have been carried out in post-process conditions [3,4], being the real-time evaluation concerning the overall morphology, chemical composition and local crystallinity really limited. Here we report on the nanofabrication and purification of ultrathin 3D Fe nanowires (<50 nm in diameter) grown by FEBID using $Fe_2(CO)_9$ precursor gas. The morphological, compositional and crystallinity changes as a function of the temperature and time have been monitored in real time by *in situ* post-growth annealing under high-vacuum conditions inside a Transmission Electron Microscope, shedding light on the nanoscale processes involved in the treatment [5]. For this purpose, the live tracking of the nanowire features has been performed by Annular Dark Field imaging and Scanning Transmission Electron Microscopy in combination with Electron Energy Loss Spectroscopy, as illustrated in Figure 1. Increasing the temperature up to 700 ºC for an as-deposited homogeneous nanocrystalline nanowire with an initial metallic content of about 40 at. % Fe induces a strong phase segregation of the components with the formation of highly pure Fe metallic regions preserving the general architecture of the nanostructure. In addition, this approach provides deeper insight in the annealing basics and give the opportunity of choosing different annealing times at each

temperature depending on the changes observed or required, tailoring the nanostructures until the desired properties are achieved.

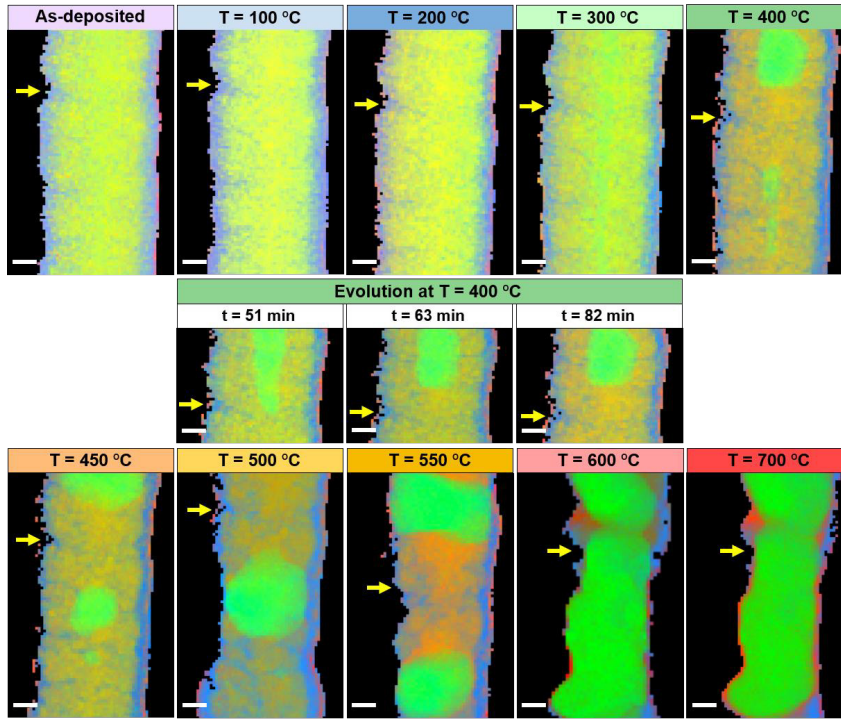

Figure 1. STEM-EELS chemical maps of the central section of an as-deposited Fe-FEBID nanowire, sequentially annealed at 100 ºC, 200 ºC, 300 ºC, 400 ºC, 450 ºC, 500 ºC, 550 ºC, 600 ºC and 700 ºC, showing the spatial distribution of Fe, O and C in green, red and blue, respectively. Yellow arrows are guides to the eye indicating the same point of the nanowire. Scale bars are 10 nm in all images.

References

1.- Fernández-Pacheco A *et al*. (2013) *Sci. Rep.* 3: 1492
2.- Pablo-Navarro J *et al*. (2017). *J. Phys. D* 50: 18LT01
3.- Pablo-Navarro J *et al*. (2018). *ACS Appl. Nano Mater.* 1: 38
4.- Martínez-Pérez MJ *et al*. (2018). *Nano Lett.* 18: 7674
5.- Pablo-Navarro J *et al*. *Acta Mater.* (in press)

High spatial resolution, low voltage and ultra-fast energy dispersive X-ray spectroscopy on a scanning electron microscope

Rosado M*, Ballesteros B

Catalan Institute of Nanoscience and Nanotechnology (ICN2), CSIC and The Barcelona Institute of Science and Technology (BIST); ICN2 building, UAB campus, Bellaterra 08193, Barcelona, Spain
*Author for correspondence: marcos.rosado@icn2.cat

Keywords: chemical analysis, EDX, electron microscopy, nanoscience, nanotechnology, SEM

Energy Dispersive X-Ray Spectroscopy (EDX) on a Scanning Electron Microscope (SEM) is a surface chemical analysis technique. When using this technique, surface means a volume of typically a few cubic microns under the real sample surface[1]. In order to acquire real surface EDX spectra, SEM operators have to work at very low electron beam energies to minimize electron beam penetration on the sample, thus reducing the analysis volume and, in turn, decreasing the signal that reaches the EDX detector. The resulting low signal spectra are not useful for semi-quantitative analysis or mapping/linescan analyses.

We have recently attached an X-Max Ultim Extreme EDX detector (Oxford Instruments) to our extreme high resolution Thermo Fisher Magellan 400L FESEM. With this detector we have been able to perform low energy EDX analysis with high energy resolution and high signal inputs, allowing us to do real surface analysis and to detect low energy peaks from elements that are typically detected at higher energies. Thanks to the high surface detecting area of the Ultim Extreme detector, mappings and linescans are done in a much shorter time than before, allowing us to acquire high signal mappings or linescans in just a few minutes, both in SEM and STEM modes, and with nanometre spatial resolution.

Here we present different analysis examples performed on our state-of-the-art EDX system, including high resolution STEM-EDX maps and linescans of multicomponent nanoparticles, such as Fe_3O_4/Mn_3O_4 nanocubes, Ni/ZnO catalyst or $AgCeO_2$ heterodimers, where features of around 10 nm can be easily resolved (see Figure 1). We will also show the capabilities for light element analysis by the detection of boron in metal-organic framework (MOF) nanosheets.

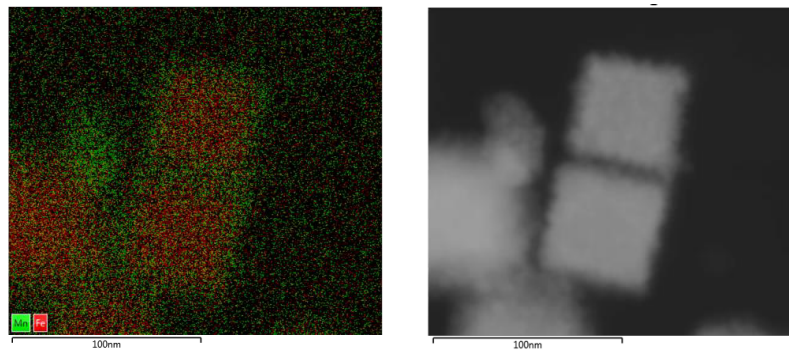

Figure 1. Fe_3O_4/Mn_3O_4 nanocubes high resolution STEM-EDX mapping. Left: STEM-EDX map showing spatial localization of Mn and Fe. Right: the corresponding SEM image.

References

1.- Goldstein J. (2003). Scanning electron microscopy and X-ray microanalysis, Springer, ISBN 978-0-306-47292-3

Acknowledgements

The authors acknowledge Alejandro Gómez and Josep Nogués (ICN2) for providing Fe_3O_4/Mn_3O_4 samples; Jordi Llorca (UPC) for providing Ni/ZnO catalyst samples; Fangchang Tan and José Giner (ICMAB) for MOF samples; and Javier Patarroyo and Víctor Puntes (ICN2) for $AgCeO_2$ heterodimer nanoparticle samples.

SESSION MS-4. INVITED SPEAKER

Direct visualization of electric and magnetic field structures in materials using differential phase contrast STEM

Gabriel Sánchez-Santolino[1,4,*], Seki T[1], Ishikawa R[1], Findlay SD[2], Kohno Y[3], Ikuhara Y[1], Shibata N[1]

1. Institute of Engineering Innovation, The University of Tokyo, Tokyo 113-8656, Japan
2. School of Physics and Astronomy, Monash University, Victoria 3800, Australia
3. Electron Optics Division, JEOL Ltd., Tokyo 196-8558, Japan
4. Present address: Department of Physics, Chalmers University of Technology, Gothenburg, Sweden
*Author for correspondence: gabriel.sanchezsantolino@chalmers.se

Keywords: aberration-corrected STEM, charge density, differential phase contrast, electric field imaging, quantitative STEM imaging

Understanding the properties of materials and devices at the atomic-scale is essential to control their functional properties. Recent advances in aberration-corrected scanning transmission electron microscopy (STEM) have made possible to directly characterize both the structure and chemistry of localized structures in materials. However, at these small scales, functionality is ultimately governed by strong confined electromagnetic fields, such as the built-in electric field at p-n junction devices. It is then a must, in order to harness the physical properties of materials and devices, to directly visualize these highly-confined fields.

Differential phase contrast (DPC) imaging in the STEM enables the study of such localized fields by exploring novel segmented detector geometries. Electrons, as charged particles, are deflected by the interactions with the electromagnetic fields present inside materials. As waves, the phase of the incident electron wave-function is shifted proportionally to the strength of the field. Therefore, if we divide the detector plane using a segmented detector, the shift of the beam and therefore the fields inside the sample can be measured by taking the difference between the signals reaching diametrically opposed segments. It is possible then to visualize local electric fields in materials, even with atomic resolution. Figure 1 shows simultaneous high angle annular dark field (HAADF) image, (b) electric field vector colour map and (c) electric

field strength map or $SrTiO_3$ along the [001] zone axis. The electric field vector and strength maps are reconstructed from quantitative DPC-STEM images. Furthermore, converting such local electric fields to charge densities it is possible to obtain the internal atomic charge density distributions, including both the positive nuclear and the negative electronic charges[4]. In this presentation, current status of atomic-resolution DPC-STEM developments and future directions will be discussed.

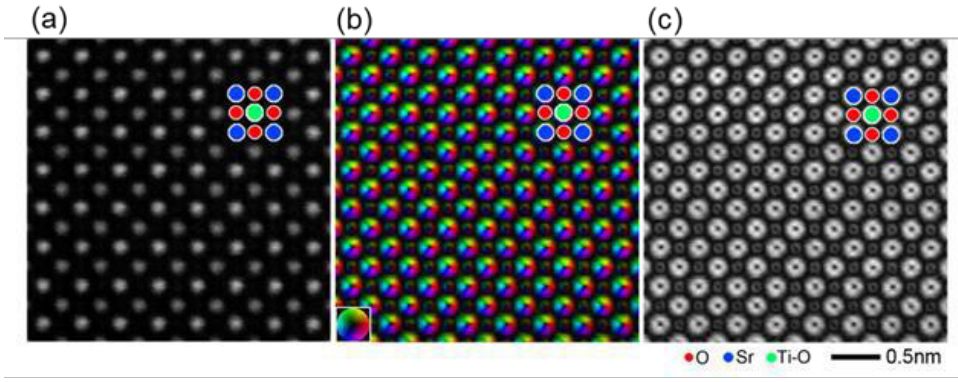

Figure 1. Atomic resolution DPC-STEM images of SrTiO3 observed from the [001] direction. (a) HAADF image. (b) Electric field vector color map and (c) electric field strength map. The inset color wheel in (b) denotes the electric field direction and strength.

References:

1.- Shibata N *et al*. (2012). Nat. Phys. 8: 6115
2.- Müller K *et al*. (2014). Nat. Commun. 5: 5653
3.- Shibata N *et al*. (2017). Nat. Commun. 8: 15631
4.- Sánchez-Santolino G *et al*. (2018). ACS Nano 12: 8875

Microstructural characterization of Ti6Al4V/Al_2O_3 joints produced using Ag-Cu sputtered coated Ti foil

Emadinia O[1,2,*], Simões S[1,2], Tavares CJ[3], Guedes A[4]

1. CEMMPRE, Centre for Mechanical Engineering, Materials and Processes, Department of Metallurgical and Materials Engineering, University of Porto, Rua Dr. Roberto Frias, 4200-465 Porto, Portugal
2. INEGI - Institute of Science and Innovation in Mechanical and Industrial Engineering, Rua. Dr. Roberto Frias, 4200-465 Porto, Portugal
3. Centre of Physics, University of Minho, Azurém, 4800-058 Guimarães, Portugal
4. Department of Mechanical Engineering, CMEMS-UMinho, University of Minho, Azurém 4800-058 Guimarães, Portugal
*Author for correspondence: omid@fe.up.pt

Keywords: alumina, interface, joining, microstructure, titanium

Advanced ceramics such as alumina are attractive materials for industrial applications where high thermal stability, wear resistance and stiffness are key requirements. A major drawback that limits the application of these materials is related to the high cost associated with the production of either large or complex shape components. This issue may be overcome by joining simple parts to produce larger components that may present more intricate geometries. Moreover, to integrate these materials into functional structures, adequate joining procedures must be developed, namely techniques able to produce sound metal/ceramic joints. This is not a straightforward process since sound metal/ceramic joints are difficult to obtain due to the different properties of metals and ceramics that generally give rise to wettability problems as well as to the formation of undesirable reaction products that hinder the performance of joints. Brazing and diffusion bonding are referred as possible routes to produce metal/ceramic joints, with the former being often considered more interesting, because it is cheaper and less demanding in terms of experimental set up[1] and the latter being more adequate to mitigate the formation of unwanted phases at the joints. This highlights the importance of understanding and controlling the microstructure evolved at the joint interfaces, which influences the mechanical properties of joints and service life of joined components.

This study evaluates the microstructure of Ti6Al4V/Al_2O_3 brazed joints using a pure titanium foil (99.99%) and a Ag-Cu sputtered coated Ti foil (Ti/Ag-Cu). Joining was conducted in a resistance furnace under a vacuum level of 8×10^{-4} Pa, with a dwelling stage of 10 minutes, at 980 and 1010 ºC with Ti/Ag-Cu and Ti foils, respectively. Afterwards, cross sections of the joints were prepared using standard metallographic techniques and analysed by Optical Microscopy (OM), Scanning Electron Microscopy (SEM), Electron Dispersive X-ray Spectroscopy (EDS) and Electron Backscatter Diffraction (EBSD).

Backscatter Electron Images (BEIs) of the interfaces obtained using the two different filler foils are presented in Figure 1. Both fillers produced sound interfaces, apparently free of pores and cracks. The interface of the joint obtained with Ti filler is composed of three distinct layers (Figure 1a and 1b): (I) fine diffusion layer of Ti_3Al phase adjacent to the alumina, (II) a thick layer of Ti(α) with large and elongated grains and (III) a layer with smaller equiaxed grains of Ti(α). Joining using Ti/Ag-Cu filler induces the formation of a more complex interface that presents a multilayered microstructure and is composed of Ti(α), Ti_2(Ag,Cu), and TiAg.

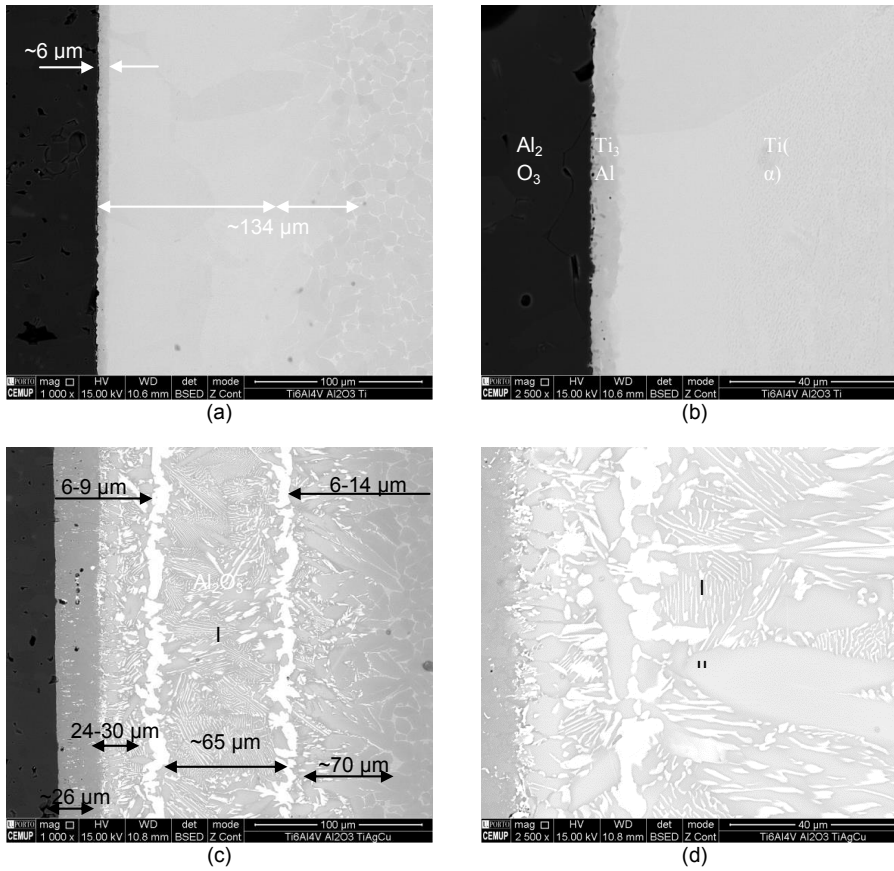

Figure 1. BEIs of Ti_6Al_4V/Al_2O_3 interfaces obtained after joining with: (a) and (b) Ti filler at 1010℃, (c) and (d) Ti/Ag-Cu filler at 980℃.

References

1.- Aldinger F, Weberruss VA (2010). Advanced ceramics and future materials: an introduction to structures, properties, technologies, methods, WILEY-VCH Verlag GmbH & KGaA: Weinheim, Germany, pp. 170-260

Acknowledgements

This work was financially supported by: Project NanoTiC-POCI-01-0145-FEDER - funded by FEDER funds through COMPETE2020 - Programa Operacional Competitividade e Internacionalização (POCI) and by national funds (PIDDAC) through FCT/MCTES.

Atomic structure and optoelectronic properties of inorganic nanotubes

Lajaunie L[1], Ramasubramaniam A[2], Serra M[3], Radovsky G[3], Panchakarla LS[4], Zak A[3,5], Calvino JJ[1], Tenne R[3], Arenal R[6,7]

1. Departamento de Ciencia de los Materiales e Ingeniería Metalúrgica y Química Inorgánica, Universidad de Cádiz, Puerto Real, Spain
2. Department of Mechanical and Industrial Engineering, University of Massachusetts Amherst, Amherst, USA
3. Department of Materials and Interfaces, Weizmann Institute, Rehovot, Israel
4. Department of Chemistry, Indian Institute of Technology Bombay, Mumbai, India
5. Faculty of Sciences, Holon Institute of Technology, Holon, Israel
6. Laboratorio de Microscopías Avanzadas, Instituto de Nanociencia de Aragón, Universidad de Zaragoza, Zaragoza, Spain
7. ARAID Foundation, Zaragoza, Spain
8. Instituto de Ciencias de Materiales de Aragón, CSIC-Univ. Zaragoza, 50009 Zaragoza, Spain
*Author for correspondence: luc.lajaunie@uca.es

Keywords: band-gap, exciton, inorganic nanotubes, STEM-EELS

In 1991, Iijima proposed that flat graphene nanoribbons transform into carbon nanotubes under appropriate conditions[1]. Following this discovery, Tenne *et al.* showed in 1992 that inorganic layered compounds can also form inorganic nanotubes (NTs)[2]. Inorganics NTs covers now a wide range of materials and structures including transition metal dichalcogenide and misfit layered compounds (MLCs)[3,4]. MLCs are materials that are composed of stacks of chemically and structurally dissimilar layers with incommensurate lattice parameters.

In this work, we report the detailed structures and chemical composition of recently synthetized[5,6] MLCs NTs elucidated by using a combination of DFT calculations and different TEM techniques including probed-corrected high-resolution scanning TEM (HR-STEM HAADF), iDPC imaging, image simulation and spatially-resolved EELS (SR-EELS).

Results obtained on quaternary chalcogenide-based misfit NTs LnS(Se)-TaS2(Se) (Ln = La, Ce, Nd, and Ho) showed that sulphur atoms were bound preferentially to lanthanum while selenium atoms were bound to tantalum[5]. Therefore, a sequence of double La-Ta and S-Se superstructure was obtained in the LaS-TaSe2 nanotubes. Results obtained on alloyed LaS-(NbxTa1-x)S2 NTs will also be presented (Figure 1)[6]. Whereas, the TaS2 in the LnS-TaS2 (Ln=lanthanide atom) compounds crystallize in the *2H* polytype, we show that, invariably MLC nanotubes prepared from 80 at% Nb content in the precursor belonged to the *1T* polytype. The characterization of a new nanotubular misfit-oxide phase, CaCoO2–CoO2 will also be discussed[7].

Finally, we also investigated the optoelectronic properties of the oxide-based MLCs nanotubes by combining monochromated low-loss spatially resolved electron energy-loss spectroscopy experiments with time-dependent hybrid density-functional theory

calculations. Experimental and calculated results independently confirm an optical gap of 1.9–2.1 eV and calculations suggest the existence of strongly bound intralayer excitons, which could allow for optoelectronic applications of these nanotubes at near-infrared to visible wavelengths.8 Likewise, excitonic properties obtained on WS2 nanotubes by using monochromated low-loss EELS will also be presented.

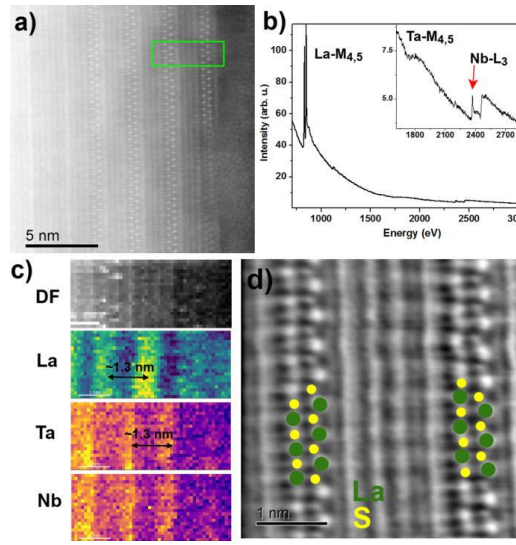

Figure 1. a) HRSTEM-ADF micrograph of a LaS-(NbxTa1-x)S2 NT. The green square highlights the area used for the acquisition of the EELS spectrum image. **b)** Corresponding EELS spectra showing the La-M4,5, Ta-M4,5 and Nb-L3 edges. **c)** (from top to bottom); dark field image acquired simultaneously with the EELS spectrum image. La, Ta and Nb chemical maps extracted from the integrated intensity of the corresponding edges. **d)** iDPC image superposed with the atomic model of the LaS sub-system.

References

1.- Iijima S. (1991). *Nature* 354 (6348): 56
2.- Tenne R *et al*. (1992). *Nature* 360 (6403): 4446
3.- Višić B *et al*. (2017). *J. Am. Chem. Soc.* 24;139 (37): 12865
4.- Serra M *et al*. (2019). *Nanoscale* 11: 8073
5.- Lajaunie L *et al*. (2017). *Inorganic Chem.* 57 (2): 747
6.- Stolovas D *et al*. (2018). *Chem Mat.* 30 (24): 8829
7.- Panchakarla LS *et al*. (2016) *ACS Nano* 27; 10 (6): 6248
8.- Lajaunie L *et al*. (2018). *Appl. Phys. Lett.* 16; 113 (3): 031102

Chemical discrimination of single atom species in a heterobinuclear Au(III)-Pd(II) complex with an hexa-aza macrocycle by advanced electron microscopy

Castillo CE, Algarra AG, Fernández-Trujillo MJ, Basallote MG, Calvino JJ, López-Haro M*

Departamento de Ciencia de los Materiales e Ingeniería Metalúrgica y Química Inorgánica, Universidad de Cádiz, Campus Rio San Pedro, 11510-Puerto Real, Cádiz.
*Authors for correspondence: miguel.lopezharo@uca.es / jose.calvino@uca.es

Keywords: chemical discrimination, HAADF-STEM, K-means clustering, single atoms

The identification of species at the level of single atoms has become crucial to understand the behaviour of novel advanced materials. In this task, modern aberration corrected microscopes are essential, given their capability to image matter with sub-Angstrom spatial resolution.

In this context, the direct visualization of single metal atoms by High Angle Annular Dark Field (HAADF) STEM is a well stablished technique.[1] However, the identification of the chemical nature of single atoms is still a challenge and only very few examples can be found by using state-of-the-art EELS or EDS spectroscopies.[2] At this respect, it is important to highlight that Egerton and Watanabe have just evidenced that such identification by spectroscopic techniques is not a trivial task because of *i)* the weak characteristic signal of a single atom, *ii)* corruption of the signal by statistical (shot) noise and *iii)* the influence of atomic displacements induced by thermal excitation under the electron beam.

To further explore the potential of HAADF STEM, in this work we have developed a novel methodology that combines very low dose imaging with smart image-denoising and image analysis techniques. In particular Principal Component Analysis (PCA) and Undecimated Wavelets transform (UWT) were used to improve the contrast of the images, and K-means clustering algorithms to visualize and identify the chemical nature of the metallic centres in a hetero-binuclear Au(III)-Pd(II) complex with an hexaaza macrocyclic ligand, of interest as precursor of nanostructured bimetallic materials.

To this end, after synthesis the complex was dissolved in acetone and 10 µL of the solution were dripped onto a lacey-carbon coated Au grid. Chemical inertness of the TEM grid was key to avoid chemical transformations of the macrocyclic complex. A FEI Titan^3 Themis 60-300 microscope operated at 200 kV was used to record 2k x 2k HAADF-STEM images of the sample using a beam current of just 7 pA, in order to avoid beam damage.

Figure 1 shows an experimental HAADF-STEM image representative of the sample after noise removal and background subtraction. The image intensities are displayed

in colour scale, with highest intensities in yellow and lowest in deep blue. Considering the origin of contrasts in HAADF-STEM images, the highest intensity areas should be assigned to locations of metallic atoms.

To isolate the pixels corresponding to the metallic entities from the background, the experimental images were analysed by the K-means clustering method, Figure 1(b). Further segmentation of the clustered images allowed us discriminating the areas corresponding to Au from those corresponding to Pd and background, Figure 1(c).

To test the reliability of the method, a simulated HAADF image of the bimetallic complex was calculated and submitted to the whole denoising, background subtraction, clustering and segmentation process, Figures 1(d,e). The comparison with the results obtained from the experimental image clearly indicates a correct assignment of the cluster numbers to Au and Pd, and validates the whole procedure.

Moreover, Au to Pd distances were measured from the segmented images and the mean value was found in good agreement with that obtained from DFT calculations.

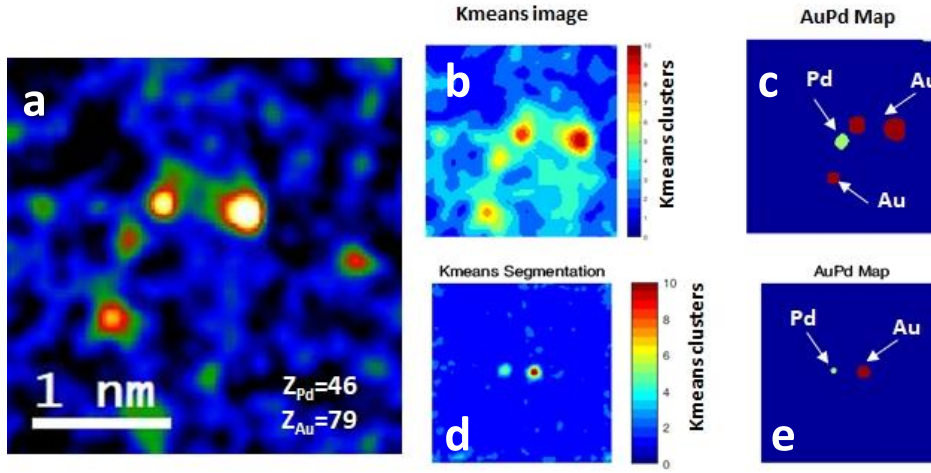

Figure 1. (a) Denoised and background subtracted HAADF-STEM image of the sample; results of the K-means analysis of (b) the experimental HAADF image and (d) the simulated image of a bimetallic cluster supported on a 10 nm thick amorphous carbon layer; (c,e) segmentation of the clustered images after assigning Au to cluster numbers comprising the highest intensities, Pd to clusters representing middle intensities and background to the clusters gathering the pixels with the lowest intensities.

References

1.- Colliex C *et al*. (2012). *Ultramicroscopy* 123: 80
2.- Suenaga K *et al*. (2012). *Nat. Photon.* 6 (8): 545

Acknowledgements

Financial support from MINECO/FEDER (MAT2017-87579-R, MAT2016-81118-P and CTQ2015-65707-C2-2-P) and Junta de Andalucía (FQM334 and FQM137) is acknowledged. Electron Microscopy data were recorded at DME SC-ICYT UCA). Carmen E. Castillo acknowledges support from the Juan de la Cierva Program (IJCI-2015-25828).

Effect of the annealing temperature on the growth and properties of (Au)-NiO_x films for electrochemical applications

Valencia LM[1,*], de la Mata M[1], Herrera M[1], Abargues R[2], Noguera J[2], Molina SI[1]

1. Departamento de Ciencia de los Materiales e Ingeniería Metalúrgica y Química Inorgánica, IMEYMAT, Facultad de Ciencias, Universidad de Cádiz, Campus Río San Pedro s/n, 11510 Puerto Real (Cádiz), Spain
2. Instituto de Ciencia de los Materiales, Universidad de Valencia, P.O. Box 22085, 46071 Valencia, Spain
*Author for correspondence: luisamaria.valencia@uca.es

Keywords: annealing temperature, Au nanoparticles, improved electrochemical performance, nickel oxide films, TEM

Nickel oxide is a p-type semiconductor of great interest due to its electrical, optical and electrochemical properties, such as wide band gap (3.6-4.0 eV), good optical transmittance in the visible region or its capability to become non-stoichiometric under certain growth conditions[1]. The applications of this transition metal oxide include batteries, LEDs, electron blockers in solar cells, Hole Transport Materials (HTMs), etc[2]. Moreover, due to its electrochemical properties, nickel oxide can be used as electrocatalyst for water splitting, in photocatalysis and as a H_2 gas sensors, among others.

One important aspect for the application of metal oxides nanomaterials is the surface characterization in terms of the crystalline phase, morphology and stoichiometry. These parameters actually rule the final performance of the nanomaterial. Metal oxide surface characteristics can be tailored by thermal annealing and has a key role on the catalytic properties. Additionally, embedding metallic nanoparticles as gold and silver inside NiOx is another strategy to improve the electro-optical properties of metal oxides[3,4], offering another degree of freedom to tune the material performance. Therefore, there is the need to correlate the effect of the thermal treatment with the material morphology, composition and structure in order to control the material properties at will. Depending on the synthesis conditions, different particle sizes may be obtained[5]; and some related properties as the conductivity and stoichiometry, change too by modifying the annealing temperature.

In this work, we analyze the role of the annealing temperature in the morphology, composition and structural properties of non-stoichiometric nickel oxide (NiO_x) films and Au NP- containing NiO_x films by means of TEM techniques. These materials are in-situ synthesized on Si substrates by spin-coating a solution of a Ni(II) and Au(0) precursors. Both, NiOx and Au NPs are synthesized simultaneously. In particular, we analyze the role of the bake temperature at 100 and 500ºC. As it can be seen in Fig. 1, the NiO_x film baked at 100 ºC is polycrystalline. The same result has been found for the film baked at 500ºC. We notice that the higher the annealing temperature, the

larger the particle size (from ~5 nm at 100ºC to ~15 nm at 500ºC) likely due to the Ostwald ripening.

Regarding the Au-NiO_x films, Fig. 2 shows a TEM micrograph where the Au particles can be observed. We have found the same trend (higher annealing temperatures result in larger particle sizes) but, surprisingly, Au NPs and NiO_x segregate apart for the higher temperature regime studies (500ºC).

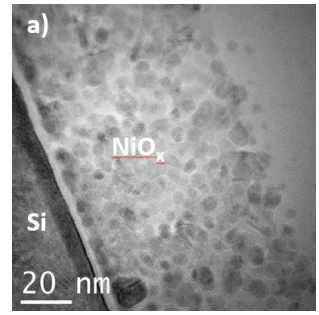

Figure 1. Characterization of NiO_x films. a) TEM image of NiO_x film growth at 100ºC.

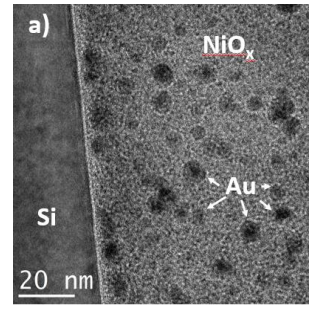

Figure 2. Characterization of Au-NiO_x films. a) TEM image of Au-NiO_x film growth at 100ºC.

References

1.- Palombari R. (2003). *J. Electroanal. Chem*. 546: 23
2.- Martínez-Gil M *et al*. (2017). *Mater. Sci. Semicond. Process.* 72: 37
3.- Ferreira FF *et al*. (2003). *Solid State Ionics* 165 (1-4): 161
4.- Fragua DM *et al*. (2015). *Adv. Mater. Interf. 2* (11): 1500156
5.- Wang CB *et al*. (2005). *Catal. Lett*. 101 (3-4): 241

Acknowledgments

National project TEC2017-86102-C2-2-R. INNANOMAT group TEP-946. Co-funding from UE. DME-SC-ICyT-UCA.

Arsenic speciation in trioctahedral clays: insights from a serpentine synthesis study

Ryan PC[1,2,*], Huertas FJ[2]

1. Geology and Environmental Studies, Middlebury College, Middlebury, Vermont 05753 USA
2. Instituto Andaluz de Ciencias de la Tierra (CSIC-University of Granada), Avda. de las Palmeras 4. 18100 Armilla (Granada), Spain
*Author for correspondence: javier.huertas@csic.es

Keywords: arsenic, mineral synthesis, serpentine, TEM-AEM

The occurrence of arsenic in minerals and amorphous solids is one of the main controls on its behavior in groundwater, sediments, soils and hydrothermal-metamorphic systems. Oxidation state ranges from As^{3-} to As^{5+}, where the low oxidation states tend to occur in sulfides and arsenides and the higher oxidations states –As^{3+}, As^{5+}– in (hydr)oxides and silicates. Previous research shows that As occurs in antigorite and chlorite as As^{3+} and As^{5+} in tetrahedral coordination. Both minerals are sources of elevated As in groundwater. Considering charge and radius of ions in silicate minerals, the occurrence of As in phyllosilicates is predictable. As(V), with a crystal radius of 0.48 Å, is a better fit in the tetrahedral sheet than Al(III) with (crystal radius of 0.53 Å), and the 0.54 Å crystal radius of As(III) is nearly identical to Al.

Paired substitutions to balance charge may include: i) As^{5+}_{tet} + As^{3+}_{tet} = 2 Si_{tet}, ii) As^{5+}_{tet} + Al^{3+}_{oct} = Si_{tet} + Mg_{oct}, and iii) As^{3+}_{tet} + Al^{3+}_{oct} = Si_{tet} + Mg_{oct}

To gain insight into the incorporation of As into trioctahedral clays, we synthesized serpentine minerals at 200 ºC over 10-day periods in alkaline solutions including varied amounts of Si, Mg, Al, As^{3+} and As^{5+}. XRD data from synthesized powders lacking Al (and with or without As) indicates 00l peaks at 7.5, 3.66, 2.47 and 1.84 Å with broad weak peaks at ~9.5 Å suggesting small amounts of interstratified or physically mixed talc-like 2:1 layers. 020 and 060 peaks indicate b-axis of 9.1 to 9.2 Å. Al-bearing solutions (with or without As) produced powders with a sharp 7.2 Å 001 as well as broad weak peaks at ~9.5 Å. FTIR data for As-bearing serpentines are consistent with those of naturally occurring chrysotile, especially peaks at 3696, 980 and 600 cm^{-1}, whereas specimens that include Al (with or without As) are more similar to spectra from naturally occuring antigorite and lizardite. TEM data from As-bearing synthesized serpentines shows tubular crystal form, consistent with XRD and FTIR evidence for chrysotile, whereas Al-bearing synthesized serpentines have hexagonal platy morphology, consistent with the presence of octahedral Al that reduces the T-O mismatch and allows planar crystals to form. As in tetrahedral sites (especially As^{5+}) preserves the mismatch and tubular crystals form.

Elemental analysis by TEM-AEM (EDX) and ICPMS of dissolved powders reveals:

- chrysotile-like crystals with up to 1 wt% As: $Mg_{2.8}(Si_{1.8}As_{0.2})O_5(OH)_4$, with average 0.2 wt% As;
- platy crystals with high Al: $(Mg_{1.8}Al_{0.7})(Si_{2.0})O_5(OH)_4$, and high Al with As^{3+} e.g. $(Mg_{2.07}Al_{0.52})(Si_{1.97}As^{3+}{}_{0.03})O_5(OH)_4$.

Syntheses indicate that either, or both, As^{3+} and As^{5+} occur in the serpentine structure. XAS confirms the presence of both As^{3+} and As^{5+} in tetrahedral sites, and indicates a preference for As^{5+} over As^{3+} in this mineral group. Low apparent octahedral content (charge <6 for $O_5(OH)_4$ unit) in many crystals is consistent with interstratified talc-like layers observed in HRTEM, i.e. interstratified 9.5 Å talc-like layers within crystals mainly comprised of 7 Å layers, including lateral transitions between these two layer types. Alkaline fluids that foster Mg clay formation also foster occurrence of the AsO_4^{3-} oxyanion, contributing to presence of tetrahedral As in Mg clays.

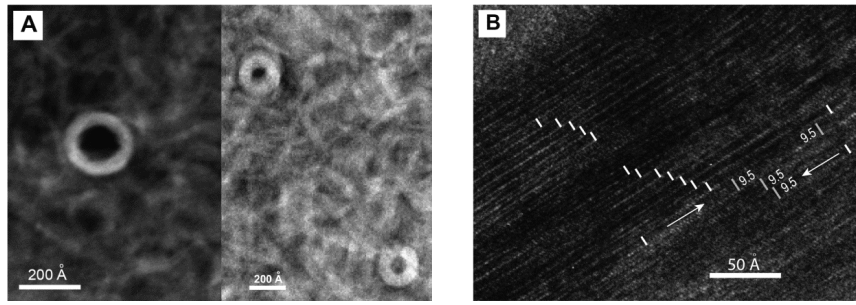

Figure 1. HRTEM images showing (A) cross-sections of vertical tubular crystals showing thickness of rolled layers as well as diameter of central hole; and (B) interstratification of 7 Å and 9.5 Å layers in a platy crystal that was oriented vertically to emphasize c-axis spacings.

Acknowledgements
Funding was provided by NSF-EAR-0959306 and the Middlebury College Undergraduate Research Office, and MINECO (CGL2014-55108-P and CGL2017-92600-EXP) with contribution of FEDER funds. XANES and EXAFS were obtained using the Inner Shell Spectroscopy beamline (8-ID) of the National Synchrotron Light Source II, a U.S. Department of Energy (DOE) Office of Science User Facility operated for the DOE Office of Science by Brookhaven National Laboratory under Contract No. DE-SC0012704. For technical expertise, the authors thank María del Mar Abad (TEM), Jody Smith (ICPMS), Lauren Pincus (XAS), and Eduardo Flores (FTIR).

(S)TEM Characterization of Plasmonic UV Nanoparticles

de la Mata M[1,*], Catalán-Gómez S[2], Nucciarelli F[1], Pau JL[2], Molina SI[1]

1. Departamento de Ciencia de los Materiales, Ing. Met. y Qca. Inorg., IMEYMAT, Universidad de Cádiz, 11510 Puerto Real, Spain.
2. Grupo de Electrónica y Semiconductores, Departamento de Física Aplicada, Universidad Autónoma de Madrid, Cantoblanco, 28049 Madrid, Spain
*Author for correspondence: maria.delamata@uca.es

Keywords: colloidal nanoparticles, single particle, (S)TEM, UV plasmonics

Plasmonics has evolved becoming an appealing branch of photonics, which provides a powerful platform for fundamental studies and manifold applications. The current knowledge on plasmonics mainly relies on noble metal nanostructures, deeply investigated through a wide variety of techniques, and whose spectral response lies within the IR-VIS range. Alternative material systems may provide plasmonic UV resonances, but, in contrast to noble metals, reports dealing with plasmonic UV materials are scarcer, and usually analyse the overall response of nanostructure ensembles[1,2]. Importantly, despite the valuable information attainable through macroscopic measurements, single particle studies are essential to understand and tune the final plasmonic response of nanostructures[3]. As several intrinsic and extrinsic parameters may influence the plasmonic performance of a given nanostructure, such as its size, shape, environment, etc., the ultimate understanding of their actual response requires from the correlation of those features at high spatial resolution. Note that these colloidal plasmonic nanoparticles may be used for the development of composites intended for additive manufacturing, where interactions between both, the polymer matrix and the neighbouring particles would play a role on the composite response. Therefore, we performed (S)TEM analyses at single UV plasmonic nanoparticles (i.e., gallium nanoparticles), rendering morphological, compositional and plasmonic detailed information on the material system.

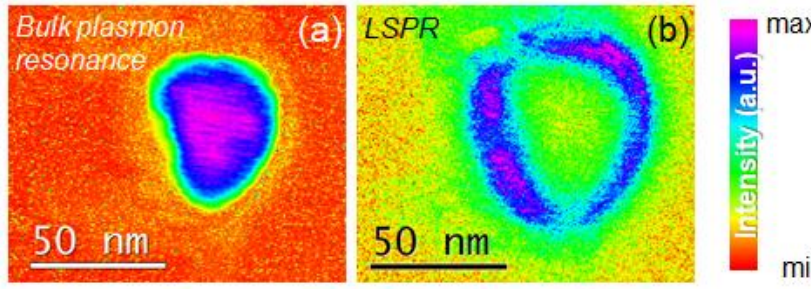

Figure 1. Plasmon resonances observed in a single UV plasmonic NP. (a) Bulk plasmon resonance, and (b) localized surface plasmon resonance (LSPR), both obtained by EELS.

References
1.- Catalán-Gómez S *et al*. (2017). *Nanotechnology* 28: 405705
2.- Losurdo M *et al*. (2016). *Nat. Mater*. 15: 995
3.- Ringe E *et al*. (2013). *Phys. Chem. Chem. Phys*. 15: 4110

Acknowledgments
TEC2017-86102-C2-2-R, PAI research group TEP-946

In-situ aberration-corrected TEM nanoindentation of silver manoparticles

Carlton CE[1,2], Aoki T[3], Zhu Y[4], Caturla MJ[5], Zorro F[6,7], Ferreira PJ[1,6,7,*]

1. Materials Science and Engineering Program, University of Texas at Austin, Austin, TX, 78712, USA
2. Samsung Semiconductor, Austin, TX, 78754, USA
3. LeRoy Eyring Center for Solid State Science, Arizona State University, Tempe, AZ 85287, USA
4. Department of Condensed Matter Physics and Materials Science, Brookhaven National Laboratory, Upton, NY, USA
5. Applied Physics Department, Alicante University, San Vicente del Raspeig, E-03690 Alicante, Spain
6. Advanced Electron Microscopy Imaging and Spectroscopy Department, International Iberian Nanotechnology Laboratory, Braga, Portugal
7. Mechanical Engineering Department and IDMEC, Instituto Superior Técnico, University of Lisbon, Av. Rovisco Pais, 1049-001 Lisboa, Portugal
   *Author for correspondence: paulo.ferreira@inl.int

Keywords: dislocations, in-situ TEM, nanoindentation, nanoparticles,

0-D nanostructures, such as single-crystalline nanoparticles exhibit intriguing size effects that provide interesting properties. Consequently, they have significant impact for applications in a wide diversity of fields, including pharmaceuticals, advanced materials, fuel cells, catalysts, as well as environmental detection and monitoring. Yet, so far, the mechanisms associated with the deformation of nanoparticles are still not well understood, especially the role played by single dislocations[1]. In this work, using in situ aberration-corrected transmission electron microscopy, we compressed silver nanoparticles with dimensions below 20 nm. Upon compression, it is was possible to observe perfect and partial dislocations within the nanoparticles. However, these dislocations were unstable and expelled towards the free surface, when the nanoindentor was removed, due to the presence of image stresses associated with the nearby surfaces. This explains why nanoparticles typically exhibit a lack of dislocations, even after significant deformation. In other words, nanoparticles appear to be self-healing, thereby ejecting dislocations towards the free surface.

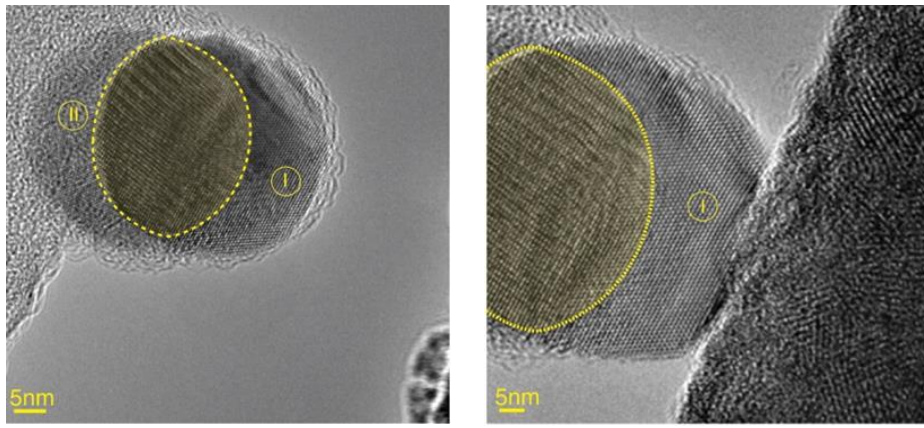

Figure 1. Aberration Corrected TEM images showing the in-situ nanoindentation process. Left, silver nanoparticles I and II before nanoindentation. Right, high magnification of the contact region, showing that upon initial contact, no dislocations are present within the nanoparticle.

References

1.- Carlton CE, Ferreira PJ. (2012). *Micron* S43: 1134

SESSION LS-1. INVITED SPEAKER

Unraveling bacterial DNA replication initiation using cryo-EM

Ernesto Arias-Palomo[1,*], Puri N[2], O'Shea Murray VL[2], Yan Q[2], Berger JM[2,*]

1. Department of Structural & Chemical Biology, Centro de Investigaciones Biológicas, CIB-CSIC 28040 Madrid, Spain
2. Department of Biophysics and Biophysical Chemistry, Johns Hopkins University School of Medicine, Baltimore, MD 21205, USA
   *Author for correspondence: earias@cib.csic.es / jmberger@jhmi.edu

Keywords: AAA+ ATPases, cryo-EM, DnaB, DnaC, DNA replication, helicase, helicase loader, structural biology

In cells, dedicated AAA+ ATPases deposit hexameric, ring-shaped helicases onto DNA to initiate chromosomal replication. However, the molecular mechanisms that control nucleotide turnover and helicase loading are not well understood. We used cryo-EM to determine sub-4 Å-resolution structures of the *E. coli* DnaB•DnaC helicase•loader complex with nucleotide in pre- and post-DNA engagement states. Our work provides the first high-resolution view of how replicative helicase loading occurs in bacteria and explains how this mechanism both parallels and diverges from homologous hexameric helicase and DNA polymerase clamp loader systems.

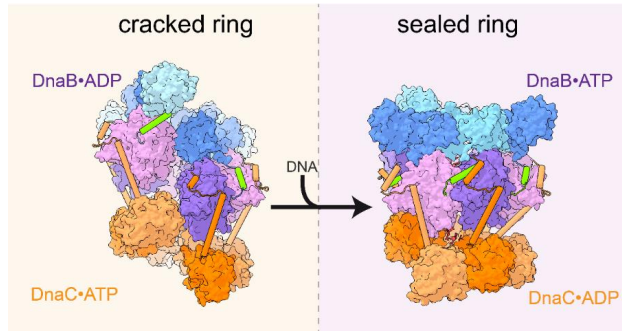

Figure 1. Cryo-EM structures of the DnaB•DnaC complex. Left, DnaC breaks the DnaB hexamer to allow DNA passage into the central channel. Right, Nucleic acid binding reseals the helicase ring that adopts a translocation-competent conformation.

Structural and functional analysis of the role of the chaperonin CCT in mTOR complex assembly

Cuéllar J[1,*], Ludlam WG[2], Tensmeyer NC[2], Aoba T[2], Dhavale M[2], Santiago C[1], Bueno-Carrasco MT[1], Mann MJ[2], Plimpton RL[2], Makaju A[3], Franklin S[3], Willardson BM[2*], Valpuesta JM[1]

1. Centro Nacional de Biotecnología, Campus de la Universidad Autónoma de Madrid, 28049 Madrid, Spain
2. Department of Chemistry and Biochemistry, Brigham Young University, Provo, UT 84602
3. Department of Internal Medicine, Nora Eccles Harrison Cardiovascular Research and Training Institute, University of Utah, Salt Lake City, UT 84112
*Author for correspondence: jcuellar@cnb.csic.es

Keywords: CCT, chaperonin, cryo-EM, folding, mLST8, mTORC, WD40, β-propeller

The mechanistic target of rapamycin (mTOR) kinase forms two multi-protein signaling complexes, mTORC1 and mTORC2, which are master regulators of cell growth, metabolism, survival and autophagy. Two of the subunits of these complexes are mLST8 and Raptor, β-propeller proteins that stabilize the mTOR kinase and recruit substrates, respectively. We have found that the eukaryotic chaperonin CCT plays a key role in mTORC assembly and signaling by folding both mLST8 and Raptor. A high resolution (4.0 Å) cryo-EM structure of the human mLST8-CCT intermediate isolated directly from cells shows mLST8 in a near-native state bound to CCT deep within the folding chamber between the two CCT rings, and interacting mainly with the disordered N- and C-termini of specific CCT subunits of both rings. These findings describe a unique function of CCT in mTORC assembly and a distinct binding site in CCT for mLST8, far from those found for similar β-propeller proteins.

Structural characterization of human tyrosine hydroxylase

Bueno-Carrasco MT[1,*], Flydal MI[2], Kleppe R[2], Martínez A[2], Valpuesta JM[1], Cuéllar J[1,*]

1. Centro Nacional de Biotecnología (CNB-CSIC), Darwin 3, 28049 Madrid, Spain
2. Department of Biomedicine, University of Bergen, Jonas Lies vei 91, N-5009 Bergen, Norway
*Author for correspondence: mtbueno@cnb.csic.es / jcuellar@cnb.csic.es

Keywords: cryo-EM, dopamine, neurodegenerative disease, regulatory domain, tyrosine hydroxylase

The aromatic amino acid hydroxylases (AAAHs) constitute a family of enzymes that catalyse the hydroxylation of aromatic amino acids using tetrahydrobiopterin (BH_4) as cofactor and di-oxygen as additional substrate[1]. Tyrosine hydroxylase (TH) is an AAAH that catalyses the conversion of L-tyrosine to L-DOPA, the first and rate-limiting step in the biosynthesis of catecholamine neurotransmitters (dopamine, noradrenaline and adrenaline). TH is a highly controlled enzyme, and the regulatory mechanisms include feed-back inhibition by catecholamine end products and phosphorylation at four different Ser/Thr sites[2]. Mutations in TH are associated with a neuropsychiatric disorder characterized by a large reduction in dopamine and noradrenaline levels, and a metabolic phenotype that is also observed in the non-motor and motor symptoms of the neurodegenerative disease Parkinson's disease (PD)[3].

TH is a 224 kDa homotetramer built by two dimers with a D2 symmetry. Each subunit consists of a regulatory ACT domain with an unstructured N-terminal tail, a catalytic domain and a C-terminal tetramerization domain. To date, only structures of truncated forms of the protein are available, such as the crystal structure of the catalytic and oligomerization domains. Improvements in the purification process have allowed to obtain an active TH with an intact N-terminus. The importance of the N-terminal region lies in its phosphorylation sites and a separated Ala-rich helical motif. These features most likely display a leading role in the regulation of TH.

In this work we have obtained a structure of the full-length human TH at 3.8 Å resolution. The data was collected in a FEI Titan Krios electron microscope equipped with a Gatan K2 Summit direct electron detector. The 3D reconstruction of the homotetramer shows a resolution range from 2.24 Å to 10 Å, corresponding to the oligomerization domains and the regulatory N-terminal domains, respectively. The lowest resolution obtained in the N-terminal tails is consistent with their high flexibility and the disordered region found between residues 1-43. This structural study shows for the first time how these regulatory domains are arranged as a dimer perpendicular to the plane formed by the four catalytic domains. This information will help complete the understanding of the hydroxylation mechanism of TH and its regulatory properties.

References

1.- Fitzpatrick PF. (1999). *Annu. Rev. Biochem.* 68: 355
2.- Dunkley PR *et al*. (2004). *J. Neurochem.* 91: 1025
3.- Willemsen MA *et al.* (2010). *Brain* 133: 1810

Mechanism of action of pyruvate carboxylase

López-Alonso JP[1,*], Gil-Cartón D[1], Lázaro M[1], Tong L[2] and Valle M[1,3]

1. Structural Biology Unit, CIC bioGUNE, Ed 800, Parque Tecnológico de Bizkaia, 48160 Derio, Spain.
2. Department of Biological Sciences, Columbia University, New York NY 10027, USA
3. Department of Biochemistry and Molecular Biology, University of the Basque Country, P. O. Box 644, 48080 Bilbao, Spain
*Author for correspondence: jplopez@cicbiogune.es

Keywords: allosteric enzyme, cryo-EM, metabolism, pyruvate carboxylase, reaction mechanism, structure

Pyruvate carboxylase is a biotin-dependent enzyme that catalyses the carboxylation of pyruvate into oxalacetate, an essential metabolite in the tricarboxylic acid cycle which is the substrate in several anabolic biosynthetic reactions as gluconeogenesis and lipogenesis. The reaction takes place in two different steps, first the ATP-mediated carboxylation of biotin followed by the transfer of the carboxyl to the pyruvate molecule. PC is a homotetramer organized in two layers, with two opposite monomers in each layer. As other biotin-dependent carboxylases it contains biotin carboxylase (BC) and carboxyltransferase (CT) domains which catalyze each consecutive reaction. In addition, PC contains a biotin-carboxyl carrier protein (BCCP) domain that transfers the product of the BC active site to the CT active site where it acts as substrate. The mechanism of action of PC requires large conformational changes with the BCCP domain traveling long distances between catalytic sites located at opposite subunits. These large movements of domains are subjected to allosteric regulation by acetyl co-enzyme A. The structure of this symmetric tetramer has been largely studied by X-ray crystallography. However, due to the flexibility of the domains that couple the two consecutive reactions, the exact mechanism of action of PC has not yet been fully resolved.

In the present study we compare the structure of *Lactococcus lactis* PC and *Listeria monocytogenes* PC. Both structures were obtained by cryoelectron microscopy at 3.5 Å resolution. This resolution allowed us to build an atomic model of the enzyme and get insights into the mechanism of action. Different classes of each protein show the BC domain opening to allow the entry and release of reaction intermediates; and the BCCP domain movement from the BC domain to the CT domain.

De novo structure determination of glutamate dehydrogenase

Lázaro M[1,*], Melero R[2], López-Alonso JP[1], Delgado S[1], Gil-Carton D[1], Valle M[1], Lisa MN[3]

1. Dept. Electron microscopy, CICBiogune, Bizkaia Science Technology Park building 800, Derio 48160, Spain
2. Centro Nacional de Biotecnología (CNB-CSIC), Darwin 3, Campus de Cantoblanco 28049, Madrid, Spain
3. Instituto de Biología Molecular y Celular de Rosario (IBR, CONICET-UNR), Ocampo y Esmeralda, S2002LRK, Rosario, Argentina
*Author for correspondence: mlazaro@cicbiogune.es

Keywords: electron microscopy, enzyme, GDH, *Mycobacterium tuberculosis*, novo model building

Mycobacterium tuberculosis (*Mtb*), the causative agent of tuberculosis, modulates its metabolism in response to nutrients available in the environment to survive within infected macrophages [1]. In *Mtb* and related species, the fate of α-ketoglutarate, a key metabolic intermediate at the crossroad between the Krebs cycle (C metabolism) and nitrogen assimilation *via* the production of glutamate, is determined by the balance of the activities of three metabolic enzymes: a glutamate dehydrogenase (GDH), an α-ketoglutarate dehydrogenase and a glutamate synthase. In turn, these enzymes are modulated by direct interaction with the regulator GarA, a molecular switch that is inactivated upon phosphorylation by the Ser/Thr protein kinase G in the presence of glutamate in the bacterial medium. Although research in this signal transduction pathway started more than ten years ago, and that some of its molecular components have been characterized and validated as drug targets for drug design against tuberculosis, a complete knowledge about the molecular basis of activity and regulation of many proteins involved is lacking. Most notably, there is no structural information concerning the enzyme GDH, the only glutamate dehydrogenase coded by *Mtb*. This enzyme uses NAD(H) to catalyze the reversible deamination of glutamate into α-ketoglutarate and is essential for the bacterial metabolic homeostasis. Composed of 180 kDa subunits, *Mtb*GDH has several predicted domains and belongs to the subfamily of high molecular weight GDHs, a subgroup exclusively found in prokaryotes and that remains structurally not characterized.

In this work we determined the structure and oligomeric state of *Ms*GDH (GDH from *M. smegmatis*, 70% sequence identity with *Mtb*GDH) by cryo-electron microscopy using the single particle technique, resulting in a 4.11Å resolution map. Only one third of the protein has homology with low molecular weight GDH. Using the diffraction data of a crystal (not resolved due to the low resolution), and the electron density map, we can assign the entire sequence using molecular replacement and coevolution analysis.

References

1.- York A. (2017). *Nat. Rev. Microbiol.* 15: 383

Structural studies of filamentous plant viruses by cryo-EM

Cuesta R.[1,*], Yuste C[2], Ponz F[2], Valle M[1]

1. Molecular Recognition and Host-Pathogen Interactions, Center for Cooperative Research in Biosciences, CIC bioGUNE, 48160 Derio, Spain
2. Center for Biotechnology and Plant Genomics (UPM-INIA), Campus Montegancedo, 28223 Madrid, Spain
*Author for correspondence: rcuesta@cicbiogune.es

Keywords: flexible filamentous virus, potyvirus, structure, viral like-particles, virus

Potyviruses constitute the second largest genus of plants viruses and cause important economic losses worldwide. Infective potyvirus virions are long flexuous filaments where coat protein (CP) subunits assemble in helical mode bound to a monopartite positive-sense single-stranded RNA [(+)ssRNA] genome. Viral like particles (VLPs) are nanostructures that resemble the structures of viruses but lack the genomic material. In this work we present the cryo-electron microscopy (cryoEM) structure of the potyvirus turnip mosaic virus (TuMV) at 5.2Å resolution and its VLPs at 7.8Å and 8.15Å resolution. TuMV virions share a very similar structure with other potyviruses and the atomic model shows a conserved fold for the CPs of flexible filamentous plant viruses. Also, several amino acids that form the RNA binding pocket are responsible of interactions within the CP and between adjacent subunits. The absence of the genomic material in the VLPs triggers structural changes in the assembly of CP subunits.

Near-atomic resolution cryo-EM structure of *Brevibacterium linens* encapsulin

Allende-Ballestero C[1,*], R. Klem[3], D. Luque[1, 2], J.J.L.M. Cornelissen[3], J.R. Castón[1,*]

1. Dept. of Structure of Macromolecules, Centro Nacional de Biotecnología (CNB-CSIC), Darwin 3, Cantoblanco. 28049 Madrid, Spain
2. Centro Nacional de Microbiología/Instituto de Salud Carlos III; Carretera de Majadahonda-Pozuelo, 28220 Madrid, Spain
3. Dept. of Biomolecular Nanotechnology Institute for Nanotechnology, University of Twente, Drienerlolaan 5, 217, Enschede, The Netherlands
*Author for correspondence: mcallende@cnb.csic.es / jrcaston@cnb.csic.es

Keywords: bacterial compartment, cryo-EM, encapsulin, HK97-like fold, nanotechnology

Encapsulins are bacterial protein macromolecular assemblies. Encapsulins from *Myxococcus xanthus* and *Thermotoga maritima* assemble into icosahedral T=3 (32-nm diameter) and T=1 (24 nm) capsid-like nanocompartments, respectively. Both particles pack proteins that protect cells from oxidative stress. The protein shell provides enzyme stability and controls the flux of substrates and products.

We used three-dimensional (3D) cryo-EM analysis to study the encapsulin from *Brevibacterium linens*, which naturally packs a dye-decolorizing peroxidase (DyP) involved in oxidative stress. DyP is assembled as a trimer of dimers, i.e., a 240 kDa hexamer [1]. The specific encapsulation mechanism of DyP is mediated by its C-terminal end, which interacts specifically with a defined region of the encapsulin inner surface. Here we determined the near-atomic resolution cryo-EM structure of *B. linens* encapsulin shell at 2.65 Å, indicating a highly porous structure. The encapsulin trimers are probably the assembly building blocks. Local resolution analysis indicated that pentameric regions are the most flexible shell regions. The polypeptide chain of encapsulin revealed a HK97-like fold, observed in the capsid proteins of tailed bacteriophages and herpesviruses. Structural alignment of encapsulins from *B. linens* with *T. maritima* showed that the hydrophobic pocket for C-terminal region of DyP binding is similar. Inter-molecular interactions of encapsulin has also been determined.

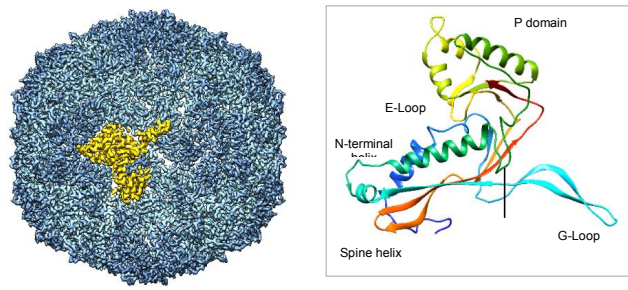

Figure 1. 3D cryo-EM map of *B. linens* encapsulin at 2.65 Å resolution. (A) Radially colored map viewed from a twofold-axis (left). Ribbon diagram represented in rainbow color (right).

References

1.- Putri RM *et al.* (2017). *ACS Nano* 11: 12796

Bacterial conjugation directly observed by optical microscopy

Carranza G, García-Cazorla Y, Arechaga I*

IBBTEC, UC-CSIC, Santander, 39011, Spain
*Author for correspondence: arechagai@unican.es

Keywords: bacterial conjugation, antibiotic resistance, optical microscopy

Bacterial conjugation is the main mechanism for horizontal gene transfer, thus contributing to the plasticity of the genome repertoire[1]. Unfortunately, this process is also the main contributor to the dissemination of antibiotic resistance genes[2]. Monitoring this process in real time can only be achieved by optical microscopy as any other technique normally used in structural biology will only provide a still picture of the process. Thus, we proceed to clone the main proteins involved in bacterial conjugation with a repertoire of fluorescent proteins integrated at the natural location in the conjugative plasmid. Then, we obtained images with state of the art optical microscopes, including STORM and SLIM. We observed that localization of these proteins in the donor cells in the absence and in the presence of recipient cells shows dramatic rearrangements upon contact between both cells. Moreover, by using at the recipient cells fluorescent constructs of SeqA, a protein that binds hemi-methylated DNA, we have found, surprisingly, that more than one event of conjugation takes place at a particular time. Altogether, these results provide new insights on the events that take place in real time during such an important biological process.

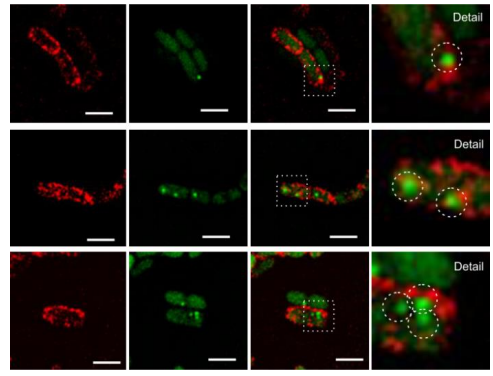

Figure 1. Bacterial conjugation monitored by optical microscopy. Donor *dam*$^{+}$ cells hosting R388_TrwBmKate2 (left panels, *red*) were mated with *dam*$^{-}$ recipient cells expressing SeqA-GFP (central panels, *green*). SeqA is a protein that only binds to hemymethylated DNA. Dam^{-} recipient cells are unable to methylate DNA and, therefore, SeqA-GFP signal will only be recorded if a strand of methylated DNA is transferred from donor to recipient cells.

References

1.- de la Cruz F, Davies J. (2000). *Trends Microbiol.* 8(3): 128
2.- Cabezón E *et al*. (2015). *FEMS Microbiol. Rev*. 39(1): 81

Understanding the mechanism of phage T7 DNA delivery to the bacterial cytoplasm

Pérez-Ruiz M, Pulido-Cid M, Cuervo A, Carrascosa JL*

Dept. Structure of Macromolecules, Spanish National Research Centre for Biotechnology (CNB), Spanish National Research Council (CSIC); Darwin 3, Madrid, E28049, Spain
*Author for correspondence: jlcarras@cnb.csic.es

Keywords: cryo-EM, DNA translocation, single-particles analyses, three-dimensional reconstruction, T7 phage

Tailed phages (Caudovirales) are the most representative and diversified class of virus group. They are traditionally divided into three families: *Myoviridae*, *Siphoviridae* and *Podoviridae*. Phage T7 belongs to the *Podoviridae* family, which presents a short and non-contractile tail, and it is an interesting system to study how these viruses puncture the double membranes of Gram-negative bacteria. It has been postulated that during infection, the internal head complex, (the core) undergoes a drastic rearrangement and their structural components exit the capsid through the tail to form a channel that traverses the bacterial membrane, in order to allow DNA translocation[1]. Here we present the near-atomic resolution cryo electron microscopy (cryo-EM) structure at 3.2 Å of this DNA translocation complex. Our results suggest that the interaction of two proteins of the core complex show a novel type of assisted folding and assembly, which correlates well with the proposed functional hypothesis.

References

1.- Hu B *et al*. (2013). *Science* 339: 576

Cryo-EM for the study of genome within the capsid of fungal dsRNA viruses

Gil-Cantero D[1,*], Luque D[2], Castón JR[1,*]

1. Dept. of Structure of Macromolecules, Centro Nacional de Biotecnología (CNB-CSIC), Darwin 3, Cantoblanco, 28049 Madrid, Spain
2. Centro Nacional de Microbiología/Instituto de Salud Carlos III, Carretera de Majadahonda-Pozuelo, 28220 Madrid, Spain
*Author for correspondence: dgil@cnb.csic.es / jrcaston@cnb.csic.es

Keywords: capsid, cryo-EM, double-strand RNA, mycovirus, viral polymerase

We are studying two fungal dsRNA viruses, Penicillium chrysogenum virus (PcV) and L-A virus of *Saccharomyces cerevisiae*. Their T=1 capsids show structural variations of the same framework, with 60 asymmetric homodimers for L-A virus and 60 monomers with a duplicated domain for PcV. PcV genome consists of four monocistronic segments that codes for the capsid protein (CP), the viral polymerase (Pol) and two proteins of unknown functions, and each segment is encapsidated separately in a similar particle. L-A genome is a single-segment dsRNA that encodes a major CP and Pol as a fusion protein with CP.

Within the capsid, fungal dsRNA viruses show a low degree of genome compaction compared to the T=1 core of reoviruses (and other dsDNA viruses), and contain one or two copies of Pol/virion. Fungal dsRNA viruses contain a single loosely packed dsRNA (~20 bp/100 nm^3 versus ~40 bp/nm^3 for reoviruses), which probably facilitates template motion. The 3D structures of PcV and L-A were determined by single-particle cryo-EM analysis at 3.7 Å resolution. The genome organization was revealed in asymmetric 3D reconstructions. Whereas PcV has an RNA layer underneath to the inner capsid surface resolved as filaments, L-A has three concentric RNA layers of filaments with a single-spooled organization. The diameter of the filaments is ~20 Å and the inter-strand spacing ~35-40 Å. Functional implications of these packaged genomes will be discussed.

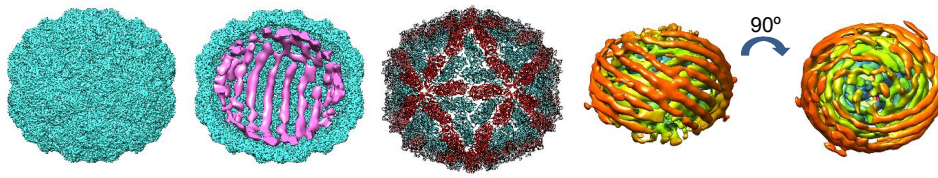

Figure 1. Structure of PcV and L-A virus. PcV capsid and outermost genome layer in contact with the capsid (left). Atomic model of the L-A capsid (centre) and packaged genome layers (right).

References

1.- Luque D *et al*. (2018). *Viruses* 10 (9): 481

Structure of a polinton-like virus, the missing link between bacteriophage and eukaryotic viruses of the PRD1-like lineage

Condezo GN[1,*], Pagarete A[2], Bratbak G[2], San Martín C[1]

1. Spanish National Centre for Biotechnology (CNB-CSIC), C/ Darwin 3, 28049 Madrid, Spain
2. Department of Biological Sciences, University of Bergen, Thormøhlensgt. 53 A/B, 5006 Bergen, Norway
*Author for correspondence: gncondezo@cnb.csic.es

Keywords: cryo-electron microscopy, double jelly roll, polinton-like virus, virus evolution, virus structure

Viruses in the PRD1-like lineage infect organisms across the evolutionary tree and build their capsids from proteins with beta-jelly rolls orthogonal to the capsid surface[1]. Polintons are large eukaryotic dsDNA transposons encoding a protein-primed DNA polymerase (POL) and a retroviral-like integrase (INT). Most of them also include a DNA-packaging ATPase and a maturation protease similar to those found in PRD1-like viruses. They also encode genes that could translate into orthogonal jelly roll proteins, suggesting that in certain conditions they could form icosahedral capsids. These observations prompted the hypothesis that Polintons may have evolved from a PRD1-like ancestor (encoding capsid proteins, POL, and ATPase), which entered a proto-eukaryotic host with a bacterial endosymbiont and acquired the protease and integrase genes by recombination with a transposon[2-3]. Subsequent evolution would have resulted in the “polintovirus” elements splitting into two different ways of life: the transposable, capsid-less integrating elements, and the bona fide viruses.

Recently, marine metagenome analyses have revealed a group of putative polinton-like viruses (PLVs) in eukaryotes. PLV genomes contain genes for single and double jelly roll proteins and a packaging ATPase, but lack the protease and integrase genes[4]. Therefore, PLVs could represent a minimal version, or a first ancestor, of the PRD1-like lineage in eukaryotic hosts. We are analyzing the structure of the only isolated virus belonging to this newly defined group: *Tetraselmis striata* virus N1 (TsV-N1)[5]. The cryo-EM capsid structure at 5.2 Å resolution corroborates the placement of TsV-N1 in the PRD1-like lineage.

References

1.- Krupovic *et al.* (2008). *Nat. Rev. Microbiol.* 6: 941
2.- Fischer *et al.* (2011). *Science* 332: 231
3.- Krupovic *et al.* (2015). *Nat. Rev. Microbiol.* 13: 105
4.- Yutin *et al.* (2015). *BMC Biol* 13: 95
5.- Pagarete *et al.* (2015) *Viruses* 7: 3937

Structural surprises in reptilian adenoviruses

Condezo GN[1], Marabini R[2], Gómez-Blanco J[1], San Martín C[1,*]

1. Centro Nacional de Biotecnología (CNB-CSIC), Madrid, Spain
2. Escuela Politécnica Superior, Universidad Autónoma de Madrid, Madrid, Spain
*Author for correspondence: carmen@cnb.csic.es

Keywords: adenovirus, capsid stability, complex viruses, minor coat proteins, virus structure

Adenoviruses (AdV) are among the most complex of the non-enveloped, icosahedral viruses. They are one of the best characterized members of the PRD1-AdV lineage, and therefore a paradigm for understanding assembly of much more complex dsDNA viruses such as African swine fever virus or mimivirus. Recombinant human AdV (HAdV) are widely used as vehicles for gene transfer, oncolysis and vaccination. The HAdV particle is composed of more than ten different proteins plus the 35 kbp dsDNA genome, totaling a mass of 150 MDa for the ~95 nm, pseudoT=25 icosahedral virion. Each capsid facet has 12 trimers of the major coat protein, hexon. At each vertex, five penton base subunits form the penton base, from which a trimeric fiber projects. Minor coat proteins IIIa, VI and VIII on the inner capsid surface, and IX on the outer surface, complete the intricate network of interactions required for capsid assembly and stabilization.

Little is known about the basic biology of non-human AdV, which have been proposed as alternative vectors to solve issues posed by preexisting immunity to HAdV. We present here the cryo-EM structure of a lizard atadenovirus, LAdV-2, at 3.4 Å resolution. This is the first high resolution structure of an AdV with non-mammalian host, and of an AdV not belonging to the Mastadenovirus genus. Atadenovirus capsids contain genus specific proteins LH3, p32k, and LH2, and are more thermostable than the more studied human AdV. We find a large conformational difference in the internal vertex protein IIIa between mast- and atadenoviruses, induced by the presence of an extended polypeptide in the region. This polypeptide, as well as α-helical clusters located beneath the icosahedral facet, likely correspond to proteins LH2 and p32k. The external genus specific protein LH3, with a trimeric β-helix fold typical of bacteriophage host attachment proteins, contacts the hexon shell surface via a triskelion structure identical to that used by protein IX in human AdV, revealing a conserved capsid binding motif and a possible gene duplication event. Altogether, this work shows how the network of minor coat proteins differs between AdV genera and relates to virus evolution and capsid stability properties.

Acknowledgments
Work supported by grants BFU2016-74868-P from the Spanish Agencia Estatal de Investigación, co-funded by the European Regional Development Fund; as well as BFU2013-41249-P and the Spanish Adenovirus Network (AdenoNet, BIO2015-68990-REDT) from the Ministerio de Economía y

Competitividad of Spain. We thank S. Chen (MRC-LMB, Cambridge) and F. de Haas (FEI) for cryo-EM data collection, and the EU-INSTRUCT I2PC for data processing.

SESSION LS-3. INVITED SPEAKER

Bringing light onto hidden complex interactions: microscopy as a tool to study sexual reproduction in trees

Losada, JM*, Lora J, Alcaraz ML, Hormaza JI

Instituto de Hortofruticultura Subtropical y Mediterránea La Mayora IHSM-CSIC-UMA. Avda Dr. Wienberg s/n. 29750 Algarrobo-Costa, Málaga, Spain
*Author for correspondence: juan.losada@csic.es

Keywords: compatibility, embryo, flower, gametes, pistil, pollen, seed development

A common feature of the sexual reproductive phase of angiosperms is the elongation of a single cell (pollen grain, the male counterpart) within a complex multicellular tissue that corresponds with the female part, the pistil. From the landing place of the pollen grains in the stigma to fertilization in the ovary, most events occur microscopically. However, in spite of the conservation of those events across plant taxa, flowering plants have developed a vast diversity of strategies to achieve double fertilization. Microscopy methods have been shown as a powerful tool to study the intricate interaction that occurs between the male and the female counterparts. Since fertilization is the ultimate condition for seed development and fruit set, the study of the progamic phase (from pollination to fertilization) is highly relevant to ensure food production.

Fruit trees offer an excellent model in which to study plant reproductive interactions, given their presence in most lineages of flowering plants, the possibility of asexual clonal propagation, and the usually “slow” timeframe from pollination to fertilization compared to most annual plant species.

In this work, we review the diversity of different microscopy methods that we use to study reproductive biology in temperate and tropical woody perennial fruit crops. In addition to the latest advances in highly sophisticated microscopy methods, we discuss how a proper combination of modern and traditional image capture, and

further analysis, can be highly efficient to study tree sexual reproduction, thus enlightening the obscure cellular interactions that take place during the reproductive phase.

It's not easy being green – Electron microscopy techniques for the study of moss

Sousa AL[1*], Pereira SG[2,3], Bonucci S[1], Becker JD[3], Bettencourt-Dias M[2], Tranfield EM[1]

1. Electron Microscopy Facility, Fundação Calouste Gulbenkian - Instituto Gulbenkian de Ciência, Rua Quinta Grande 6, 2780-156, Oeiras, Portugal
2. Cell Cycle Regulation, Fundação Calouste Gulbenkian - Instituto Gulbenkian de Ciência, Rua Quinta Grande 6, 2780-156, Oeiras, Portugal
3. Plant Genomics, Fundação Calouste Gulbenkian - Instituto Gulbenkian de Ciência, Rua Quinta Grande 6, 2780-156, Oeiras, Portugal
*Author for correspondence: alsousa@ign.gulbenkian.es

Keywords: chemical fixation, correlative light-electron microscopy, electron microscopy, high-pressure freezing - freeze substitution, *Physcomitrella patens*

Biological electron microscopy (EM) is a powerful technique for the study of many organisms, including plants. In fact, it is an irreplaceable technique for the ultrastructural descriptions of the features that compose living organisms.

Although important, EM is a technique that needs considerable processing methods before being able to visualize the samples under the electron beam. All the protocols are technically demanding and most of the times troublesome to optimize. There is the potential to unintentionally introduce artifacts that can have a large impact on the final ultrastructural observation. This problem is even more pronounced when it comes to processing plant samples.

Plant cells have a distinctive feature, the cell wall, composed of cellulose[1]. The cell wall provides strength and rigidity to plant cells, and consists of several layers that gives protection against mechanical stress. These intrinsic characteristics also function as a barrier for fixatives and impose an additional challenge for the accurate preservation of the structures contained within.

The objective of this study was to characterize the locomotory apparatus that assembles in the motile sperm cells of the moss *Physcomitrella patens.* These sperm cells develop inside an antheridium which is located at the tip of the gametophore, a complex structure composed of leaves, rhizoids and both sexual organs (antheridia and archegonia)[2].

To be able to resolve the complex ultrastructure of the *P. patens* sperm cells, the investigation focused on the optimization and integration of three electron microscopy techniques that are capable of preserving the structures of interest. The three types of techniques were: chemical fixation, high-pressure freezing–freeze substitution and correlative light-electron microscopy.

Chemical fixation allowed us to carefully identify the different stages of development and to do the initial ultrastructural characterization. Different ways to dissect the

antheridia and several fixative combinations were tested in the optimization process which allowed us to describe the main structures and events occurring during spermatogenesis.

High-pressure freezing – freeze substitution was used to avoid the artifacts induced by chemical fixation and allow a more accurate and detailed ultrastructural characterization of each structure. Furthermore, electron tomography was applied in conjunction with this technique to better describe the structures in three-dimensions.

Correlative light-electron microscopy (CLEM), was used to elucidate the protein composition of the sperm cells' locomotory apparatus. After all the work developed for the description of the structure, CLEM allowed us to validate some of the compositional results obtained by light microscopy and associate them to the structures observed by electron microscopy.

In summary, the three different techniques individually helped us to characterize aspects of the locomotory apparatus of *Physcomitrella patens'* sperm cells. Combined, these complementary approaches gave us a much broader and interconnected structural understanding of the conserved and unique structures assembled during *P. patens* spermatogenesis.

References

1.- Keegstra K. (2010). *Plant Physiol.* 154: 483
2.- Prigge MJ, Bezanilla M. (2010). *Development* 137: 3535

Ultrastructural analysis of carotenoid storage cells in aril of *Bixa orellana* L.

Louro, RP[1,2*], Freitas, YG[1,3], Santiago, LJM[3]

1. Laboratório de Ultraestrutura Vegetal, Departamento de Botânica, Instituto de Biologia, Universidade Federal do Rio de Janeiro,Bloco A Avenida Carlos Chagas Filho, 373. Centro de Ciências da Saúde (CCS), Cidade Universitária, Rio de Janeiro, RJ. Brazil, CEP: 21941-902
2. Centro Nacional de Biologia Estrutural e Bioimagem, Unidade de Microscopia Avançada, Bloco M, Unidade 3. Avenida Carlos Chagas Filho, 373. Centro de Ciências da Saúde (CCS), Cidade Universitária, Rio de Janeiro, RJ. Brazil
3. Laboratório de Biodiversidade e Biotecnologia, Departamento de Botânica, Instituto de Biociências, Universidade Federal do Estado do Rio de Janeiro, Rio de Janeiro, Av. Pasteur 458, S. 301, Urca, Rio de Janeiro, RJ. Brazil CEP: 22290-240
*Author for correspondence: louro@biologia.ufrj.br

Keywords: aril, *Bixa orellana*, confocal, FIB-SEM, seed

Bixa orellana L. (Bixaceae), also known as urucum in Brazil, is a native shrub of Central and South America (1) cultivated in tropical areas worldwide. The aril of urucum seeds accumulate the carotenoids bixin and norbixin, important pigments, which are utilized in the food and pharmaceutical industries. These pigments are stored in specialized cells denominated carotenoid storage cells – CSC (2). Studies have been carried out on chemical and deposition of these compounds (2,3) and seed coats and endosperm cells (4,5). However, the cellular biology on seed development in CSCs remains poorly known with relation to carotenoids synthesis. With this purpose, in this study the aril of the urucum seeds will be analyzed on transmission electron microscopy, focused ion beam-scanning electron microscope (FIB-SEM) and confocal microscopy. Seeds were fixed with 4% PA, 25% GA in 1.25% Pipes buffer, pH = 7.3, post-fixed with 1 % osmium tetroxide, dehydrated in acetone series and embedded in Spurr's resin or observed in natural conditions. For the studies in TEM, samples were examined with a Morgagni 286 transmission microscope, the tomographic datasets were obtained using the ‘‘slice and view’’ technique using a Zeiss Auriga 40 dual beam microscope and the fluorescence analyses was obtained in Zeiss Elyra confocal microscope. The results demonstrated that the aril was formed by an outer epidermal cell layer with large specialized cells (CSC) (Figs 1. A and B). The confocal analysis demonstrated that the content of these cells was mainly autofluorescence between 400 - 440 nm (Fig 1. C) which corresponded to bixin, localized in both, cytoplasm and vacuole. The ultrastructural analyses (Figs 1. D, E and F) evidenced that the formation of these pigments occurs inside of the chromoplast. These substances were transported outside of the chromoplast and may fused one to each other, inside or outside of the chromoplast, forming a larger electron dense structure widely dispersed in the cytoplasm. During the formation of CSCs, the pigments are transported from de cytoplasm towards the vacuole, passing through the tonoplast, being storage in the central region of the vacuole. Three different deposition

types can be seen in the vacuole, small droplets highly electron dense, large droplets electron dense and a crystalline structure. Studies are still necessary to understand the biological processes involved in the formation and targeting of the pigments, as well as to identify these different deposits found in the vacuole.

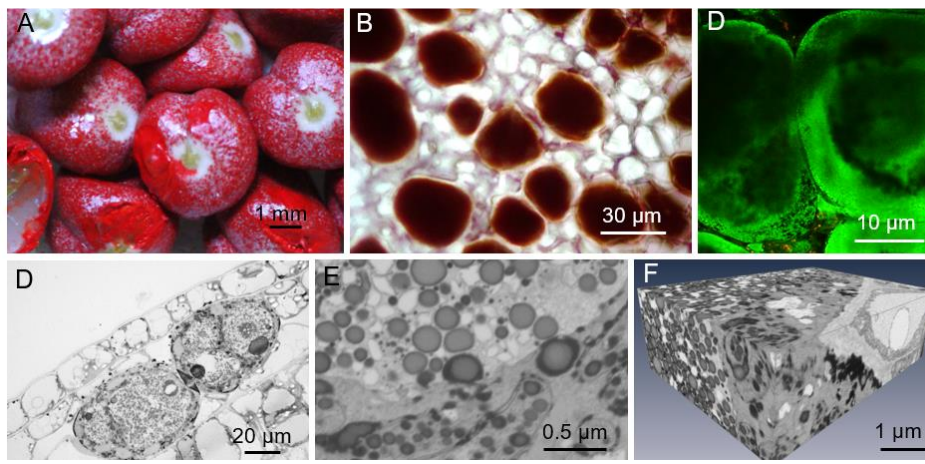

Figure 1. Characterization of *Bixa orellana* L. seed. A, Detail of the seed. B, paradermic view of the aril showing the carotenoid storage cell (CSC). C, paradermic view observed in confocal microscope. D, E, TEM micrograph of carotenoid storage cells. F, 3D model obtained in FIB-SEM microscope.

References

1.- Venugopalan A *et al*. (2011). *Ind. J. Fund. Appl. Life Sci.* 1: 9
2.- Louro RP, Santiago LJM. (2015). *Protoplasma* 253 (1): 77
3.- Scotter MJ *et al*. (1998). *J. Agr. Food Chem.* 46: 1031
4.- Amaral LIV *et al*. (2001). *Acta Bot. Bras.* 15: 125
5.- Amaral LIV *et al*. (2009). *Trees* 23: 287

Developmental analysis of glutathione reductase localization in the olive (*Olea europaea* L.) seed tissues

Lima-Cabello E, Soria A, Jiménez-López JC, Alché JD*

Dept. Biochemistry, Cell & Molecular Biology of Plants, Estación Experimental del Zaidín, Spanish National Research Council (CSIC), C/ Profesor Albareda 1, Granada 18008, Spain
*Author for correspondence: juandedios.alche@eez.csic.es

Keywords: antioxidant, glutathione reductase, immunolocalization, olive, seed, signalling

The olive seed is a promising byproduct generated by the olive oil related industries, with increasing interest because of its nutritional value and potential nutraceutical properties. Knowledge concerning the antioxidant capacity of this new alimentary material is scarce. Moreover, oxidative homeostasis and signalling involved in physiological processes such as development, dormancy and germination in the olive seed are also unknown.

Glutathione reductase (GR, EC 1.8.1.7) catalyses the reduction of the oxidized (GSSG) to the reduced form of glutathione (GSH), of paramount importance in maintaining control of oxidative stress and a reducing environment within the cell.

Considering recent information gained through molecular-genetic studies, the current work presents an overview of the cellular localization of GR protein in olive seeds of the 'Picual' and 'Arbequina' cultivars, which will point out unexplored aspects in the current context for future studies.

Olive fruits at three developmental stages (green, veraison and mature fruits) were collected, and the endocarps (stones) separated from the mesocarps + epicarps (pulp) with either a knife or a de-stoning device. The seeds were carefully dissected into two parts: on the one hand the seed coat and the endosperm were treated together, on the other hand the embryo was carefully excised. The plant materials were fixed with 4 % (w/v) paraformaldehyde and 0.2 % (v/v) glutaraldehyde in 0.1 M cacodylate buffer (pH 7.2) for 2 h at 4 °C. Samples were dehydrated in ethanol series and embedded in Unicryl resin at −20°C using ultraviolet light. Semithin (1µm) sections were obtained with a Reichert-Jung Ultracut E microtome using a glass knife. Sections were placed on Biobond-coated slides and used for cytochemical and immunohistochemical staining. For histological observations, sections were stained with a mixture of basic dyes [0.05% (w/v) methylene blue and 0.05% (w/v) toluidine blue]. For immmunolocalization, semithin sections were sequentially treated with a blocking solution [5% (w/v) bovine serum albumin, 0.1% (v/v) Tween 20 in phosphate-buffered saline], a diluted (1:50) solution of the anti-GR (AS06181, Agrisera) antiserum in blocking solution, a 1:1000 solution of the secondary antibody (Alexa Fluor 488 goat anti-rabbit IgG, ThermoFisher). DAPI sections were stained with 4µM DAPI for 15

minutes. The glass slides were washed in a 1x phosphate buffer saline (PBS) solution for 5 minutes. Negative control sections were treated as above but omitting the anti-GR antibody. Sections were examined with a Nikon Eclipse Ti inverted epifluorescence microscope equipped with a Cool LED epifluorescence system and a TIS-DFK-72AUCO2 camera. Transmitted light images were captured using Nomarski optics.

The endosperm of the olive seed showed conspicuous developmental changes as regard to the organization and quantity of the oil bodies (OBs)/protein bodies (PBs). Equivalent changes were also detected in the embryo tissues. Moreover, the presence of differentially stained PBs was detected in both tissues. No differences were found between the 'Picual' and 'Arbequina' cultivars. Immunolocalization studies using the anti-GR primary antibody yielded an intense fluorescence specifically located in the PBs present in the embryo at the early developmental stages. On the contrary, the endosperm only showed a low basal fluorescent signal with no developmental changes. Labelling of the negative controls processed by omitting the primary antibody was negligible. The observed changes were quantified in terms of fluorescence density. Such changes suggest a relevant role for this enzyme in redox metabolism and signalling events of the olive seed, without discarding the possible generation of applications for the agri-food industries.

Acknowledgments

This work was supported by ERDF con financed research projects BFU-2016-77243-P, RTC-2015-4181-2 and RTC-2017-6654-2.

Localization of Seed Storage Proteins (SSPs) in seeds of olive and nuts of agricultural/alimentary interest

M'rani-Alaoui M, Zafra A, Lima-Cabello E, Jiménez-López JC, Alché JD*

Dept. Biochemistry, Cell & Molecular Biology of Plants, Estación Experimental del Zaidín, Spanish National Research Council (CSIC), C/ Profesor Albareda 1, Granada 18008, Spain
*Author for correspondence: juandedios.alche@eez.csic.es

Keywords: ß-conglutins, cotyledon, endosperm, histology, olive, oil bodies, protein bodies, radicle, seed, seed storage proteins, SSP, testa

Olive oil production is an important economic engine in the Mediterranean area. Olive oil is obtained mainly by mechanical processes, by using the whole fruit as the primary raw material. However, the olive seed is also becoming an interesting emerging material itself when obtained after alternative processing of the olive fruit. The olive seed is used for the production of a differential oil and a unique flour among other bioactive products, with increasing uses and applications in cosmetics, nutrition and health. Other seeds of alimentary interest include almond, walnut, cashew, pistachio, hazelnuts, chestnuts and others.

Accumulation of seed storage proteins of the 7S-type (ß-conglutins) in the seed tissues has been assessed by molecular and biochemical methods in several plants. These proteins represent hallmarks of seed development, as well as important protein components with broad nutritional and even nutraceutical properties. Moreover, they have been described as important food allergens.

In the present work, detailed subcellular localization of 7S proteins in the endosperm of a wide panel of nuts (and in the olive seed as a comparison) is described. For this purpose, samples of mature olive seeds of the Picual cultivar, and a wide panel of commercial crude nuts were processed for both LM/TEM immunolocalization of 7S proteins. Samples were fixed in a mix of paraformaldehyde/glutaraldehyde, and embedded in Unicryl resin (BBinternational) at low temperature. Immunolocalication of ß-conglutins was performed on ultrathin sections (70 nm) obtained using a Reichert-Jung ultramicrotome and picked up using 200 mesh nickel grids coated with formvar. The grids were then sequentially treated with a blocking solution (5% (w/v) bovine serum albumin, 0.1% (v/v) Tween 20 in phosphate-buffered saline), a diluted (1:100) solution of an anti-7S antiserum (custom made antibody) in blocking solution, a 1:1000 solution of the secondary antibody (goat anti-rabbit IgG:30 nm gold, BBInternational), and finally contrasted using a 5% (w/v) uranyl acetate alternative solution (Ted Pella INC. CA) and observed in a JEM-1011 (JEOL) transmission electron microscope. Negative control sections were treated as above but using preimmune serum instead

of the anti-conglutin antiserum. Morphometric measurements were performed using the UTHSCSA ImageTool (version 3.00 for Windows) software.

Immunolocalization studies using the anti-ß-conglutin primary antibody yielded an intense labelling by gold particles specifically located in the protein bodies present in the endosperm of most of the nuts analysed, and in the olive seed, independently of the different histological characteristics of the different materials. Labelling in the lipid bodies, any other cell structures (cell wall, nucleus, testa) and in the negative controls processed by either omitting the primary antibody or using the pre-immune serum was negligible.

The results indicate a common distribution of the protein, likely indicating similar functions in the different seeds. They also confirm cross-reactivity of the antibody, and provide clues regarding the differential quantitative presence of the protein in the nuts analysed.

Acknowledgements

This work was supported by ERDF con financed research projects BFU-2016-77243-P, RTC-2015-4181-2 and RTC-2017-6654-2.

What's a protein like you doing in a place like this? Localization of a bacterial group II intron encoded protein in *Arabidopsis thaliana* protoplasts

Nisa-Martínez R[1], Jiménez-Zurdo JI[1], Frugier F[2], Crespi M[2] and Toro N[1,*]

1. Estación Experimental del Zaidín (Consejo Superior de Investigaciones Científicas), C/ Profesor Albareda 1,18008 Granada, Spain
2. Institut de Sciences des Plantes Paris-Saclay, Rue de Noetzlin-Plateau du Moulon Bâtiment 630, 91190 Gif-sur-Yvette, France
*Author for correspondence: ntoro@eez.csic.es

Key Words: *Arabidopsis*, group II intron, maturase, nuclear speckles, nucleolus, nucleus, protoplasts, reverse transcriptase, spliceosome

Group II introns are large catalytic ribozymes[1] and mobile retroelements that were initially identified in the mitochondrial and chloroplast genomes of lower eukaryotes and plants, but were subsequently found in bacteria and archaea[2]. Group II introns splice via a lariat intermediate, a similar mechanism used by spliceosomal introns[3]. Whereas intron excision from eukaryotic mRNA requires a set of host-cell snRNA molecules and proteins, a single maturase protein, encoded within intron domain IV is enough to assist the appropriate folding and excision of group II introns *in vivo*[4].

It is thought that both nuclear spliceosomal introns and some components of the telomerase and LINE elements evolved from mobile group II introns[5]. According to this hypothesis, group II introns originated in bacteria and invaded the nucleus of a primitive eukaryote, possibly from the alphaproteobacterial progenitor of the mitochondria; they were then fragmented to form the spliceosome[6]. Furthermore, it has been suggested that the spread of group II introns created a strong selective pressure, triggering compartmentalization of the nucleus and cytoplasm and their decay into spliceosomal introns[7].

RmInt1 is a mobile group II intron initially identified in the nitrogen-fixing endosymbiotic bacterium *Sinorhizobium meliloti* that encodes a Reverse Transcriptase-maturase (Intron Encoded Protein, IEP) [8]. We have investigated the subcellular localization patterns of the RmInt1 IEP in *Arabidopsis thaliana* protoplasts upon transient expression of translational fusions of the full-length protein and several mutant variants to the reporter EGFP (Figure 1) [9]. Following the expression of these constructs, we found that the full-length IEP was localized exclusively in the nucleolus, whereas the maturase domain alone targeted EGFP to nuclear speckles. In conclusion, the distribution of the bacterial RmInt1 IEP in plant cells protoplasts suggests that the compartmentalization of eukaryotic cells into nucleus and cytoplasm does not prevent group II intron invasion of the host genome, but it may control proliferation of the intron. The trafficking of the IEP between the nucleolus and the

speckles upon maturase inactivation is consistent with the hypothesis that the spliceosomal machinery evolved from group II introns.

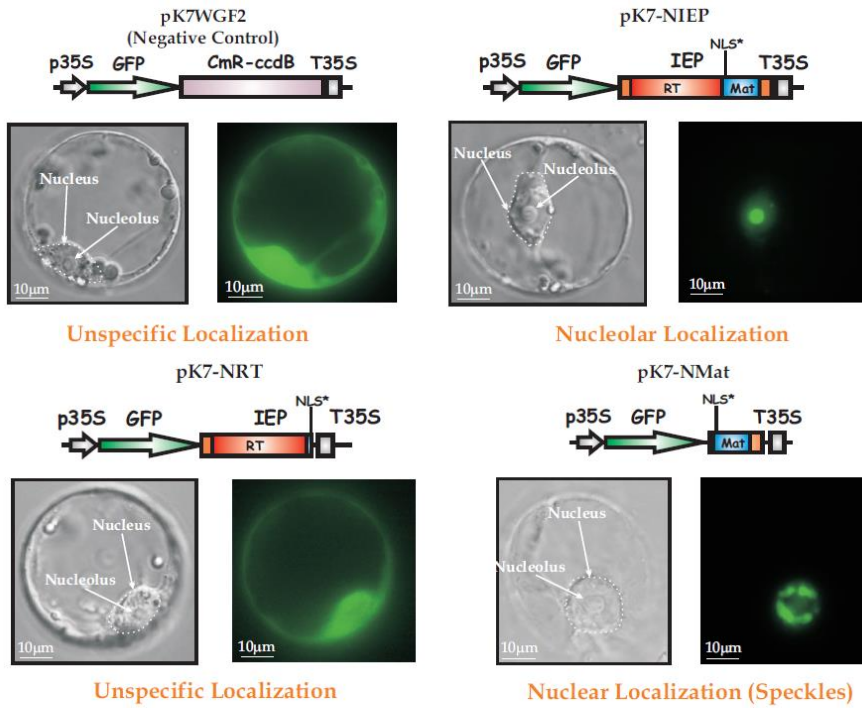

Figure 1. Subcellular localization patterns of the RmInt1 IEP in *Arabidopsis thaliana* protoplasts. Transient expression of translational fusions of the full-length protein and several mutant variants to the reporter EGFP.

References

1.- Michel F. *et al*. (1982). *Biochimie* 64:867
2.- Toro N. *et al*. (2007). *FEMS Microbiol. Rev*. 31: 342
3.- Wojciech P. *et al* 2018, *Chem.Rev.,* 118: 4156
4.- Keating K.S. *et al*., 2010, *RNA* 16: 1
5.- Rogozin I.B. *et al*., 2012, *Biol Direct* 7: 11.
6.- Vosseberg J. *et al*., 2017, *Biol Direct* 12: 30.
7.- Martin W. *et al*., 2006, *Nature* 440: 41
8.- Toro N. *et al*., 2018, *Front Microbiol*. 9: 627
9.- Nisa-Martínez R. *et al*., 2013 *PLoS One*, 8(12): e84056.

Live-cell imaging of storage lipid dynamics in pollen tubes

Castro AJ*

Plant Reproductive Biology and Advanced Imaging Laboratory, Department of Biochemistry, Cell and Molecular Biology of Plants, Estación Experimental del Zaidín (CSIC), 18008 Granada, Spain
*Author for correspondence: antoniojesus.castro@eez.csic.es

Keywords: antibody microinjection, caleosin, confocal live-cell imaging, fluorescent probes, lipid body, pollen tube, TEM

The success of fertilization in flowering plants largely depends on the ability of the pollen grain to form a pollen tube, which must be able to penetrate the stigma surface and move down the style towards the embryo sac. Pollen tubes exhibit a markedly asymmetric functional behavior in many cellular processes including ion fluxes, cell wall assembly and cytoskeletal arrangements. Since the vegetative cell is haploid, this model is of great interest for genetic and molecular studies as well. Pollen for most of plants is easy to germinate *in vitro*, so it can be manipulated under controlled conditions using a wide range of technologies.

The pollen grain is an active site in storage lipid biosynthesis. These lipids are stored in the form of sphere-shaped organelles called lipid bodies (LB). This energy supply might allow the pollen tube to grow autonomously at the onset of germination. Moreover, the stored lipids can be also the origin of signaling lipids regulating pollen tube growth. Therefore, pollen tubes constitute a good model to study storage lipid dynamics[1-2].

In this work, we used confocal live-cell imaging in combination with vital stains to study lipid body distribution, motility and behavior within pollen tubes. We also used distinct fluorescent probes in combination with live-cell imaging and TEM techniques to localize four enzymes directly involved in lipid body mobilization, namely TAG lipase, 13-lipoxygenase, caleosin/peroxygenase and phospholipase A2, in mature and germinated pollen grains. Finally, we carried out functional analysis of some of these lipid body-associated proteins combining live-cell imaging and microinjection techniques using different molecules such as antibodies and chemical inhibitors.

References

1.- Zienkiewicz K *et al*. (2010). J. Exp. Bot. 61: 1537
2.- Zienkiewicz A *et al*. (2013). J. Exp. Bot. 64: 293

Acknowledgements

This work was supported by ERDF co-financed grants AGL2013-43042-P and AGL2017-84298P from Spanish Ministry of Economy and Competitiveness (MINECO).

SESSION LS-3. INVITED SPEAKER

The art of selecting and applying electron microscopy techniques to understanding biomedical research questions

Bonucci S, Sousa AL, **Erin M Tranfield***

Electron Microscopy Facility, Fundação Calouste Gulbenkian - Instituto Gulbenkian de Ciência, Rua da Quinta Grande, 6, 2780-156, Oeiras, Portugal
*E-mail for correspondence: etranfield@igc.gulbenkian.pt

In the Electron Microscopy Facility at the Instituto Gulbenkian de Ciência, we support scientists studying a broad range of biomedical research questions across a diverse spectrum of animal models. Each of these experiments requires careful methodological planning with the aim of addressing the question of interest while introducing the fewest number of biological artifacts. In this talk, I will introduce how we approach our experimental planning to specifically target a biological question, within the time and budget constraints of the research project. I will feature several of the different technical approaches we use for two and three-dimensional transmission electron microscopy imaging as I introduce you to several of the projects we are working on in the facility.

Searching for mechanical biomarkers of pathologies: some applications of Atomic Force Microscopy to tissue and cell mechanics

Ciasca G[1,*], Papi M[1], Rossi C[2], De-Giorgio F[3], Minnella A[4], Minelli E[1], Nardini M[1], Mazzini A[1], De Spirito M[1]

1. Institute of Physics, Catholic University of Sacred heart; Largo F. Vito 1, 00168,Rome, Italy
2. Institute of Biochemistry and Clinical Biochemistry, Catholic University of Sacred heart; Largo F. Vito 1, 00168,Rome, Italy
3. Institute of Public Health, Catholic University of Sacred heart; Largo F. Vito 1, 00168,Rome, Italy
4. Institute of Ophthalmology, Catholic University of Sacred heart; Largo F. Vito 1, 00168,Rome, Italy

*Author for correspondence: gabriele.ciasca@unicatt.it

Keywords: Alzheimer's disease, Atomic Force Microscopy, brain cancer, macular pathologies, red blood cells

A large body of evidence has emerged that mechanical stimuli and physical forces play a key role in tissue growth and maintenance, deeply influencing human physiology. Similarly, in pathological conditions, cells and tissues' mechanical properties undergo profound modifications, which also contribute to disease progression. Such mechanical modifications can be investigated at nanoscale level using Atomic Force microscopy (AFM) in the spectroscopy mode, with the aim to search for and validate novel mechanical biomarkers of pathologies. Here we present some AFM application to the study of cell and tissue biomechanics in several human pathologies, which include malignant and benign brain cancers, Alzheimer's disease, ocular pathologies of surgical interest and colorectal cancer. AFM application to forensic science, with regard to the determination of the time since death are also discussed. Information coming from AFM data are systematically compared with other imaging techniques such as tissue histological sections, electron and confocal microscopy, US elastography, and computational techniques such as molecular dynamics. Taken together, our results confirm that AFM has the potential to positively impact on the development of novel diagnostic and monitoring tools.

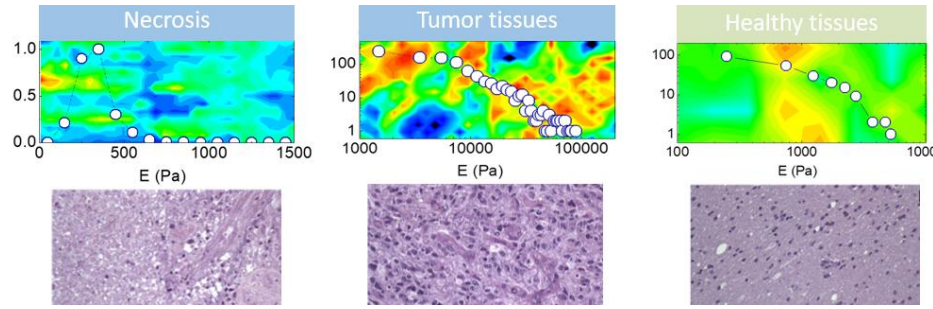

Figure 1. Mechanical fingerprint of brain cancer tissues. Young's modulus maps and frequency histogram of brain tissues obtained from patients diagnosed with Glioblastoma: Necrotic tissues (left), non-necrotic cancer tissues (centre) and healthy tissues (right), together with histological sections.

References

1.- Ciasca G *et al*. (2016). *Nanoscale* 8.47: 19629

Using CLEM to unravel intracellular membrane trafficking defects

Lopes-da-Silva M*, Falcao AS, Escrevente C, Tenreiro S, Seabra MC*

CEDOC – Chronic Diseases Research Center, NOVA Medical School|Faculdade de Ciências Médicas, Universidade NOVA de Lisboa, Lisbon, Portugal
*Authors for correspondence: Mafalda.silva@nms.unl.pt / miguel.seabra@nms.unl.pt

Keywords: autofluorescence, intracellular vesicle, lipofuscin, melanin, melanolipofuscin, RPE

Intracellular membrane traffic is essential for cellular homeostasis and function. Although recent advances in light microscopy imaging have allowed increases in resolution, Electron Microscopy still allows the observation of structures like no other technique. Correlative Light and Electron Microscopy (CLEM) combine these two imaging techniques and allows for a more detailed analysis of intercellular structures at the nanoscale resolution.

The retinal pigment epithelium (RPE) in the eye contains three major types of pigment granules; melanosomes, lipofuscin and melanolipofuscin. Melanosomes in RPE cells are formed during embryogenesis and mature during early postnatal life while lipofuscin and melanolipofuscin granules accumulate as a function of age and certain diseases. Using CLEM, we investigate the biogenesis and functional role of melanin and lipofuscin granules in RPE cells and what are their functional role during the progression of Age-related Macular Degeneration (AMD).

We have developed an *in vitro* model where human primary RPE cells are fed Photoreceptor Outer Segments (POS) which over time leads to lysosome dysfunction and the accumulation of autofluorescence intracellular vesicles, reminiscent of those found in patients with AMD. While these autofluorescent vesicles are abundant, we were unable to identify them by convention Transmission Electron Microscopy (TEM). Thus, we proceeded to image them first using confocal microscopy and then process the sample for TEM, using cells seeded on gridded coverslips to aid in cell localization.

We hypothesis that with improved knowledge of the molecular mechanisms involved in the biogenesis and maintenance of these vesicles, we will be better equipped to find novel therapies for AMD treatment.

Imaging induced antiinflamatory response in human cell cultures and *ex vitro* blood cultures

Lima-Cabello E, Jiménez-López JC, Alché JD*

Dept. Biochemistry, Cell & Molecular Biology of Plants, Estación Experimental del Zaidín, Spanish National Research Council (CSIC); Profesor Albareda 1, Granada 18008, Spain.
*Author for correspondence: juandedios.alche@eez.csic.es

Keywords: antioxidant, glutathione reductase, immunolocalization, olive, seed, signalling

The presence and the abundance of pro-oxidant and anti-oxidant products in olive derived materials was assessed in human systems through different experimental procedures. They include their co-culture with in vitro cell cultures (CACO-2, PANC-1) as well as *ex vitro* analysis of whole blood, plasma or isolated PBMCs (Peripheral Blood Mononuclear Cells) in all cases challenged with different inflammatory agents like LPS. Different redox/antioxidant markers were used in these assays, which were analysed for the presence of transcripts (mainly analyzed by qPCR) or enzymes (commonly analyzed by ELISA) corresponding to inducible nitric oxide synthase (iNOS), peroxidases, catalases, superoxide dismutases, glutathione-related enzymes and superoxide-generating enzymes (OeRboH).
Some of these markers were also tested at the cellular level, either by using specific fluorochromes (i.e. DAF-2DA to detect NO formation) or antibodies (i.e to different interleukins, TNF alpha, Reactive Carbonyl Species, antioxidant enzymes and others). Imaging was carried out by fluorescence and confocal microscopy, and quantification of the signal was made in order to assess correlation with molecular and biochemical markers.

Acknoledgements
This work was supported by ERDF con financed research projects BFU-2016-77243-P, RTC-2015-4181-2 and RTC-2017-6654-2.

Live cell imaging of soybean Bowman-Birk inhibitors internalization in HT29 colorectal cancer cells

Castro AJ[1], Sabio A[2], Olías R[2], Marin-Manzano MC[2], Clemente A[2,*]

1. Plant Reproductive Biology and Advanced Imaging Laboratory, Department of Biochemistry, Cell and Molecular Biology of Plants, Estación Experimental del Zaidín (CSIC), C/ Profesor Albareda 1, 18008 Granada, Spain
2. Department of Physiology and Biochemistry of Animal Nutrition, Estación Experimental del Zaidín (CSIC), Camino del Jueves s/n, 18100 Armilla, Granada, Spain
*Author for correspondence: alfonso.clemente@eez.csic.es

Keywords: Bowman-Birk inhibitors, cell internalization, CyDye, fluorescent probes, HT29 cells, legumes, live-cell imaging, protein labeling

Bowman-Birk inhibitors (BBI) from legumes are resistant to both acidic conditions and the action of digestive proteases, as well as the proteolytic and metabolic activity of intestinal microbiota[1]. *In vitro* and *in vivo* studies have demonstrated that BBI might exert a protective and/or suppressive effect against inflammatory and carcinogenic processes within the gastrointestinal tract *via* protease inhibition[2,3]. Indeed, it is essential to known the internalization mechanism and exact localization of BBI proteins in colon cancer cells in order to identify their potential therapeutic targets.

Individual proteins chemically labeled with fluorescent dyes can be localized and tracked in real time experiments in order to get insights about the site and molecular mechanism of action[4]. Here, we first adapted a protocol to label BBI proteins with CyDye Fluors, which was originally developed for DIGE applications, to be used for live cell imaging. Then, we carried out live cell assays of CyDye-labeled soybean major BBI isoinhibitors, IBB1 and IBBD2[5], either alone or combined with other fluorescent probes, in order to get insights about the dynamics and to determine their internalization mechanism in HT29 colorectal adenocarcinoma cells.

The IBB1 and IBBD2 proteins assayed were taken up by HT29 colon cancer cells in a time-dependent manner, being the bulk of the internalized proteins localized in the cytoplasm over a period of three hours of culture. The chemically inactivated forms of IBB1 and IBBD2 also enter HT29 cells but the process is slightly delayed compared with the native proteins. Both cyanide-labeled BBI proteins colocalized with FM4-64, an endosomal lipophilic marker, implying that they enter HT29 cells by endocytosis (Figure 1). Accordingly, internalization of both molecules was completely abolished at 4ºC. At longer times of culture, the IBB1 signal colocalized with DAPI, thus indicating that this protein is able to escape from endosomes into the nuclear/cytosolic compartments, where it might interact with potential therapeutic target/s, including the proteasome.

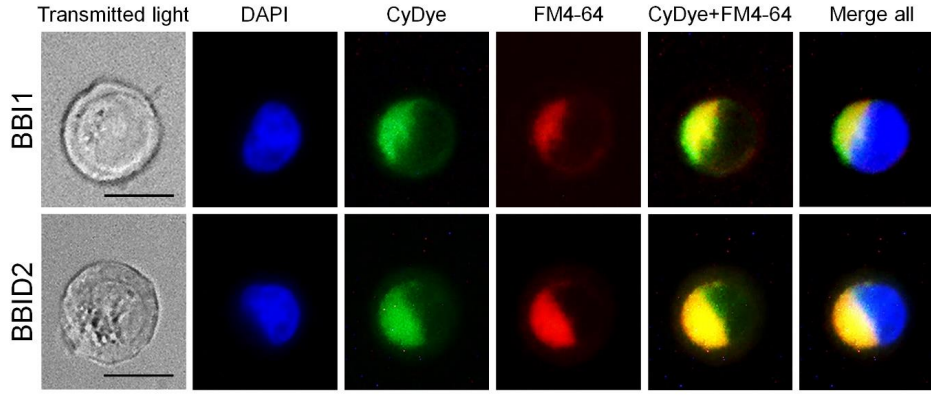

Figure 1. Internalization of soybean IBB1 and IBBD2 proteins into human colorectal cancer HT29 cells by endocitosis. The native IBB1 and IBBD2 proteins (~25 µg each) were labelled with CyDye2. HT29 cells were cultured *in vitro* for 90 min before chemical fixation and imaging. Nuclei were stained with DAPI. Photomicrographs were taken in an Eclipse Ti-U fluorescence microscope. Bars= 10 µm.

References

1.- Marin-Manzano MC *et al*. (2009). Br. J. Nutr. 101: 967
2.- Clemente A *et al*. (2012). Br. J. Nutr. 108: S135
3.- Utrilla MP *et al*. (2015). Mol. Nutr. Food Res. 59: 807
4.- Toseland CP. (2013). J. Chem. Biol. 6: 85
5.- Clemente A *et al*. (2010). Mol. Nutr. Food Res. 54: 396

Acknowledgments

This work was financially supported by the grant AGL2017-83772-R funded by the Spanish Ministry of Science, Innovation and Universities.

Exploring neuronal subcellular architecture in the mouse brain

M. Rosario Fernández-Fernández

Centro Nacional de Biotecnología, Spanish National Research Council (CSIC), C/ Darwin 3, Cantoblanco, 28049 Madrid, Spain
*Author for correspondence: mrfernandez@cnb.csic.es

Keywords: animal models, electron tomography, fast-freezing techniques, Huntington's disease, subcellular architecture

Eukaryotic cells are organized into compartments that act as local functional modules. The morphology of these compartments, their spatial distribution and the relationships amongst them constitute the subcellular architecture, which is tightly related to cell function and specialization. The analysis of the alterations in the subcellular architecture can contribute to gain insights into the pathophysiological basis of diseases, serve as a biomarker and enable the identification of new therapeutic targets.

In the latest years we have developed a protocol for the preservation of mouse brain tissue in close-to-native conditions and we have applied it to the analysis of striatal neurons and their alterations in Huntington's disease (HD) mouse models. We use electron tomography (ET) and focused ion beam-scanning electron microscopy (FIB-SEM) as fundamental 3D imaging tools. The combination of this tool kit has allowed the identification of new functionalities for subcellular organelles as well as architectural alterations associated to HD.

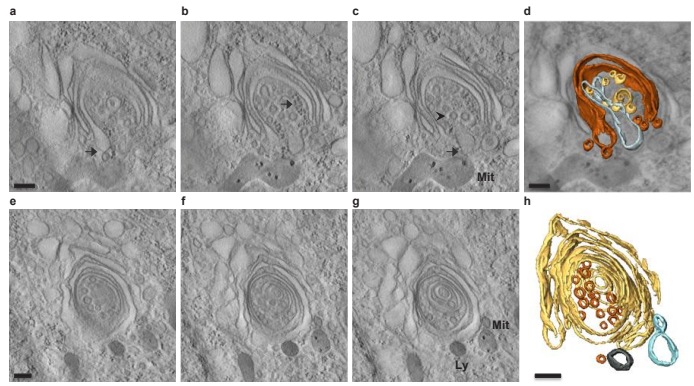

Figure 1. Visualization of the 3D architecture of an engulfing Golgi. Representative slices from 3D volumes of engulfing Golgis in the open (a to c) and closed states (e to g). 3D views of the models with segmented membranes (d and h). In (d) the model is visualised on a background showing the projection of the whole structure.

References

Fernández-Fernández MR *et al*. (2017). J. Cell Sci. 130: 83

Fast and automated diffraction tomography: how to acquire 3D electron diffraction in a systematic and accurate way

Plana-Ruiz S[1,2,*], Krysiak Y[3], Portillo J[4,5], Alig E[6], Estradé S[2], Peiró F[2], Kolb U[1,7,*]

1. Institut für Angewandte Geowissenschaften, Technische Universität Darmstadt, Schnittspahnstrasse 9, 64287 Darmstadt, Germany.
2. LENS, MIND/IN2UB, Departament d'Enginyeria Electrònica i Biomèdica, Universitat de Barcelona, Martí i Franquès 1, 08028 Barcelona, Spain.
3. Institute of Physics, Czech Academy of Sciences, Cukrovarnická 10/112, 16200 Prague, Czech Republic.
4. Centres Científics i Tecnològics, Universitat de Barcelona, Lluís Solé i Sabarís 1-3, 08028 Barcelona, Spain.
5. NanoMegas SPRL, Blvd Edmond Machtens 79, B-1080 Brussels, Belgium.
6. Institut für Anorganische und Analytische Chemie, Goethe-Universität Frankfurt, 60438 Frankfurt am Main, Germany.
7. Institut für Anorganische Chemie und Analytische Chemie, Johannes Gutenberg-Universität Mainz, Duesbergweg 10-14, 55128 Mainz, Germany.
*Author for correspondence: sergiplana@hotmail.com / kolb@uni-mainz.de

Keywords: automated acquisition, crystal structure determination, electron diffraction tomography, high-throughput characterization, nanobeam diffraction

The usual methods to determine the structure of new materials deal with x-ray diffraction. However, x-rays are inconvenient in some cases because they cannot sample diffraction information from isolated nanocrystalline domains. Although this may not be a problem for single-phase powders or “big-enough” crystals, it becomes a challenge when crystallographic analyses at the nanometre scale are required, i.e., identification of new crystal structures in mixed phases, nanocrystals embedded in different phase matrices or disordered crystals. Electron diffraction tomography (EDT) can be a valuable method to overcome the aforementioned challenges by enabling the reconstruction of the intensity-weighted reciprocal lattice from a single nanocrystal. However, its main limiting factors are tiresome acquisition times and lack of automatization.

In this context, a new module has been developed in Digital Micrograph scripting as well as in Matlab environment in order to provide a versatile platform for EDT acquisition. The new acquisition method, so-called Fast-ADT (Fast & Automated Diffraction Tomography), is based on tilting the goniometric stage two times; a first one to generate a file containing the displacement of the crystal with the tilt angle, and a second one for the EDT acquisition. The program has been developed in such a way that TEM or STEM mode can be used, thus extending an EDT acquisition software for the different specifications of the available microscopes. Crystals of $BaSO_4$ have been used to demonstrate the validity and accuracy of the acquisition method. Finally, to show the method potential, a new polymorph of a commercially available organic pigment (DRED1) with space group *P-1* has been solved *ab initio*, showing all the 46

non-hydrogen independent atoms on the Fourier potential maps. In this way, the authors intend to provide an all-in-one platform to characterize different kinds of materials in a more systematic and automated way.

Quantitative evaluation of the accuracy of compressed sensing electron tomography reconstructions using material-realistic 3D-phantoms

Bouzaine A[1], Muñoz-Ocaña JM[2], Rodriguez Chia A[2], Hungría AB[1] Calvino JJ[1], López-Haro M[1,*]

1. Departamento de Ciencia de los Materiales e Ingeniería Metalúrgica y Química Inorgánica, Universidad de Cádiz, Campus Rio San Pedro, 11510 Puerto Real, Cádiz, Spain
2. Departamento Estadística e Investigación Operativa, Universidad de Cádiz, Campus Rio San Pedro, 11510 Puerto Real, Cádiz, Spain
*Authors for correspondence: jose.calvino@uca.es / miguel.lopezharo@uca.es

Keywords: 3D nanometrogy, catalysis, compressed sensing, nanoparticles, STEM-HAADF tomography

Electron tomography (ET) has become a powerful tool to reveal structural and compositional data, out of reach for 2D techniques, to better rationalize the relationships between materials synthesis and function. Typically, a large number of tilt projections, with small increments of angles, *e.g.* 2°, are recorded to obtain a reliable volume reconstruction. However, in these experimental conditions many materials suffer morphology changes during the tilt series acquisition due to beam damage. To avoid this, the number of projection images is often reduced during the experiment, this leading to degradation of the reconstruction quality.[1]

Therefore, recent efforts in the field of ET have aimed not only at improving the reliability of the 3D information, by dumping the influence of the artefacts, but also at decreasing the total number of STEM-HAADF images required to reconstruct the volumes with sufficient accuracy. In this regard, the use of reconstruction algorithms based on so-called Compressed Sensing (CS) start to be more widespread. In particular, Total Variation Minimization (TVM) based algorithms have proven very efficient for 3D nanometrology.[2] However, providing an estimate of the errors of magnitudes estimated from reconstructed and segmented volumes is in fact an important issue which has not been properly addressed because a perfectly known reference is needed. The problem particularly complicates in the case of multicomponent material systems.

A reasonable procedure to estimate the error in the tomographic analysis would be establishing a quantitative comparison between the parameters determined directly from models closely representative of the investigated problem and those obtained after their reconstruction and segmentation.

In this work, we have developed an improved volume reconstruction/segmentation method which incorporates advanced processing strategies. Then, we have stablished an approach to evaluate in quantitative terms the accuracy of TVM reconstructions, which considers the influence of relevant experimental parameter like the range of tilt

angles, noise level or object orientation. The approach is based on the analysis of material-realistic, 3D phantoms which include the most relevant features of the system under analysis.

As an illustration, Figure 1(a) shows a 3D phantom built to study the 3D analysis of nanocatalysts consisting of metal nanoparticles, of varying size, supported on cube-shaped crystallites of a heavy oxide. To approach real experimental conditions, prior to the reconstruction, the image series were corrupted with a mixture of Gaussian and Poisson noise and further denoised using Undecimated Wavelet Transforms (UWT). Figure 1b, shows on its hand the segmentation of its reconstruction using the TVM 3D algorithm, considering tilts in the -70º to 70º and 5º steps.). Then, the volume of each individual nanoparticle has been quantified and compared to those corresponding to the original 3D phantom, as illustrated in Figure 1c.

Note that the particles appear slightly smaller in the segmented/reconstructed volume. For the three particles, the volume is underestimated by roughly the same amount (ca. 1000 cubic voxels), but the relative error is much smaller in the case of the large particles (≈20%) than in the small ones (≈100%). This result provides a close estimate of the error expected in the analysis of experimental series, under the simulated conditions, which must be taken into account when comparing nanometrological measurements with others obtained by complementary techniques.

Reconstructing the 3D-phantom under different conditions (noise level, orientation of the sample, tilt range, tilt increment, different prefiltering or reconstruction methods…), an apriori knowledge about the best experimental approach to solve a particular 3D characterization problem can be obtained.

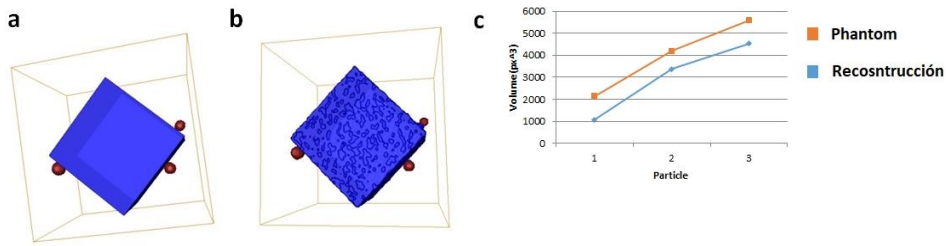

Figure 1. a) 3D phantom of a Metal/Oxide system. b) reconstructed/segmented volume using UWT-TVM 3D, tilts in the -70º to 70º range in 5º steps. c) Comparison of the particle volumes in the phantom and in the reconstructed/segmented volume.

References

1.- Midgley PA, Bals S. (2009). Electron Tomography, in Handbook of Nanoscopy, G Van Tendeloo, D Van Dyck, SJ Pennycook (Eds.), Wiley-VCH, chapter 7, vol. 1, pp. 253-280

2.- López-Haro M. (2018). *Part. Part. Syst. Charact.* 35: 1700343

Acknowledgements

This work received financial support from MINECO/FEDER (MAT2017- 87579-R, MAT2016-81118-P, MTM2016-74983-C2-2-R).

Scanning transmission electron microscopy as a tool to optimise and characterise encapsulated agrochemicals in fully-organic reservoirs

Trasobares S[1,2], Mejías FJR[1], López-Haro M[1,2], Varela R[1], Molinillo JMG[1], Macías FA[1], Calvino JJ[1,2]

1. Facultad de Ciencias, Universidad de Cádiz, Campus Río San Pedro, 11510 Puerto Real, Cádiz, Spain
2. IMEYMAT. Instituto de Microscopía Electrónica y Materiales, Universidad de Cádiz, Spain
*Author for correspondence: susana.trasobares@uca.es

Keywords: 2D and 3D STEM, agrochemicals, beam sensitive materials, encapsulated bioactive compounds

Nowadays final applications of natural products in weed control are still limited by their water solubility and bioavailability. In this context, encapsulation emerges as a relevant route to enhance physicochemical properties of natural compounds. Moreover, using fully-organic reservoirs ensures that the target activity is retained while respecting environmental issues. In this paper we will show how state of the art electron microscopy can be applied not only to optimize the encapsulation process but also to characterize the beam sensitive encapsulated moiety.

Scanning Transmission Electron Microscopy Imaging and Spectroscopic techniques have been combined first to optimize the encapsulation process of disulfide model molecules within lithocholic acid (LCA) nanotubes and secondly to characterize Metal-Organic Frameworks containing other S-bearing bioactive molecules.

Spatially resolved spectroscopic techniques as EELS and XEDS have been used to monitor the distribution of the guest molecules within the organic nanotubes. In particular, the appearance of the sulfur and nitrogen signals in the analytical maps has allowed us to detect the presence of the bioactive disulfide molecule and to determine its location in the sample. Figure 1 (top) illustrates the EDS sulfur (yellow) and carbon (blue) maps of a disulfide compound hosted within the organic LCA nanotubes and the EELS signal corresponding to the hosted molecule and organic nanotubes. Moreover, STEM analytical tomography experiments have confirmed that the bioactive molecule is actually embedded within the nanotubes.

Once the encapsulation synthesis was optimized, the process was extrapolated to use shell agents that incorporate trace elements (Zn), which are well-known to play an important role in living cells. In this context, a Metal-Organic Framework was used to host specific bioactive molecules which showed promising results against HeLa cell lines (uterine cancer)[3]. In terms of electron microscopy, the characterization of this new structures is particularly challenging, since damage effects characteristic of the extremely beam sensitive MOFs adds up to the requirement of discriminating the two (host-guest) organic components. As reported by Zhu et al., ZIF8 crystals begin to

lose crystallinity when the accumulated dose reaches 25 e- $Å^{-2}$ and are completely damaged at a dose of 75 e- $Å^{-2}$. In the present work we have identified the MOF´s crystallinity structure by Integrated Differential Phase Contrast STEM (iDPC-STEM) imaging using a probe current lower than one picometer. EELS maps allowed us detecting the location of the guest molecules within the MOF structure.

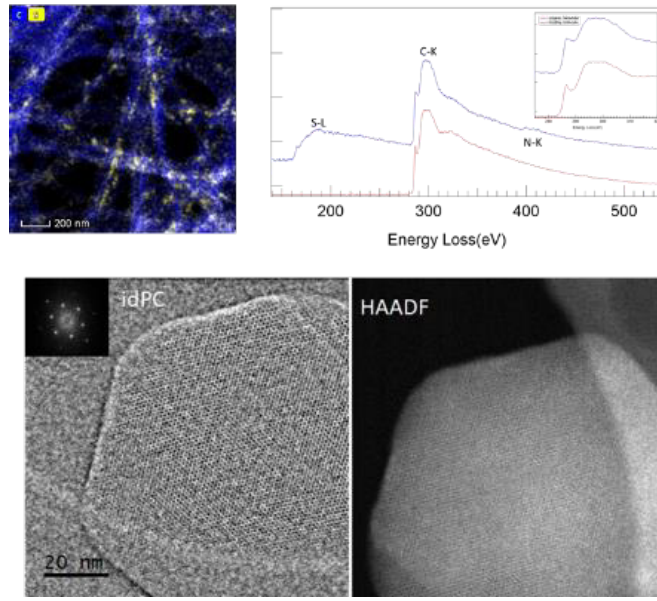

Figure 1. Characterization of encapsulated bioactive molecules on organic nanotubes and MOFs. Upper images, spectroscopy EDS and EELS signals for organic nanotubes. Lower image, iDPC and HAADF images of encapsulated MOFs structure.

References

1.- Arroyo E et al. (2010). *Mutat. Res. - Genet. Toxicol. Environ. Mutagen.* 695 (1-2): 81

2.- Zhu Y *et al*. (2017). *Nat. Mat.* 16 (5): 532

Acknowledgements

This project has received funding from the European Union's Horizon 2020 research and innovation programme under Grant 823717−ESTEEM3. Financial support from Junta de Andalucía (FQM334), MINECO/FEDER (Projects MAT2017-87579- R, MAT2016-81720-REDC) is also acknowledged. STEM studies were performed at SC-ICYT DME-UCA.

Negative-staining: a simple technique with modern applications in biological research

Bonucci S*, Tranfield EM

Electron Microscopy Facility, Fundação Calouste Gulbenkian - Instituto Gulbenkian de Ciência, Rua da Quinta Grande, 6, 2780-156, Oeiras, Portugal
*Author for correspondence: sbcosta@igc.gulbekian.pt

Keywords: carbon, electron beam, Electron Microscopy, grid, negative-staining

Electron Microscopy is an old technique that has been evolving and improving since it was first introduced. In 2017 the importance of the cutting-edge technique cryo-electron microscopy was acknowledged when its developers received the Nobel Prize. However, that is not to say that all the old techniques should be forgotten as new exciting ones are developed. Within the field of Electron Microscopy there is a wide spectrum of complexity of the methods ranging from negative-staining to correlative light and electron microscopy to cryo-electron microscopy. Simplicity is not automatically correlated with less or poorer
information. Sometimes the best method to start is with a simple and direct approach that will yield a very good initial data set and help guide the ongoing progress of the experiments.

For the purpose of the work presented herein, we have chosen to step back and to focus on the power of the relatively low-tech method of negative-staining to show that sometimes less is more in experimental techniques. In this body of work, we will show many examples of how negative staining, and negative staining in combination with immune-gold labelling has led to very informative results for the users of our EM Facility.

The main principle of this technique is the difference in electron diffraction caused by the interaction with the beam between the sample and the stain that is added on top of the sample. Although negative-staining is a simple, easy and fast technique to prepare samples for electron microscopy, there will exist artifacts in the final results. For example, the sample distortion due to the drying process on the grid, or the artifacts that might appear associated to the uneven spread of the stain on the sample. However, the type of problems that might arise will decrease with the level of experience of the person executing the technique since experience leads towards an increasing level of criticism and knowledge, allowing the choice of the best way to apply the negative-staining for each unique biological question.

To summarize, we are not suggesting negative staining is the perfect solution to every biological process but it is a useful technique to remember in the face of so many new fancy ways of doing things. It is a technique that can be done within an hour and can be suitable for simple qualitative or quantitative studies of proteins, antibodies,

bacteriophages, vesicles, virus, bacteria, as well as used in single or double immunolabeling, or as an essential step of quality control for a more advanced technique such as single particle analysis by cryo-electron microscopy. Although negative staining is not a new approach it is a very valuable one, and one that warrants being used more regularly when applied to appropriate biological questions.

Applications and challenges of SEM in Biomedicine

Zuzarte M*, Girão H

iCBR, Faculty of Medicine, University of Coimbra, Azinhaga de Sta Comba, 3000-548 Coimbra, Portugal
*Author for correspondence: mzuzarte@uc.pt

Keywords: scanning electron microscopy, low-vaccuum, biomedicine, tissues, cells

Variable-pressure scanning electron microscopes are currently available allowing low-vacuum observations of non-conductive specimens without pre-processing. This technique is quite relevant enabling the observation of biological samples in their native state. Nevertheless, some samples remain difficult to image due to their high water-content and lack of contrast, with biomedical samples being the major challenge. To overcome these limitations some technical improvements have been developed by manufactures. For example, the use of a cryo-stage can enable a better preservation of the samples and avoid out-gassing. Specific detectors can also be attached such as ultra-variable-pressure detectors to allow a superior imaging of the sample's surface at low-accelerating-voltages and low-vacuum conditions. Moreover, autofocus, auto brightness and auto contrast controls, enable optimized imaging performance with minimal time and effort. For more challenging samples, methodological improvements can also be considered. For example, cell and tissue cultures should be established on silicon wafers instead of glass coverslips. This improves conductivity and avoids charging effects. Furthermore, a conductive layer can be applied to the samples using ionic liquid which replaces the water and maintains the shape of sample without vaporization under vacuum. Overall, these improvements enable an efficient observation and high quality imaging of biomedical samples and avoid the multistep tedious sample preparation required for high vacuum imaging that inevitably causes artefacts.

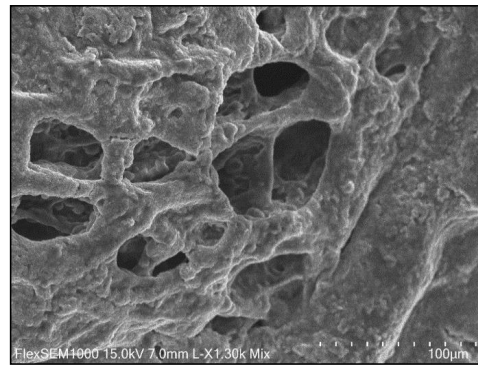

Figure 1. Lung tissue – Observation of a sample of defrosted lung tissue without pre-processing under a Flex SEM1000 (Hitachi).

Acknowledgments
We acknowledge the support of PPBI-Portuguese Platform of BioImaging: POCI-01-0145-FEDER-022122.

The Instruct Image Processing Center (I2PC): support to structural biologists

Melero R*, Carazo JM*

Dept. of Macromolecular Structures, CNB, Spanish National Research Council (CSIC), C/ Darwin nº 3, Madrid, Spain
*Author for correspondence: rmelero@cnb.csic.es / carazo@cnb.csic.es

Keywords: Corbel, image processing, iNEXT, instruct

The Instruct Image Processing Center (I2PC) at the CNB-CSIC (Madrid-Spain) is the European Reference Center for infrastructure provision in Image Processing in Transmission Electron Microscopy and X-ray Microscopy. We provide support to structural biologists, helping them to maximize the extraction of biological knowledge from their electron microscopy images in three differents platforms: Instruct, iNEXT and Corbel. In iNEXT we give support at sample level, with analysis of EM grids and acquisition of EM images using a FEI Talos Artica and a Falcon III direct detector. In Instruct we give support for full EM image processing using SCIPION package, including movie alignment, particle picking, classification, volume reconstruction and atomic structure determination. In Corbel we link the structural data with genomics and proteomics databases, with annotations of 3D protein structures at residue level using proteomic and genomic sources including UniProt and ENSEMBL databases, diseases and genomic variants, protein domain families, disordered regions, short linear motifs and immunological epitopes.

Microscopical detection of ROS and RNS in plant samples by using chromogenic and fluorescent probes

Alché JD*

Dept. Biochemistry, Cell & Molecular Biology of Plants, Estación Experimental del Zaidín, Spanish National Research Council (CSIC), C/ Profesor Albareda 1, Granada 18008, Spain
*Author for correspondence: juandedios.alche@eez.csic.es

Keywords: DAB, hydrogen peroxide, hydroxyl, NBT, nitric oxide, Ro-GFP, superoxide.

Reactive oxygen and nitrogen species (ROS and RNS) are highly reactive molecules resulting from aerobic metabolism, whose production is enhanced in several types of biotic and abiotic stresses. Moreover, small deviations of the basal levels of these molecules participate in signalling events in biological systems, thus participating in plant/animal physiology.

Detection of these molecules is extremely challenging in many cases, due to their low concentration, and their short life span. Different microscopical approaches have been designed to image and quantify the presence of molecules like peroxides (hydrogen peroxide), superoxide, hydroxyl and nitric oxide among others.

In this short review, most commonly used methods and probes are described for their use in LM, FM, CLSM and TEM microscopy applications. They include chromogenic detection of hydrogen peroxide by DAB and superoxide by TMB. As fluorescent probes, examples of the use of 2',7'-dichlorofluorescein diacetate (DCF-DA) to detect peroxides, dihydroethidium (DHE) to detect superoxide, rhodamine B hydrazide to detect hydroxyl, and 4,5-diaminofluorescein-2 diacetate (DAF- 2DA) to detect nitric oxide will be displayed, alone or in combination with different ROS/NO donors and scavengers.

Microscopy imaging of samples with newly developed fluorescent probes, including ro-GFP, a redox sensitive green fluorescent protein capable to dynamically monitoring changes in the cellular glutathione pool (as an indicator of cellular redox state), will be also displayed and discussed.

Acknowledgements
This work was supported by ERDF con financed research projects BFU-2016-77243-P, RTC-2015-4181-2 and RTC-2017-6654-2.

SCIENTIFIC PROGRAMME
ABSTRACTS
POSTERS

MS-P01. Characterization of brittle phases in EN 1.4462, 1.4482 and 1.4410 duplex stainless steels in heat treatments

Ruiz A*, Nuñez A, Vargas A, Almagro JF

Technical Department, Metallurgical Laboratory, Acerinox Europa S.A.U., Polígono Industrial Palmones s/n, Los Barrios 11379, Spain
*Author for correspondence: andres.ruiz@acerinox.com

Keywords: brittle phases duplex, crystalline phases, EBSD, FEGSEM, heat treatments, stainless steel, superduplex,

Duplex stainless steels are characterized by a two-phase structure made of α-ferrite and γ-austenite grains, within the 40/60 %[1] range as supplied material. Duplex stainless steel applications are based on its outstanding combination of high mechanical properties and corrosion resistance. Its main drawback is related to holding the material under annealing/aging conditions (temperatures between 600 and 1000 ºC) [2], which results in precipitation phenomena of brittle phases, predominantly in the grades with higher Cr and Mo contents. Consequently, a decrease in the corrosion resistance occurs in the material and an adverse effect in its mechanical properties. Duplex stainless steels have a wide precipitation range in temperatures and kinetics, which is very important in its production process. The characterization of the precipitation kinetic is essential for the process windows of the materials production.

In this research, different phases are characterized within EN 1.4462, 1.4482 and 1.4410 duplex stainless steels, after a 1-hour heat treatment at 950 ºC in air by FEGSEM and EBSD[3]. The latest technique, which analyses diffraction patterns known as Kikuchi bands, allows to identify and classify each phase within a specified structure of a certain material. According to this study, brittle phases and precipitates after the heat treatment are studied. This technique emerges as an automated and competitive method when compared to more conventional procedures, such as optical metallography. Fig. 1 shows EN 1.4410 superduplex phases characterization and quantification by EBSD, where a different colour were assigned to each phase by the software. Fig. 2 shows same characterization in another type of material, EN 1.4482.

The results point out the presence of fragilizing phases and precipitates in EN 1.4462 and superduplex EN 1.4410, predominating in EN 1.4410. However, there is no evidence of fragilizing phases in EN 1.4482, which is in good agreement with the expected results, according to each material's composition.

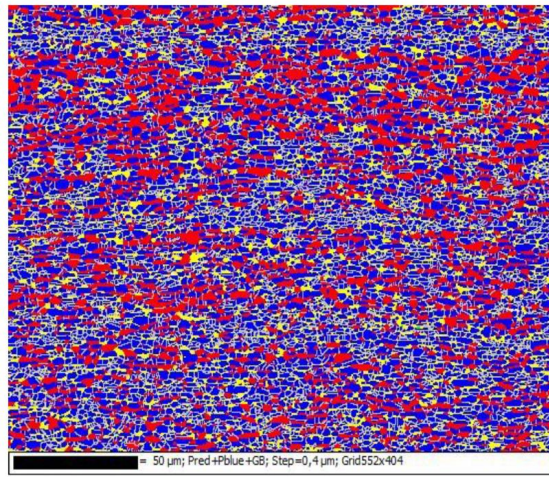

Figure 1. Characterization of brittle phases in EN 1.4462 duplex. Red areas, BCC phase (26.3%); Blue areas, FCC phase (59.6%); Yellow areas, sigma phase (13.4%); and Green areas, chi phase (0.10%).

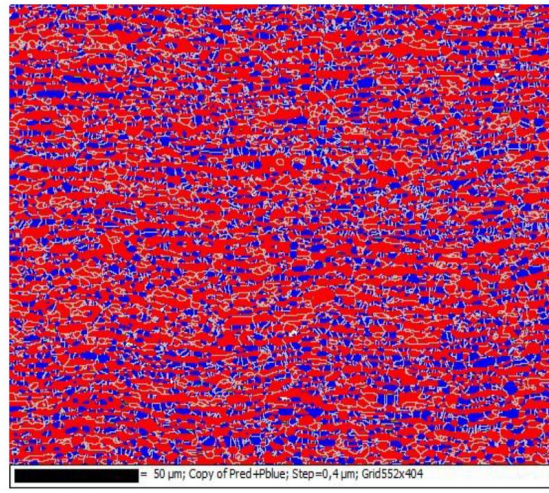

Figure 2. Characterization of brittle phases in EN 1.4482 duplex. Red areas, BCC phase (67.1%); Blue areas, FCC phase (32.1%).

References

1.- Kahar SD. (2017). *Int. J. Engin. Res. Appl.* 7 (4, Part -4): 27
2.- Llorca-Isern N *et al*. (2016). *Mat. Char.* 112: 20
3.- HKL Technology Inc. (2005). EBSD Applications Catalogue. App 7, pp. 32-35

MS-P02. Strain glass state in Ni-rich Ni-Ti-Zr shape memory alloys

Xu S[1], Pons J[1,*], Santamarta R[1], Karaman I[2], Noebe RD[3]

1. Departament de Física, Universitat de les Illes Balears, E07122 Palma de Mallorca, Spain.
2. Dept. Materials Science and Engineering, Texas A&M University, College Station, TX 77843, USA
3. Materials and Structures Division, NASA Glenn Research Center, Cleveland, OH 44135, USA
*Author for correspondence: jaume.pons@uib.es

Keywords: high temperature shape memory alloys, martensitic transformation, strain glass

Slightly Ni-rich Ni-Ti-Hf and Ni-Ti-Zr alloys are potential candidates for high temperature shape memory alloy applications. As a matter of fact, good shape memory and superelasticity in tension has been reported in $Ni_{50.3}Ti_{34.7}Zr_{15}$ and $Ni_{50.3}Ti_{29.7}Zr_{20}$ alloys reinforced by nanoprecipitation of the so-called H-phase[1-2]. The stability of Ni-Ti-Hf/Zr alloys under prolonged aging in austenite at 520 K (value close to the *Af* temperature) was also studied. For Ni-Ti-Zr alloys, the martensitic transformation was found to be suppressed after 1 week ageing at 520 K[3].

Shape memory alloys are considered as ferroic systems that exhibit a ferroelastic transition (the martensitic transformation), the lattice strain being the ferroic degree of freedom. In the last years, a novel state of locally disordered lattice strain was found in alloys with suppressed ferroelastic (martensitic) transition, denoted as *strain glass*[4]. The strain glass state appears in systems with nanometric spatial heterogeneities that frustrate the long-range ferroelastic transition, typically originating from point defects (excess Ni atoms), onset of nanoprecipitation, dislocation tangles or ordered domains with nanometric antiphase boundaries[5]. The strain glass is typically detected by AC mechanical tests and TEM. The main signatures are a frequency dependence of the temperature of the elastic modulus (E) minimum and the internal friction (IF) maximum, following a Vogel-Fulcher relationship, and presence of streaking in the diffraction patterns that, at low temperature, form diffuse spots at positions close to the martensite phase reflections[4]. In the present work, new results will be provided to demonstrate the achievement of the strain glass state in Ni-rich Ni-Ti-Zr.

Alloys with nominal compositions $Ni_{50.3}Ti_{29.7}Zr_{20}$ and $Ni_{50.9}Ti_{24.1}Zr_{25}$ were produced by induction melting from high purity elemental constituents and solution heat treated (SHT) at 1170 K. Some samples were subsequently aged at 520 K in air for different times and water quenched. Dynamic Mechanical Analysis (DMA) tests were conducted on a Q800 TA instrument in single cantilever mode with 2 K/min cooling rate and multi-frequency mode (0.2-20 Hz). TEM observations were performed in a Hitachi H600 model at 100 kV.

Figure 1 presents the DMA results of the $Ni_{50.9}Ti_{24.1}Zr_{25}$ SHT alloy (with supressed martensitic transformation), which exhibit a clear frequency dependence. The modulus dip temperatures fit reasonably well with a Vogel-Fulcher-type frequency dependence,

as shown in the inset of Fig. 1, with an equilibrium temperature for the freezing process T_0 = 220 K. In turn, the $Ni_{50.3}Ti_{29.7}Zr_{20}$ SHT alloy presents the normal martensitic transformation. However, after ageing for 14 days at 250ºC the transition is supressed and frequency dependence appears in the DMA signals, with T_0 = 230 K. Fig. 2 presents the electron diffraction patterns of the $Ni_{50.9}Ti_{24.1}Zr_{25}$ SHT alloy. Some diffuse streaking is observed at room temperature, as reported in [3], indicative of short range reordering processes. At 120 K, the streaking enhances and form diffuse spots at positions close to those corresponding to the 111-type reflections of martensite, but the fundamental spots keep the cubic symmetry of the B2 phase (frustrated transformation). A similar behaviour is found in $Ni_{50.3}Ti_{29.7}Zr_{20}$ aged at 250ºC. These results are clear signatures of the strain glass state in Ni-Ti-Zr alloys[4].

As the H phase is richer in Zr and lean in Ti compared to the B2 matrix, the decomposition process at 520 K likely starts with a short range segregation of Zr and Ti atoms leading to the formation of very small domains (roughly nanometric in size) with modified compositions that constitute precursor nuclei of the H phase. Such fine spatial heterogeneity creates the strain glass state in the present alloys. Increasing the Ni content to 50.9 at% and Zr content to 25 at% makes the alloy more prone to H-phase precipitation and to the B2 phase instability, which already occurs during quenching after the SHT with no additional ageing. The present results demonstrate another case of strain glass state induced by the onset of a nanoprecipitation process, similar to the Ni_4Ti_3-type nanoprecipitation in binary Ni-Ti alloys.

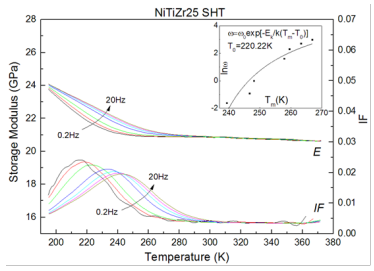

Figure 1. DMA results of $Ni_{50.9}Ti_{24.1}Zr_{25}$ and fitting of the Vogel-Fulcher equation with experimental data

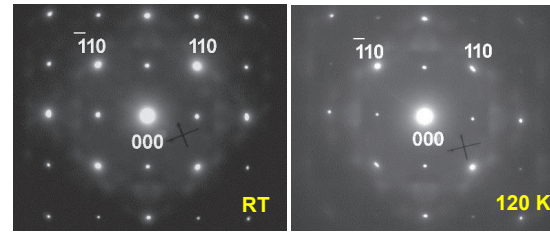

Figure 2. SAEDPs taken from $Ni_{50.9}Ti_{24.1}Zr_{25}$ SHT alloy at room temperature (left) and at –150 ºC (right).

References

1.- Evirgen A *et al*. (2014). *Scr. Mater.* 81: 12
2.- Evirgen A *et al*. (2016). *Mat. Sci. Eng. A* 655: 193
3.- Perez-Sierra AM *et al*. (2016). *Scr. Mat.* 124: 47
4.- Sarkar S *et al*. (2005). *Phys. Rev. Lett.* 95: 205702
5.- Monroe JA *et al*. (2015). *Acta Mater.* 101: 107

Acknowledgements

Support from the Spanish government and FEDER under project MAT2014-56116-C4-1-R is highly acknowledged.

MS-P03. Characterization of 3D superconducting WC nanotubes fabricated by a novel Focused Ion-Beam Induced Deposition direct-write method

Ibarra A[1,*], Córdoba R[2,3], Mailly D[4], de Teresa JM[1,3]

1. University of Zaragoza, INA, LMA, E-50009 Zaragoza, Spain
2. Instituto de Ciencia Molecular (ICMol), University of Valencia, E-46980 Valencia, Spain
3. Instituto de Ciencia de Materiales de Aragón (ICMA), CSIC-University of Zaragoza, E-50009 Zaragoza, Spain
4. University Paris Saclay, Univ Paris Sud, CNRS, Ctr Nanosci & Nanotechnol, F-91120 Palaiseau, France

*Author for correspondence: aibarra@unizar.es

Keywords: 3D nanoprinting, electron tomography, He-FIB fabrication, hollow nanowires, superconductivity, TEM characterization, tungsten carbide

Superconductors allow the transport of electricity without energy losses. This property, makes possible applications such as energy generators and storage devices, high-frequency filters and switches and magnetic sensors. Their miniaturization, reaching the nanoscale in the range of their superconducting coherence length, makes appear novel physical phenomena[1] and can optimize their functionality. Moreover, the design of three-dimensional nanosuperconductors allows to conceive new schemes for such applications.

In this contribution, we introduce a novel template-free nano-lithography method to fabricate in a single-step nano-elements by means of focused ion beam induced deposition (FIBID) with arbitrary shape and in the three dimensions, opening fascinating novel routes in the fields of material science and nanotechnology.

Particularly, 3D superconducting crystalline WC nanotubes with controllable inner and outer diameters have been fabricated[2]. Their magnetotransport properties exhibit 1.5 times higher superconducting critical temperatures (6.4 K) as well as 1.5 times higher upper critical magnetic fields (≈14 T) when compared to nanowires grown by the analogous technique Ga^+ FIBID.

Transmission electron microscopy studies have been carried out in order to know the crystallographic structure and relate it with the superconductivity properties. Moreover, the relationship between the composition into the wire (growth parameters) and the structure has been analysed. On the other hand, the resulting hollow nanowire geometry produced by the highly focused He^+ beam, which confers them a high potential for applications in a broad range of fields, has been studied by electron tomography technique.

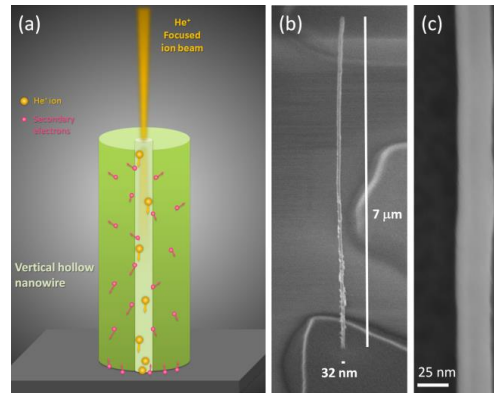

Figure 1. (a) Vertical growth of WC hollow nanowire using a He^+ FIB focused to ~1 nm. (b) SEM image of a vertical 3D WC hollow nanowire (52° tilted stage). (c) High magnification SEM image of the WC nanowire.

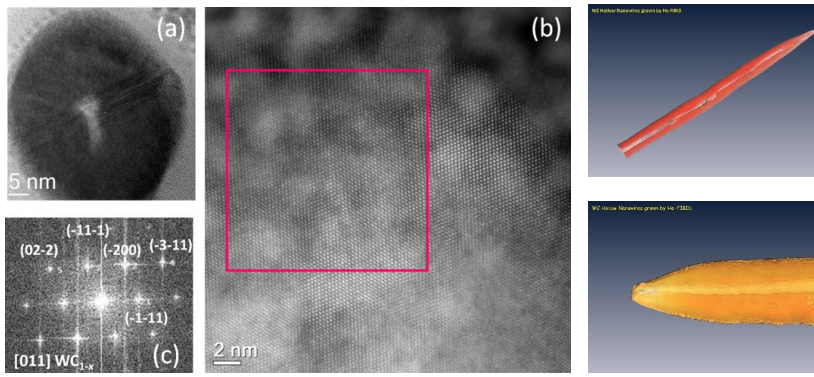

Figure 2. (a) HRTEM image of a cross-sectional view of a typical WC hollow nanowire. (b) HRSTEM image of a cross-sectional view of the WC nanowire in panel a. (c) Fast Fourier transform of the squared area in panel b, showing the crystalline nature of the material and indexed as the [011] zone axis of the FCC WC_{1-x} structure. (d and e) Tomography snapshot of the hollow nanowires.

References

1.- Córdoba R *et al.* (2013). *Nat. Commun.* 4: 1437
2.- Córdoba R *et al.* (manuscript in preparation)

MS-P04. Hierarchical porous Ni_3S_4 with enriched high-valence Ni sites as a robust electrocatalyst for efficient oxygen evolution reaction

Zhang T[1], Wan K[2], Luo J[2,3,5], Zhou C[2], Lu X[6], Mao B-W[5], Zhang X[3], Fransaer J[3], Arbiol J[1,4,*]

1. Catalan Institute of Nanoscience and Nanotechnology (ICN2), CSIC and BIST, Campus UAB, Bellaterra, 08193 Barcelona, Spain
2. Department of Materials Engineering, KU Leuven, Leuven 3001, Belgium
3. Collaborative Innovation Center of Clean Energy, Longyan University, Longyan 364012, China
4. ICREA, Pg. Lluís Companys 23, 08010 Barcelona, Spain
5. State Key Laboratory of Physical Chemistry of Solid Surfaces and Department of Chemistry, College of Chemistry and Chemical Engineering, Xiamen University, Xiamen 361005, China
6. MOE of the Key Laboratory of Bioinorganic and Synthetic Chemistry,The Key Lab of Low-carbon Chem and Energy Conservation of Guangdong Province, KLGHEI of Environment and Energy Chemistry, School of Chemistry, Sun Yat-Sen University, Guangzhou 510275, China

*Author for correspondence: arbiol@icrea.cat

Keywords: hydrogen evolution reaction (HER), metal-organic frameworks (MOFs), Ni_3S_4, oxygen evolution reaction (OER), water splitting

Hydrogen is an environmentally friendly and renewable energy carrier for green energy supply and storage. Hydrogen evolution reaction (HER), as the half reaction of electrochemical water splitting, is one way to produce hydrogen[1]. However, the sluggish kinetics of the oxygen evolution reaction (OER) that is the other half reaction of electrochemical water splitting significantly limits the overall energy conversion efficiency of water splitting[2]. Hence, it is urgent to develop high-efficient electrocatalysts for the OER in order to improve the overall efficiency of electrochemical water splitting[3]. In this work, an active and stable Ni_3S_4 architecture is designed as an advanced electrocatalyst for OER. The obtained Ni_3S_4 showed a large nanoflake structure with a uniform distribution of Ni and S, which was proved by electron energy loss spectroscopy (EELS). Meanwhile, the high-resolution transmission electron microscopy (HRTEM) images indicate that the nickel sulphide has a good crystallinity, which is in agreement with the cubic phase of Ni_3S_4 (space group: Fd3mS). In addition, this sample exhibited a relatively low overpotential of 257 mV at 10 mA/cm^2 and had a long-term stability due to the high concentration of Ni^{3+} and the meso–macro hierarchical porous structure. The water-splitting electrolyzer using the Ni_3S_4 as the anode catalyst and Pt/C as the cathode catalyst achieves a low cell voltage of 1.51 V at 10 mA/cm^2. Therefore, this work provides a new strategy for the rational design of active OER electrocatalysts.

References

1.- Wan K *et al.* (2019). *Adv. Func. Mater.* 29: 1900315
2.- Bo Y, Yujie S. (2018). *Acc. Chem. Res.* 51: 1571
3.- Wang J *et al.* (2017). *Adv. Mater.* 29: 1605838

MS-P05. The rocking phase plate – another step towards improved stability

Barragán Sanz K*, Irsen S

Research Center Caesar; Ludwig-Erhard-Allee 2, 53175 Bonn, Germany
*Author for correspondence: kristina.barragan@caesar.de

Keywords: cryo electron microscopy, phase contrast, phase plate, phase shift, single-particle analysis

Phase plates are promising tools for enhancing contrast, especially in cryo-transmission electron microscopy (cryo-TEM). As alternative to defocusing, contrast of weak phase objects -like most cryo samples- can be improved in close to focus images by inserting a phase plate into the back focal plane of the TEM[1]. The phase plate adds an additional phase shift of ideally π/2 to the scattered electrons and thus enhances image contrast. Their advantages for electron tomography and single particle acquisition have been demonstrated recently[2]. Nevertheless, phase plates are still no tool for routine application. This is mostly due to difficult handling and limited durability of actual phase plate designs.

For more than 15 years, carbon based Zernike phase plates have been the most used type [3]. Recently, a new type of hole free phase plates -Volta phase plate- has been made available. The hole free design has reduced ringing artifacts due to the missing hole edge. This is on cost of a variation of the phase shift over time.

Here, we present our experimental results from a rocking phase plate. We use a classical Zernike type phase plate which is based on a thin iridium film instead of carbon. This improves the long term stability of the phase plate.
To overcome the ringing artifact problem, we move the phase plate on a circular path during acquisition (see figure 1). This rocking mode virtually smooths the edge of the central hole. Additionally, the diameter of the central hole can be larger compared to classical Zernike phase plates which facilitates the positioning of the phase plate inside the TEM. The rocking mode is possible due to a special, piezo based positioning system, which can position the phase plate with nanometer precision[4].

We were able to show that the rocking mode settings can be used without interference of the phase plate hole edge during image recording. Furthermore, we could not find any resolution loss caused by the moving phase plate. Figure 2 shows a comparison between the phase plate in a) steady and b) rocking mode. No cutoff can be detected in the power spectra of the rocking phase plate in comparison to the power spectrum calculated from a micrograph recorded with a not moving phase plate.

In conclusion, the rocking mode could be an alternative method to acquire phase plate data. Currently, we are recording high-resolution single particle datasets to demonstrate up to which resolution the rocking phase plate can be used.

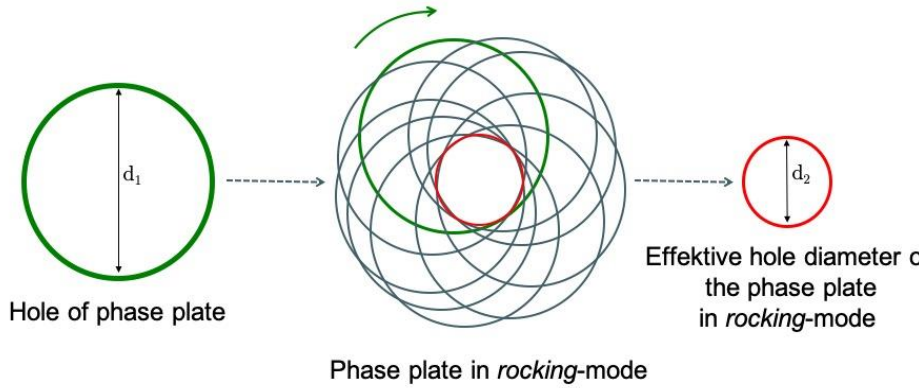

Figure 1. Illustration of the phase plate rocking mode.

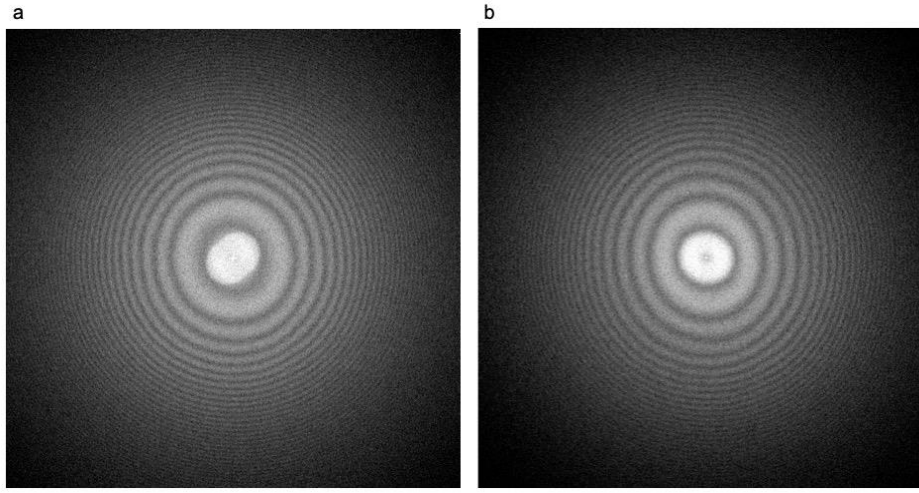

Figure 2. Power spectra of TEM-micrographs in a) steady mode and b) rocking mode.

References

1.- Danev R, Nagayama K. (2001). *J. Phys. Soc. Jpn.* 70: 696
2.- Fan X *et al*. (2017). *Structure* 25: 1623
3.- Nagayama K, Danev R. (2008). *Philos. Trans. R. Soc. Lond. B Biol. Sci.* 363: 2153
4.- Kurth P *et al*. (2014). *Microsc. Microanal.* 20: 220-221

MS-P06. TEM characterization of nanocomposite polymer membranes with MOF fillers for nanofiltration

Navarro M[1,2,*], Paseta L[1], Echaide, C[1], Benito J[3], Gascón I[3], Coronas J[1,4], Téllez C[1,4]

1. Instituto de Nanociencia de Aragón (INA) and Chemical and Environmental Engineering Department, Universidad de Zaragoza, 50018 Zaragoza, Spain
2. Laboratorio de Microscopías Avanzadas (LMA), Edificio I+D, C/ Mariano Esquillor s/n, 50018 Zaragoza, Spain
3. Departamento de Química Física, Facultad de Ciencias, Universidad de Zaragoza, 50009 Zaragoza, Spain
4. Instituto de Ciencia de Materiales de Aragón (ICMA), CSIC-Universidad de Zaragoza, 50018 Zaragoza, Spain
*Author for correspondence: martanv@unizar.es

Keywords: electron diffraction, interfacial polymerization, metal organic framework, sample preparation, STEM-EDS/EELS, TEM, thin film nanocomposite membrane

Thin film composite (TFC) membranes consist of a polyamide (PA) thin film (35-100 nm thick) as a selective layer, grown via interfacial polymerization (IP) of monomeric acid chlorides and amines on top of an asymmetric polyimide support, cast over a polypropylene non-woven backing material by phase inversion[1]. This type of membrane is very competitive for organic solvent nanofiltration, where chemical stable polymers are mandatory. In order to increase membrane flux without decreasing rejection, nanoparticles are incorporating during the IP process, giving rise to Thin film nanocomposite (TFN) membranes (Fig. 1a). Their performance is determined by the structural and physicochemical properties of the fillers and PA thin film. Metal organic frameworks (MOFs), built from organic linkers and metal-containing clusters, have been extensively included as fillers in TFN membranes[2], showing exceptional affinity with polymer chains and improved solvent permeation.

The combination of nanoscale visualization via conventional Transmission electron microscopy (TEM) and Scanning transmission electron microscopy (STEM), and spectroscopic analysis via energy dispersive X-ray spectroscopy (EDX) and Electron energy loss spectroscopy (EELS), are some of the most potent techniques for shedding further light into the connection between the nanostructure of the MOF-PA film and their transport and rejection properties[3].

Sample preparation is a key step to examine the presence, distribution and morphology of MOF nanoparticles within the PA film, but also to confirm their crystallinity after the IP process by electron microscopy, given the multilayer and heterogeneous character of these membranes and but also because of the beam-sensitive nature of MOFs. Here, we report different sample preparation protocols for applying TEM, STEM-EDS/EELS and electron diffraction depending on the nature of the TFN sample and on the characterization aim:

1. When the aim was to confirm the presence, distribution and morphology of two types of MOFs of different chemical composition in the PA layer, a fragment of the MOF-PA film was detached from the polyimide support in the last stage of the IP process. The fragment was removed from the distilled water bath and placed onto a carbon film grid. TEM and STEM-EDS techniques were applied[4].
2. When the objective was to check the distribution of the MOF nanoparticles within the TFN membrane and their crystallinity, a MOF-TFN membrane was synthesized over a non-crosslinked polyimide support without backing material. Then, the membrane was immersed in N,N-dimethylformamide at room temperature for 5 min to dissolve the polyimide support. The separated PA top layer was placed onto a carbon film grid. TEM and electron diffraction were applied[5].
3. When the goal was to verify the presence of a defect free MOF monolayer film in between the two polymer layers (Fig. 1b), transferred by the Langmuir-Schaefer (LS) technique, a lamella (~80 nm thick) was obtained from the upper 2 μm of the TFN membrane using cryo-focused ion beam (FIB) equipment (Dual Beam 3 Nova 200) and Ga atoms for the etching. STEM-EDS/EELS techniques were applied (Fig. 1c)[6].

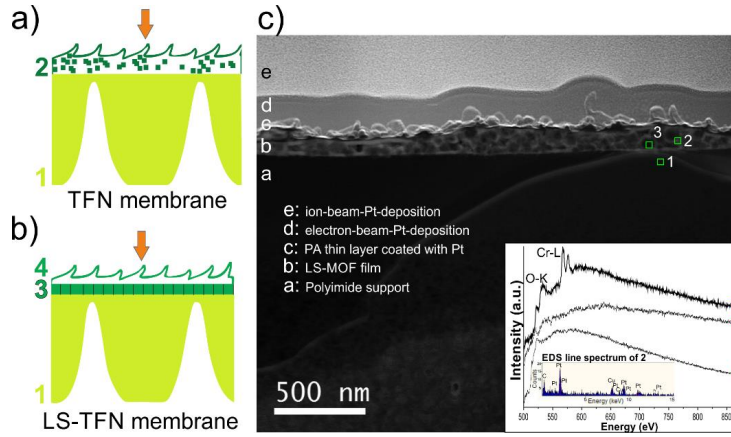

Figure 1. a) TFN and **b)** LS-TFN membranes and their components: (1) polyimide support, (2) PA layer with MOFs, (3) LS-MOF monolayer, and (4) PA layer and MOFs inside. Orange arrows show the flux direction. **c)** STEM images of the LS-TFN lamella. 1, 2, and 3 indicate areas where EELS and EDS spectrum images have been collected.

References

1.- Vandezande P *et al*. (2008). *Chem. Soc. Rev.* 37: 365
2.- Sorribas S *et al*. (2013). *J. Am. Chem. Soc.* 135: 15201
3.- Pacheco FA *et al*. (2010). *J. Membr. Sci.* 358: 51
4.- Echaide-Gorriz C *et al*. (2017). *Dalton Trans.* 46: 6244
5.- Paseta L *et al*. (2019). *J. Ind. Eng. Chem.* (in press). DOI: 10.1016/j.jiec.2019.04.057
6.- Navarro M *et al*. (2018). *ACS Appl. Mat. Interfaces* 10: 1278

Acknowledgements

Financial support from the Research Project MAT2016-77290-R (MINECO/AEI/FEDER, UE) is gratefully acknowledged.

MS-P07. Study of epitaxy in proximity coupled semiconductor - ferromagnetic insulator - superconductor heterostructures for majorana-based topological quantum computing

Koch C[1,*], Liu Y[2], Martí-Sánchez S[1], Krogstrup P[2], Arbiol J[1,3]

1. Catalan Institute of Nanoscience and Nanotechnology (ICN2), CSIC and BIST, Campus UAB, Bellaterra, 08193 Barcelona, Catalonia, Spain
2. Center for Quantum Devices, Niels Bohr Institute, University of Copenhagen & Microsoft Quantum Materials Lab Copenhagen, Denmark
3. ICREA, Pg. Lluís Companys 23, 08010 Barcelona, Catalonia, Spain
*Author for correspondence: christian.koch@icn2.cat

Keywords: electron energy loss spectroscopy, epitaxy, ferromagnetic insulator, geometrical phase analysis, nanowire, semiconductor, superconductor, topological quantum computing, transmission electron microscopy

One of the current endeavors in quantum technology consists of the development of topological quantum computers, which stand out as promising candidates because, contrary to the quantum states of ordinary individually trapped particles such as electrons, the topological properties of the quantum system ensure a higher stability when subjected to small perturbations[1]. Among the different classes of topological states, the so-called Majorana bound states are of great interest, as signatures of their appearance have been observed recently in hybrid III-V semiconductor-superconductor nanowires[2-3].

A way to induce the topological properties, without the need of external magnetic fields that could modify the band structure of the nanowire, is given by the coupling to ferromagnetic insulators. Composite tri-crystals of semiconductor-ferromagnetic insulator-superconductor materials, such as InAs-EuS-Al, have been proposed to overcome the challenge of building adequate topological systems4, where the absence of crystal defects and impurities, particularly at the interfaces between materials, is of extreme importance[5-6].

Therefore, our work is centered around the study of the crystal quality of the nanostructures, especially focusing on the epitaxial relationship between the composing materials. Mainly by the means of High-angle annular dark-field (HAADF) imaging in Scanning Transmission Electron Microscopy (HAADF-STEM), where we analyze the crystal phases and interfaces at atomic scale and check the coupling of different materials atom by atom (column), combined with Electron Energy Loss Spectroscopy (EELS) in order to gain data on the chemical composition distribution, we study nanostructures grown by different techniques, in varying geometrical layouts and growth conditions.

Namely, we have analyzed vertically grown nanowires of InAs by the Vapor-Liquid-Solid (VLS) method, with selective covering of the several facets with EuS and Al to

observe possible favored crystal orientations depending on the faceting, planar samples of EuS layers grown on InAs by Molecular Beam Epitaxy (MBE), which is the preferred synthesis method due to its ultra-pure environment, and also the growth of InAs on GaAs substrate in the form of nanowires forming networks created by the method of Selective Area Growth (SAG)[7-10], since the development of said networks is one of the final goals for the construction of the logic gates used for the calculations in a topological quantum computer. By applying Geometric Phase Analysis (GPA) to HAADF-STEM micrographs with atomic resolution, we are able to detect structural defects and deformations, such as twin boundaries, misfit dislocations, rotation and compression/dilatation within the crystal phases of these nanostructures.

References

1.- Collins G. (2006). *Sci. Am.* 294 (4): 56
2.- Albrecht SM *et al*. (2016). *Nature* 531: 206
3.- Lutchyn RM *et al*. (2010). *Phys. Rev. Lett.* 105: 077001
4.- Sau JD *et al*. (2010). *Phys. Rev. Lett.* 104: 040502
5.- Krogstrup P *et al*. (2015). *Nat. Mat.* 14: 400
6.- Chang W *et al*. (2015). *Nat. Nanotech.* 10: 232
7.- Friedl M *et al.* (2018). *Nano Lett.* 18: 2666
8.- Krizek F *et al.* (2018). *Phys. Rev. Mat.* 2: 093401
9.- Vaitiekėnas S *et al.* (2018). *Phys. Rev. Lett.* 121: 147701
10.- Aseev P *et al.* (2019). *Nano Lett.* 19: 218

MS-P08. Study of structural variations in the homologous series $Na_xGa_{4+x}Ti_{n-4-x}O_{2n-2}$ by electron microscopy techniques: influence on its luminescent properties

García-Fernández J[1,*], García-Carrión M[2], Torres-Pardo A[1], Martínez-Casado R[2], Ramírez-Castellanos J[1], Nogales E[2], Méndez B[2], González-Calbet JM[1,3]

1. Departamento de Química Inorgánica, Facultad de Ciencias Químicas, Universidad Complutense de Madrid, 28040 Madrid, Spain
2. Departamento de Física de Materiales, Facultad de Ciencias Físicas, Universidad Complutense de Madrid, 28040 Madrid, Spain
3. ICTS Centro Nacional Microscopía Electrónica, Universidad Complutense de Madrid, 28040 Madrid, Spain

*Author for correspondence: javgar07@ucm.es

Keywords: optical properties, transparent semiconductor oxides, tunnel superstructures, scanning transmission electron microscopy, sodium-gallium-titanium oxides

The Na-Ga-Ti-O system has attracted particular interest due to their multifunctional features, especially as potential materials in batteries and photocatalysts[1-2]. In this contribution, we have addressed the synthesis, characterization and study of optical properties of the homologous series with chemical composition $Na_xGa_{4+x}Ti_{n-4-x}O_{2n-2}$ (n = 5, 6 and 7 with x ≈ 0.7, labelled as NGT1, NGT2 and NGT3, respectively). The X-ray diffraction characterization shows that the NGT1 and NGT2 terms crystallize in the space group C2/m, while the n = 7 member does in the Pbam. Electron microscopy images by STEM-HAADF mode and their corresponding EELS "mappings" show that those terms are formed by an ordered intergrowth of β-Ga_2O_3 chains and TiO_6 octahedra (Figure1a). On the other hand, the NGT3 member is formed by TiO_6 octahedra that share vertices with GaO_4 tetrahedra and GaO_6 octahedra. In all cases, hexagonal or orthogonal tunnels are formed, where the Na^+ cation is visualized in the centre by ABF mode.

These structural characteristics are directly related to their optical properties. The luminescence bands have been studied by cathodoluminescence (CL) and photoluminescence (PL) techniques. In the case of terms NGT1 and NGT2 the luminescent spectra are composed by a broad band in the visible range, centred on 2.5 eV, and less intense bands in the UV range (3.7 - 4.8eV). However, for the term NGT3, a band in the infrared range is observed, at 1.5 eV, as well as a band wider but less intense in the visible, centred at 2.8 eV (Figure 1b). Finally, the values of the band gap, by PL of excitation (PLE), have been obtained, which have been confirmed by simulations by the Density Functional Theory (DFT) method. This characterization confirms the structural-properties relationships. These results can widen the performance and applicability of these materials in the field of tunable optoelectronic devices.

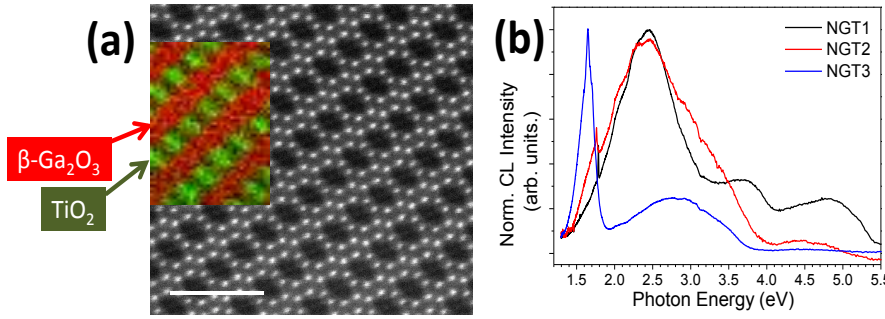

Figure 1. (a) HAADF image and EELS mapping of NGT2 sample along [010]. (b) CL spectra of all oxides.

References

1.- Edwards DD, Empie NH, Meethong N, Amoroso JW. (2006). *Solid State Ionics* 177: 1897-1900
2.- Sanford S, Misture ST, Edwards DD, (2013). J. Solid State Chem. 200(2013)189–196.

MS-P09. Transmission electron microscopy investigation of graphene oxide flakes

Hettler S[1,*], David Valenzuela S[1], Arenal R[1,2,3]

1. Laboratorio de Microscopías Avanzadas, Instituto de Nanociencia de Aragón, Universidad de Zaragoza, Zaragoza, Spain
2. ARAID Foundation, Zaragoza, Spain
3. Instituto de Ciencias de Materiales de Aragón, CSIC-Univ. Zaragoza, 50009 Zaragoza, Spain
*Author for correspondence: hettler@unizar.es

Keywords: electron energy-loss spectroscopy, graphene oxide, transmission electron microscopy

A significant amount of research has been done on (reduced) graphene oxide ((r)GO) due to its controllable properties and because it is widely used as a starting point for graphene production and functionalization[1]. Although the chemical model of GO is very complex[2], it is well established that its properties are mainly controlled by the different functional groups present, the percentage of incorporated oxygen and the ratio between sp2 and sp3-hybridized C bonds[3].

Here we present our experimental results on transmission electron microscopy (TEM) investigation of GO acquired with an image-corrected FEI Titan3 operated at 80 kV. Using TEM imaging, electron diffraction and electron energy-loss spectroscopy (EELS), GO can be characterized in detail and properties such as composition, size, thickness or fraction of sp2-hybridized C bonds can be determined with high spatial resolution.

Figure 1 shows a TEM image of a GO flake with a size of about 3 µm suspended on an amorphous carbon film. Three EEL spectra showing the background-corrected C-K edge of different GO flakes are depicted in Figure 2. The C-K edge exhibits a sharp pre-peak at 284 eV, whose intensity corresponds to the fraction of sp2-hybridized C bonds, followed by a broad peak starting at 290 eV. The spectra were acquired using a selected-area aperture in order that the EEL signal only stems from a small sample area. While the black line shows a spectrum of a highly oxidized flake (17 %), the red and green curves were obtained from flakes with a low oxygen content.

In summary, TEM is highly suited for an in-depth analysis of GO. The obtained information on structure, composition and alien material present in the GO allows to better understand the macroscopic properties of GO and its use in applications.

Figure 1. TEM image of GO flake. Scale bar is 400 nm.

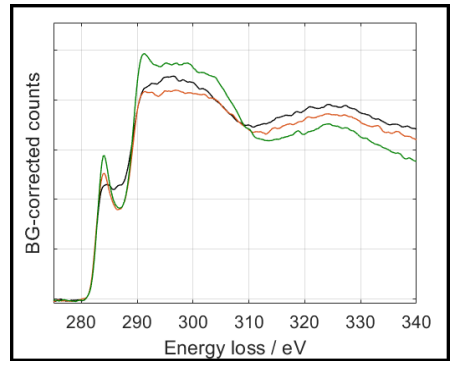

Figure 2. Comparison of EEL spectra of GO flakes with different ratio between sp2 and sp3-hybridized C bonds.

References

1.- Mao S *et al*. (2012). *RSC Adv*. 2: 2643
2.- Boukhvalov DW, Katsnelson M. (2009). *J. Am. Chem. Soc.* 130: 10697
3.- Gross K *et al*. (2016). *Nanotech.* 27: 365708

Acknowledgements

Research supported by the Spanish MINECO (MAT2016-79776-P, AEI/FEDER, EU), Government of Aragon through project DGA E13_17R (FEDER, EU) and European Union H2020 programs "ESTEEM3" (823717), Flag-ERA GATES (JTC 2017) and Graphene Flagship (785219).

MS-P10. Comparative characterization of selective-area growth and vapour-liquid-solid III-V semiconductor-superconductor nanowire networks for topological quantum computing

Botifoll M[1,2,*], Martí-Sánchez S[1], Yücelen E[2], Caroff P[2], Arbiol J[1,3]

1. Catalan Institute of Nanoscience and Nanotechnology (ICN2), CSIC and BIST, Campus UAB, Bellaterra, 08193 Barcelona, Catalonia, Spain
2. Microsoft Station Q at Delft University of Technology, 2600 GA Delft, Netherlands
3. ICREA, Pg. Lluís Companys 23, 08010 Barcelona, Catalonia, Spain
*Author for correspondence: marc.botifoll@icn2.cat

Keywords: InSb-Al heterojunction, nanowire networks, selective-area growth (SAG), strain, topological quantum computing

The fabrication of reproducible and defect-free nanowire networks with a semiconductor-superconductor heterojunction is a crucial step that needs to be achieved to generate stable enough Majorana states for topological quantum computing.

Current approaches involve direct vertical growth of the nanowires by vapour-liquid-solid (VLS), which are arranged in networks due to the growth on tilted surfaces and their coincidence during the growth process, forming only a limited number of interconnections[1]. However, this process has obvious limitations in terms of planar integration and manipulation of the individual nanowires. On the other hand, in order to overcome the practical limitations of this method, alternative horizontal (on-plane) growth processes have arisen in the last few years, being guided growth (GG) and selective-area growth (SAG) the most promising ones[2-6].

On this basis, SAG by means of molecular beam epitaxy (MBE) is being widely studied for the growth of III-V semiconductors, mainly InAs and InSb, in perfect epitaxy with the superconducting metallic layer that is typically formed by aluminium[6]. Therefore, a detailed characterization of the interface between InSb and Al in SAG nanowire networks, as well as VLS ones, is presented and compared, in order to shine light on the strain mechanisms involved in their growth mechanisms and their origin in terms of growth methods.

References

1.- Gazibegovic S *et al.* (2017). *Nature* 548: 434
2.- Oksenberg E *et al.* (2017). *ACS Nano 11:* 6155
3.- Friedl M *et al.* (2018). *Nano Lett.* 18: 2666
4.- Krizek F *et al.* (2018). *Phys. Rev. Mat.* 2: 093401
5.- Vaitiekėnas S *et al.* (2018). *Phys. Rev. Lett.* 121: 147701
6.- Aseev P *et al.* (2019). *Nano Lett.* 19: 218

MS-P11. The characterization of the process of electrochemical oxidation of Cu_2S into CuO nanowires by using transmission electron microscopy

Han X[1,*], Zhang T[1], Zuo Y[2,3], Liu Y[4], Sivula K[4], Cabot A[2,5], Arbiol J[1,5]

3. Catalan Institute of Nanoscience and Nanotechnology (ICN2), CSIC and BIST, Campus UAB, Bellaterra, 08193 Barcelona, Spain
4. Catalonia Institute for Energy Research – IREC, Sant Adrià de Besòs, Barcelona 08930, Spain
5. Departament d'Electronica, Universitat de Barcelona, 08028 Barcelona, Spain
6. Laboratory for Molecular Engineering of Optoelectronic Nanomaterials (LIMNO), École Polytechnique Fédérale de Lausanne (EPFL), Station 6, CH-1015 Lausanne, Switzerland
7. ICREA, Pg. Lluís Companys 23, 08010 Barcelona, Spain
*Author for correspondence: xu.han@icn2.cat

Keywords: HRTEM, metal chalcogenides, metal oxides, oxygen evolution, STEM

Transition metal oxides and hydroxides serving as the main alternative to the corresponding noble metals play an enormous role in catalytic conversion. There are many methods to synthesize these nanostructures[1]. Compared with metal oxides, metal chalcogenides are thermodynamic unstable and are inclined to transform into more stable oxides or hydroxides during oxygen evolution in alkaline media. Interestingly, the transformation of structures and chemical compositions of the copper sulfides makes corresponding copper oxide display high electrocatalytic performance. The detailed TEM-STEM characterization and EELS chemical analysis at the nanoscale has been employed to elucidate the formation and morphology evolution of this transformation. By studying the mechanism of this electrochemical oxidation process, we could get more information about intermediate stages which could be extended to more systems.

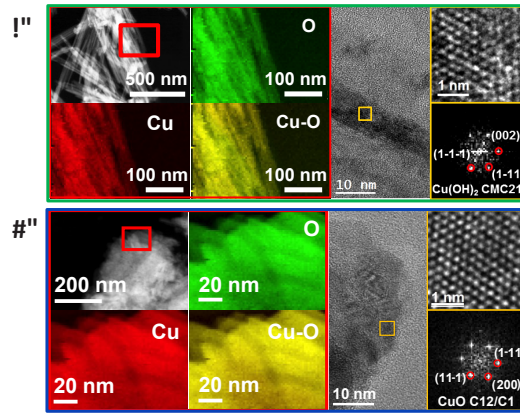

Figure 1. EELS chemical composition maps and HRTEM micrograph of $Cu(OH)_2$ and CuO.

References

1.- McCrory CCL *et al*. (2015). *J. Am. Chem. Soc.* 137 (13): 4347

MS-P12. Atomically resolved La-Mn-O nanomanganites

Ruiz-González ML[1,*], Cortés-Gil R[1], Sigcho Villacís K[1], Azor Lafarga A[1], Alonso J[2], González-Calbet JM[1]

1. Departamento de Química Inorgánica, Facultad de Ciencias Químicas, UCM, 28040 Madrid, Spain
2. Instituto de Ciencia de Materiales, CSIC, Sor Juana Inés de la Cruz s/n, 28049 Madrid, Spain
*Author for correspondence: luisarg@ucm.es

Keywords: aberration-corrected electron microscopy, defects, EELS, nanomanganites, magnetoresistance

Manganese related perovskites occupy a prominent play among the functional advanced materials because of their magnetoresistant properties. Reducing the particle size to the nanoscale has brought to light new magnetic and electric behaviors in $La_{1-x}A_xMnO_3$ related systems[1], which in order to be explained requires a deep effort of syntheses and characterization. Here we present some preliminary results on the study of simplest system, in terms of composition, La-Mn-O. Nanoparticles of $LaMnO_3$ nominal composition were prepared using a molten salt approach[2]. The XRD study shows the presence of broad diffraction peaks that can be indexed on the basis of a perovskite cell, while low TEM confirms the stabilization of particles of nanometric size (figure 1 a). Average compositional study, by means of EMPA and, more locally, EDS, indicated the presence of cationic vacancies either at the La and Mn sublattices. In order to go deeper in this characterization, we have performed an atomically resolved STEM-HAADF-EELS study in the individual nanoparticles (figure 1b) revealing the presence of defects as well as the coexistence of Mn^{3+} and Mn^{4+} according to the presence of cationic vacancies and also in agreement to the observed magnetic behavior.

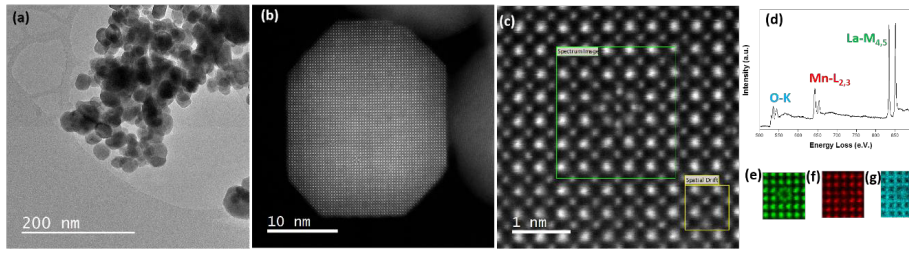

Figure 1. (a) Low magnification TEM (b) HAADF image of an individual particle (c) High resolution HAADF of an area of b (d) Sum spectra corresponding to the area marked in d (e-g) chemical maps showing the La, Mn and O distribution.

References

1.- Gao X *et al*. (2016). *Nature Comm.* 7: 11260
2.- N'Goc T *et al*. (2017). *Adv. Mater.* 29: 1604745

MS-P13. Crystal structure and local ordering in epitaxial Fe1 00−xGax/MgO (001) films

Ibarra A[3,4,*], Ciria M[1,2], Proiettia MG[2], Corredor EC[1,2], Coffey D[1,2], Begué A[1,3], de la Fuente C[1,2], Arnaudas JI[2,3,4]

1. Instituto de Ciencia de Materiales de Aragón, Consejo Superior de Investigaciones Científicas, Zaragoza, Spain
2. Dep. Física de la Materia Condensada, Universidad de Zaragoza, Zaragoza, Spain
3. Instituto de Nanociencia de Aragón, Universidad de Zaragoza, Zaragoza, Spain
4. Laboratorio de Microscopias Avanzadas (LMA), Universidad de Zaragoza, Zaragoza, Spain

*Author for correspondence: aibarra@unizar.es

Key Words: EXAFS, Fe-Ga alloys, RHEED, TEM, thin films, X-ray diffraction

Iron-gallium alloys (Fe100−xGax) have become an important material for magnetostrictive applications because of their large tetragonal magnetostriction at low field for alloys around 18.4 % Ga[1], whereas, at the same time, they provide good corrosion resistance and mechanical hardness[2]. Large magnetoelastic (ME) coupling is a rewarding property in thin films and patterned elements, as the ME anisotropy can control the orientation of the magnetization M. Epitaxial Fe100−xGax thin films have shown a remarkable potential for microwave and energy conversion applications[3], by using a piezoelectric layer to control the magnetic anisotropy through the modification of the strain in the magnetic layer by means of an applied voltage.

In this work we present a study of the structural properties of Fe100−x Gax (x<30) films grown by Molecular Beam Epitaxy on Mg0(100). We combine long range and local/chemically selective X-ray probes (X-ray Diffraction and X-ray absorption spectroscopy) together with real space imaging by means of Transmission Electron Microscopy and surface sensitive in situ Reflected High Energy Electron Diffraction. For substrate temperature Ts below 400ºC we obtain bcc films while, for x ≈ 24 and Ts ≥ 400ºC the nucleation of the fcc phase is observed. For both systems a Ga anticlustering or local range ordering phenomenon appears. The Ga/Fe composition in the first and second coordination shells of the bcc films is different from that expected for a random Ga distribution and is close to a $D0_3$ phase, leading to a minimization of the number Ga-Ga pairs. On the other side, a long-range $D0_3$ phase is not observed indicating that atomic ordering only occurs at a local scale.

Overall, the epitaxial growth procedure presented in this work, first, avoids the formation of a long range ordered $D0_3$ phase, which is known to be detrimental for magnetostrictive properties, and second, demonstrates the possibility of growing fcc films at temperatures much lower than those required to obtain bulk fcc samples (see figure 1).

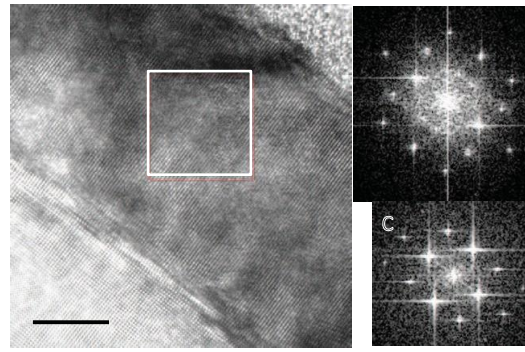

Figure 1. (a) Transmission electron microscopy image of the S1-24 film showing the MgO and FeGa layer perpendicular to the [110] direction. (b) FFT of the area marked in (a), corresponding to the FeGa film and (c) FFT of the MgO.

References

1.- Clark AE *et al*. (2003). *J. Appl. Phys.* 93 (103): 8621
2.- Atulasimha J, Flatau AB. (2011). *Smart Mater. Struct.* 20 (4): 043001
3.- Dan Onuta T *et al*. (2011). *Appl. Phys. Lett.* 99 (20): 10

MS-P14. Atomic structure of defects in GaSe/InSe heterostructure

Grzonka J[1,*], Claro M[1], Sadewasser S[1], Ferreira PJ[1,2,3]

1. INL - International Iberian Nanotechnology Laboratory, Av. Mestre José Veiga s/n, 4715-330 Braga, Portugal
2. Mechanical Engineering Department and IDMEC, Instituto Superior Técnico, University of Lisbon, Av. Rovisco Pais, 1049-001 Lisboa, Portugal
3. Materials Science and Engineering Program, The University of Texas at Austin, TX 78712, USA
*Author for correspondence: justyna.grzonka@inl.int

Keywords: GaSe, InSe, MBE, STEM

Large area epitaxy growth of two-dimensional (2D) layered materials is an important step in realizing novel device applications. The properties of 2D materials are usually very different from their 3D counterparts, which has resulted in the creation of many other 2D atomic crystals. Stacking different 2D crystals together may cause charge redistribution between the neighboring crystals in the stack or they can induce structural changes within each other. The use of semiconducting monolayers leads to the creation of optically active heterostructures. Most of the 2D heterostuctures are built by direct stacking of individual monolayer flakes of different materials. The direct growth of heterostructures by molecular beam epitaxy (MBE) or chemical vapor deposition (CVD) can accelerate that process[1].

Both gallium selenide (GaSe) and indium selenide (InSe) belongs to the group of layered III-VI binary chalcogenides, which crystallize in hexagonal-type structures. Each layer contains four monoatomic sheets – two layers of either Ga or In sandwiched between two layers of Se. Each Ga or In atom is bound through covalent bonds with three equally distant neighboring Se atoms and with the equivalent metal atom, Ga or In, bounded to another three Se atoms. There are no dangling bonds in this system therefore such layers are bonded together through weak van der Waals interactions. That weak inter-layer interaction allows the formation of several polytypes, due to possible different stacking sequences of the layers along the c direction. Both GaSe and InSe are layered materials and it was found that twinning and stacking disorder can be easily introduced during the growth. An understanding of how these defects are related to the atomic structure and properties is currently lacking. In this context, the use of advanced atomic resolution TEM/STEM is critical, as it allows us to observe the defect structure at the atomic scale.

In this study the growth of GaSe/InSe epilayer on c-plane sapphire substrates was performed by the MBE method. The observations of the atomic structure were conducted by HAADF STEM, as it provides Z contrast and allows us to distinguish the metal atoms of In and Ga sandwitched between Se atoms. The STEM observations show that the growth starts from nucleating domains which further coalescence and

create a continuous film. The high density of stacking faults was observed. The EDS measurements show that within the GaSe layer a strong interdiffusion of In occurs at the GaSe/InSe interface. The aim of this research is to fundamentally understand the behaviour of GaSe and InSe growth in the context of creating 2D heterostructures. The results of this study can be used to design GaSe/InSe heterostructures at the atomic scale with desired properties for different applications.

References

1.- Novoselov KS *et al*. (2016). *Science* 353: aac9439

LS-P01. Cytoskeletal scaffolding proteins as modulators of the functional responses of thylakoid membranes

Jiménez-López JC[1,2,3*]

1. Dept. Biochemistry, Cell & Molecular Biology of Plants, Estación Experimental del Zaidín, Spanish National Research Council (CSIC); Profesor Albareda 1, Granada 18008, Spain.
2. The UWA Institute of Agriculture and School of Agriculture and Environment, The University of Western Australia, 35 Stirling Highway, Crawley, Perth, WA, 6009, Australia.
3. Department of Biological Sciences, Purdue University, 201 S. University Street, West Lafayette 47907-2064 (IN) USA.
*Author for correspondence: josecarlos.jimenez@eez.csic.es

Keywords: actin dynamics, cytoskeletal membrane-associated proteins, actin-ABPs signalling, capping protein, F-actin, thylakoids membranes

The actin cytoskeleton is a dynamic structure, and a major regulator of cell morphogenesis, and cellular responses to extracellular stimuli. Cytoskeletal functioning is coordinated through a plethora of actin-binding proteins (ABPs)[1]. Heterodimeric capping protein (CP) is a major actin cytoskeleton regulator through direct interaction with phosphatidic acid, a major component of plant membranes, and its association with plant cell membranes[2].

Plant physiological processes rely mainly on energy, which depends on the light efficient capture and conversion by the chloroplast throughout its optimal photosynthetic performance in response to different environmental light conditions. Lack or excess of light can have negative effects on plants, and remodelling of thylakoid membranes in response to different illumination can be considered as one of the fundamental processes for the regulation of photosynthesis and photo-protection for light damage.

Despite the significance of plant cytoskeleton in the actin-based chloroplast movement (anchoring/positioning) and its role in the chloroplast import apparatus, there is no information so far linking actin cytoskeleton dynamics and photosynthesis associated functional and mechanical processes. The aim of this study was to elucidate this functional association.

Complementary biochemical and microscopy approaches were used to elucidate possible CP-membrane particular association with membrane-bound chloroplast organelle fractions in Arabidopsis leaf.

The outcomes of this study are helping to demonstrate the functional and structural role of cytoskeleton dynamics in thylakoid membranes and their photosynthesis associated processes. The results demonstrated for the first time the presence of cytoskeletal elements in chloroplast internal components (stroma and thylakoids), and the potential functional interactions between cytoskeleton and thylakoid elements, and the involvement of cytoskeleton in the maintenance and repairing processes of

thylakoid membranes for light damage. This will add a new layer of complexity to the chloroplast mechanisms to perform adequate responses of the photosynthetic machinery to light stress.

References

1.- Jiménez-López JC *et al*. (2011). ICAR 2011, Book of abstracts, communication no. 301
2.- Jiménez-López JC *et al*. (2014). *Plant Physiol.* 166 (3): 1312

Acknowledgements

This study was partially funded by the Physical Biosciences program of the Office of Basic Energy Science, US Department of Energy grant ref. DE-FG02-04ER15526; and by the Spanish MINECO grant ref. RYC-2014-16536 (Ramon y Cajal Research Program) to JCJ-L. Author thanks Purdue University and Prof. CJ Staiger for various antibodies kindly provided for this study.

LS-P02. Functional association between storage proteins mobilization and redox metabolism signalling in narrow-leafed lupin (*Lupinus angustifolius*) cotyledons driving seed germination and seedling development

Lima-Cabello E, Rodriguez-Pöhnlein AM, Molina-Borrego F, Alché JD, Jiménez-López JC*

1. Dept. Biochemistry, Cell & Molecular Biology of Plants, Estación Experimental del Zaidín, Spanish National Research Council (CSIC); Profesor Albareda 1, Granada 18008, Spain.
2. The UWA Institute of Agriculture and School of Agriculture and Environment, The University of Western Australia, 35 Stirling Highway, Crawley, Perth, WA, 6009, Australia.
*Author for correspondence: josecarlos.jimenez@eez.csic.es

Keywords: sweet lupin seeds, cotyledon, 7S-type globulin, vicilin, glutathione, redox signalling

Narrow-leafed lupin or NLL (*Lupinus angustifolius*) is characterized by multiple agricultural benefits such as the protective function of seed β-conglutin proteins against necrotrophic pathogens attack[1]. It is also characterized by its adaptation to drought stress. However, desiccation tolerance is an essential process that has to be achieved during seed maturation as adaptive strategy to enable seed survival during storage and to cope with severe environmental conditions, and to yield seeds of high germination potential.

Numerous events at cellular and biochemical level, such as the formation of specialized storage organelles, synthesis and accumulation of storage proteins, adequate mobilization of seed storage compounds upon imbibition, particularly proteins from conglutins families in the case of NLL[2], oligosaccharides, and activation of antioxidant capacity of scavenging ROS for avoiding deleterious damage, appear associated with the acquisition of desiccation tolerance of seeds.

Furthermore, redox metabolism activation is crucial processes to set proper conditions for seed germination, seedling establishment and plant growth. Thus, antioxidant enzymes have been considered of particular importance for acquiring seed maturation and the capacity of germination (vigour).

Despite the importance of these physiological cues for breaking dormancy leading the seed to germinate, little information is known about regulatory features underlying biochemical, molecular and signalling processes taking place during NLL seed germination[3].

The aims of this study are to 1) characterize the cellular changes occurring in *NLL* cotyledons during and after germination; 2) determine the composition and pattern of proteins (conglutins α, β, γ and δ) mobilization from storage membrane-surrounded organelles, and genes expression during transformation of the cotyledons tissue into leaf-like photosynthetic (autotropic) organs; and 3) determine the extent of redox

metabolism changes, as regulator of ROS-dependent signalling driving NLL seed germination and seedling growth.

The study outcomes evidence functional changes of key molecular and regulatory signalling pathways and the implications of particular isoforms of conglutin α, β and γ proteins as key players in functional and metabolic changes, and regulatory networking underlying morphogenesis and developmental processes closely-related to the seed germination capability. Such processes are taking place after dormancy breaking and during the initial germination stages.

References

1.- Jiménez-López JC *et al*. (2016). *Front. Plant Sci*. 7: 1856

2.- Foley RC *et al*. (2015). *BMC Plant Biol.* 15: 106

3.- Lima-Cabello E *et al*. (2017). ICLGG 2017, Book of abstracts, communication no. ICLGG2017/P/67

Acknowledgements

This study was partially funded by the EU Marie Curie grant PIOF-GA-2011-301550, the Spanish MINECO grants RYC-2014-16536 (Ramon y Cajal Research Program) and BFU2016-77243-P, and by the CSIC - Intramural project ref. 201540E065.

LS-P03. How three enzymes play during the long famine in terrestrial snails

Porcel D.

Centro de Instrumentación Científica, Universidad de Granada. Calle Profesor Ossorio s/n, Campus Fuentenueva. 18071 Granada, Spain
*Author for correspondence: dporcel@ugr.es

Keywords: acid phosphatase, alkaline phosphatase, digestive gland, esterase, snail, starvation

A seasonal pattern of the enzyme activity in the process of starvation (induced in laboratory) was studied in the terrestrial snail *Helix aspersa*. In natural conditions, specimens suffer latency due to the environmental conditions and the availability of food. The snails were kept in starvation in a laboratory under controlled conditions. We studied how the physiology of the cells of the digestive gland changed during this period. By following these procedures, we show the distribution of hydrolytic enzymes in the digestive gland and how it changed for 12 months. The snails were starved for 1-3 months (short time group) and 6-12 months (long time group).

When snails settled on starvation, they lost weight. The short time group (STG) lost 15% and the long time group (LTG) up to 45%. The frequency of different cell types (digestive, excretory and calcium) was altered during the period of experimentation. In STG digestive cells represent up to 80% of the adenomere. However, in LTG, especially in nine and twelve months, these cells cannot be seen. On the other hand, excretory cells reached 20% in one month, but in twelve months they increased up to 70%. The acid phosphase (Pac) had a relevant role until three months of inanition, whereas, esterases had the main role in twelve months concurring with the increase of the cell death. Alkaline phosphatase (Pal) activity was related to metabolic acidity during a starvation and an extracellular pH balance.

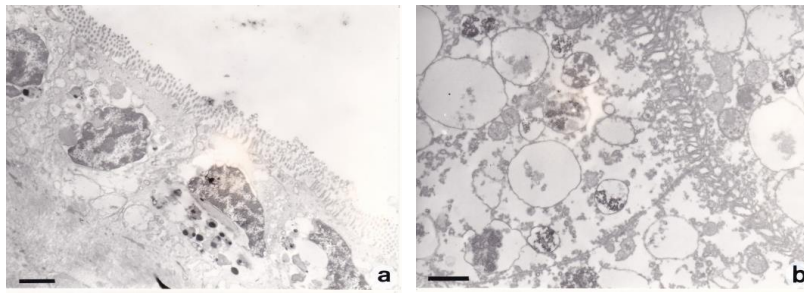

Figure 1. Nine months in starvation. Death Pac cells (a) and Pac positive digestive vacuoles (b). Bars= 2 µm.

References

1.- Porcel D *et al.* (1996). *Comp. Biochem. Physiol.* 115A (1): 11

LS-P04. *VIPP1* develops a crucial function in the maintenance of chloroplast membrane integrity and survival of tomato plants

Capel C[1], Micol-Ponce R[1], García-Alcázar M[1], Yuste-Lisbona FJ[1], Pineda B[2], Capel J[1], Moreno V[2], Lozano R[1,*]

1. Centro de Investigación en Biotecnología Agroalimentaria (BITAL). Universidad de Almería. 04120 Almería, Spain
2. Instituto de Biología Molecular y Celular de Plantas (UPV-CSIC), Universidad Politécnica de Valencia. 46022 Valencia, Spain
*Author for correspondence: rlozano@ual.es

Keywords: chlorophyll biosynthesis, chloroplasts morphogenesis, Crispr/Cas9, thylakoid membrane, tomato

VESICLE-INDUCING PROTEIN IN PLASTIDS 1 (VIPP1) develops a crucial function in the biogenesis and integrity of thylakoid membranes and therefore, in the control of photosynthesis. Moreover, as an essential protein for physiology of chloroplasts, VIPP1 is highly conserved among oxygenic photosynthetic organisms, including plants, algae and cyanobacteria. Indeed, recent studies indicated that VIPP1 directly binds to membranes and induces membrane remodeling through its lipid-binding property. Such biochemical function is a requirement for the proposed roles of VIPP1 in the maintenance of chloroplast membranes. Functional analyses of VIPP1 in plants have been performed in the model species *Arabidopsis thaliana,* however, its involvement in plant development has not been characterized in other plant species.

Here we report the isolation of the tomato *VIPP1* gene from the screening of an insertional mutant collection. Tomato *vipp1-1* mutant plants exhibit albinism and early postembryonic lethality. Phenotype characterization of novel silencing and knock-out alleles generated either by RNAi and CRISPR/Cas9 technologies, supported that abnormalities of *vipp1-1* plants were caused by the loss of function of *VIPP1*. Chloroplast membranes were examined by transmission electron microscopy and confocal microscopy, and results showed severe abnormalities in the structure and arrangement of thylakoid membrane. Such developmental alterations in the membranes prevent chlorophyll biosynthesis, and are ultimately responsible for the premature death of tomato seedlings. Together, our results prove that *VIPP1* is required for the maintenance of thylakoid membrane and hence, for tomato plant survival.

LS-P05. Establishing TCTP1 secretion pathway using TEM immunocytochemistry

Hafidh S[1,*], Lima-Cabello E[2], Alché JD[2]

1. Laboratory of Pollen Biology, Institute of Experimental Botany CAS, Rozvojovà 263, 165 02 Prague 6, Czech Republic.
2. Plant Reproductive Biology and Advanced Imaging Laboratory, Department of Biochemistry, Cell and Molecular Biology of Plants, Estación Experimental del Zaidín, CSIC, Granada, Spain.

* Authors for correspondence: hafidh@ueb.cas.cz / juandedios.alche@eez.csic.es

Secreted bioactive membrane extracellular vesicles such as exosomes are an integral component that mediate cell-to-cell crosstalk in most organisms. In our previous studies[1-3], we showed that some of the proteins required for pollen tube-pistil communication with the female reproductive tissues, could be secreted from pollen tubes *via* these nanovesicles. Translationally Controlled Tumor Protein (TCTP) is one of such proteins. Using reverse genetics, we showed that Arabidopsis *tctp1* is male sterile and that TCTP1 is essential for long-distance pollen tube guidance (through and exit the transmitting tract) as well as in the short-distance guidance (through the funiculus and the micropylar entry) during pollen tube-pistil interaction[2]. Here we have used immunocytochemistry with a combination of confocal laser scanning microscopy (CLSM) and TEM to establish TCTP1 dynamic localization in pollen tubes. Evidence from both CLSM and TEM hinted that TCTP1 is present at the proximity of the cell wall of 4hrs *in vitro* grown pollen tubes and is secreted to the extracellular matrix. To emphasize TCTP-nanovesicles connection, we are currently using TEM to study the association of TCTP with extracellular vesicle resident proteins such as glutathione *S*-transferase (GST) to better understand TCTP secretion pathways to the extracellular matrix in pollen tubes.

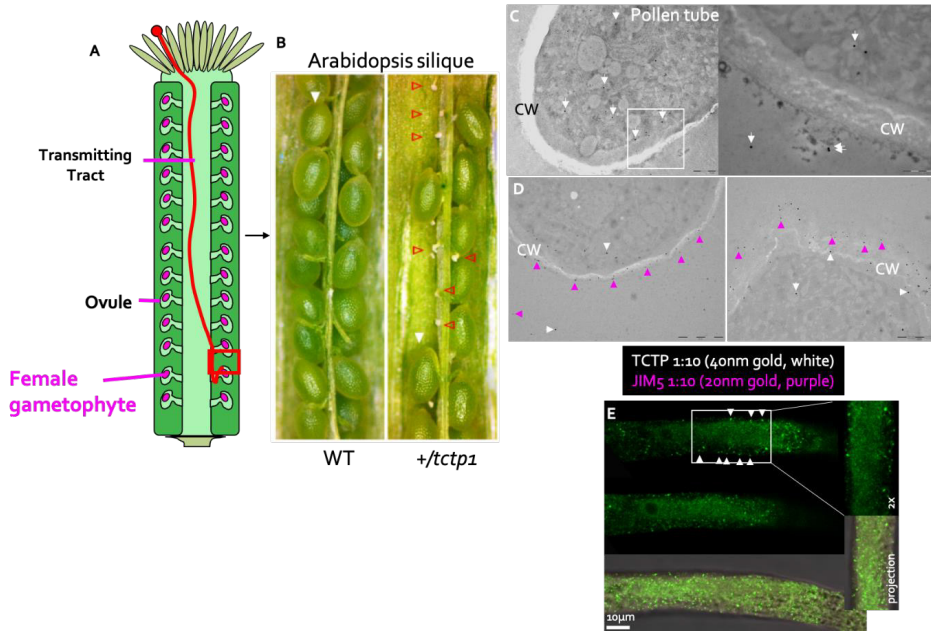

Figure 1. TCTP is a male factor required for pollen tube guidance. (A) Sketch cartoon of pollen tube guidance in Arabidopsis pistil. (B) Dissected siliques showing fertilization defect of tctp1 mutant. (C-D) TEM-immunocytochemistry of TCTP and pectin (JIM5 antibody). (E) Immunolocalization of TCTP with CLSM showing vesicular structures near the cell wall (CW).

References

1.- Hafidh S et al. (2014). *Biochem. Soc. Trans*. 42 (2): 388
2.- Hafidh S et al. (2016). *Genome Biol*. 17: 81
3.- Hafidh S et al. (2018). *Plant Physiol*. 178: 258

Acknowledgements

This project is supported by EMBO STF7107 and STF8202, GACR 17-23203S and 18-02448S. The work was also supported from European Regional Development Fund-Projects “Centre for Experimental Plant Biology” (No. CZ.02.1.01/0.0/0.0/16_019/0000738) and BFU-2016-77243-P.

LS-P06. ABA and ET involvement in the nodule-specific response on drought in yellow lupine.

Kućko A[1], Wilmowicz E[2,3*], Przywieczerski T[2], Alché JD[4,*]

1. Department of Plant Physiology, Warsaw University of Life Sciences-SGGW (WULS-SGGW), 159 Nowoursynowska Street, 02-776 Warsaw, Poland
2. Chair of Plant Physiology and Biotechnology, Nicolaus Copernicus University, 1 Lwowska Street, 87-100 Toruń, Poland
3. Centre for Modern Interdisciplinary Technologies, Nicolaus Copernicus University, 4 Wileńska Street, 87-100 Toruń, Poland
4. Department of Biochemistry, Cell and Molecular Biology of Plants, Estación Experimental del Zaidín, CSIC, 1 Profesor Albareda Street, 18008 Granada, Spain
*Authors for correspondence: juandedios.alche@eez.csic.es / emwil@umk.pl

Keywords: abscisic acid, drought, ethylene, lupine, nitrogen fixation, nodule, phytohormones.

Lupine-*Bradhyrhizobium* infection activates the formation of nodules, which are a place of nitrogen fixation – the process that substantially affects crop production and improves agricultural soil in such significant element. This consequently leads to better grain production of subsequent plants. Nowadays, the nodule functioning is strongly disrupted by global climate changes, such as soil drought. Given this fact, the emphasis should be given to extending the knowledge concerning the markers of early plant' response on water deficit to prevent crop losses and increase yield potential. Therefore, our aim was to answer the question regarding the phytohormones contribution in the drought-dependent nitrogen fixation, exclusively in the nodules of *Lupinus luteus* (L.). Water deficit stress significantly decreased the number of nodules, their water content, the expression of gene encoding leghemoglobin (*LlLbl*), as well as iron and nitrogen concentration. Moreover, drought changed the cellular structure of the symbiosome in a way that indicated its degradation. Phytohormones immunolocalization studies revealed that the stress caused the accumulation of abscisic acid and 1-aminocyclopropane-1-carboxylic acid – ethylene precursor in the nodule cells infected by *Rhizobia* but also surrounded cells. Collectively, we proposed a model of ABA/ET-dependent regulation of nodules functioning under drought stress, which provides an excellent basis for understanding the mechanisms of water-deficit responses.

Acknowledgments:
This research was supported by the Polish Ministry of Agriculture and Rural Development (grant number 149/2011) and the ERDF co-funded projects BFU-2016-77243-P and RTC-2017-6654-2.

LS-P07. The EPIP peptide as a crucial component of phytohormonal-dependent pathway regulating flower shedding in yellow lupine

Wilmowicz E[1,2,*], Kućko A[3], Panek K[1], Burchardt S[1], Alché JD[5,*]

1. Chair of Plant Physiology and Biotechnology, Nicolaus Copernicus University, 1 Lwowska Street, 87-100 Toruń, Poland
2. Centre for Modern Interdisciplinary Technologies, Nicolaus Copernicus University, 4 Wileńska Street, 87-100 Toruń, Poland
3. Department of Plant Physiology, Warsaw University of Life Sciences-SGGW (WULS-SGGW), 159 Nowoursynowska Street, 02-776 Warsaw, Poland
4. Chair of Plant Physiology and Biotechnology, University of Gdańsk, 59 Wita Stwosza Street, 80-308 Gdańsk, Poland
5. Department of Biochemistry, Cell and Molecular Biology of Plants, Estación Experimental del Zaidín, CSIC, 1 Profesor Albareda Street, 18008 Granada, Spain

*Authors for correspondence: juandedios.alche@eez.csic.es / emwil@umk.pl

Keywords: catalase, EPIP peptide, flower abscission zone, *INFLORESCENCE DEFICIENT IN ABSCISSION-LIKE*

The loss of a plant organ is a natural process that takes place in a specialized group of cells called the abscission zone (AZ). The proper functioning of this structure ensures also detachment of generative organs and consequently yielding of many crops characterized by high agronomic potential, like lupins. We have previously shown that activation of flower AZ is accompanied by a strong accumulation of *INFLORESCENCE DEFICIENT IN ABSCISSION-LIKE* (*LIIDL*) mRNA in yellow lupine (*Lupinus luteus* L.). The C-terminal LIIDL amino acid sequence contains EPIP motif (Wilmowicz et al. 2018) which determines IDA/IDL activity (Santiago et al. 2016, Stenvik et al. 2008). We revealed that the application of EPIP peptide synthesized based on the predicted amino acid LIIDL sequence increased the flower abortion rate and led to the cellular changes similar to those characteristics for naturally active AZ (Wilmowicz et al. 2018). All these events were accompanied by significant changes in the phytohormonal homeostasis reflected by an accumulation of transcripts of genes coding enzymes crucial for abscisic acid (zeaxanthin epoxidase, *LIZEP*) and ethylene (synthase and oxidase of 1-aminocyclopropane-1-carboxylic acid, *LIACS*, *LIACO*) biosynthesis. Additionally, exogenous EPIP peptide changed the content of abscisic acid and precursor of ethylene, but also influenced their specific localization in the whole AZ area. Furthermore, the AZ redox state was disturbed by treatment with EPIP peptide which was confirmed by changing localization and activity of catalase.
Our results provide novel information about the role of EPIP peptide in the phytohormonal-regulated pathway of flower abscission in lupine.

Acknowledgments:
This research was supported in part by the National Science Centre of Poland (grant number 2018/02/X/NZ1/01229) and the Spanish MINECO (BFU-2016-77243-P).

References

1.- Wilmowicz E *et al*. (2018). Plant Growth Regul. 85: 91
2.- Santiago J *et al*. (2016). eLife 8: e15075
3.- Stenvik GE *et al*. (2006). Plant Cell 18:1467

SPONSORS INFORMATION

SPONSORSHIP

INSTITUTIONAL PARTNERS

MINISTERIO DE CIENCIA, INNOVACIÓN Y UNIVERSIDADES

CSIC Consejo Superior de Investigaciones Científicas

eez Estación Experimental del Zaidín

SME

Sociedade Portuguesa de Microscopia SPMicros

EMS European Microscopy Society

Ayuntamiento de Granada

SABOR GRANADA saborgranada.es

Diputación de Granada

COMPANY SPONSORS

PLATINUM SPONSORS

ZEISS Seeing beyond

GOLD SPONSORS

Izasa Scientific A Werfen Company

ThermoFisher SCIENTIFIC

BRONZE SPONSORS

abbelight Now, we see.

iesmat

OTHER SPONSORS

Leica MICROSYSTEMS

OXFORD INSTRUMENTS

PHOTON LINES Soluciones ópticas

FEDELCO SL

Aname

Gold sponsor

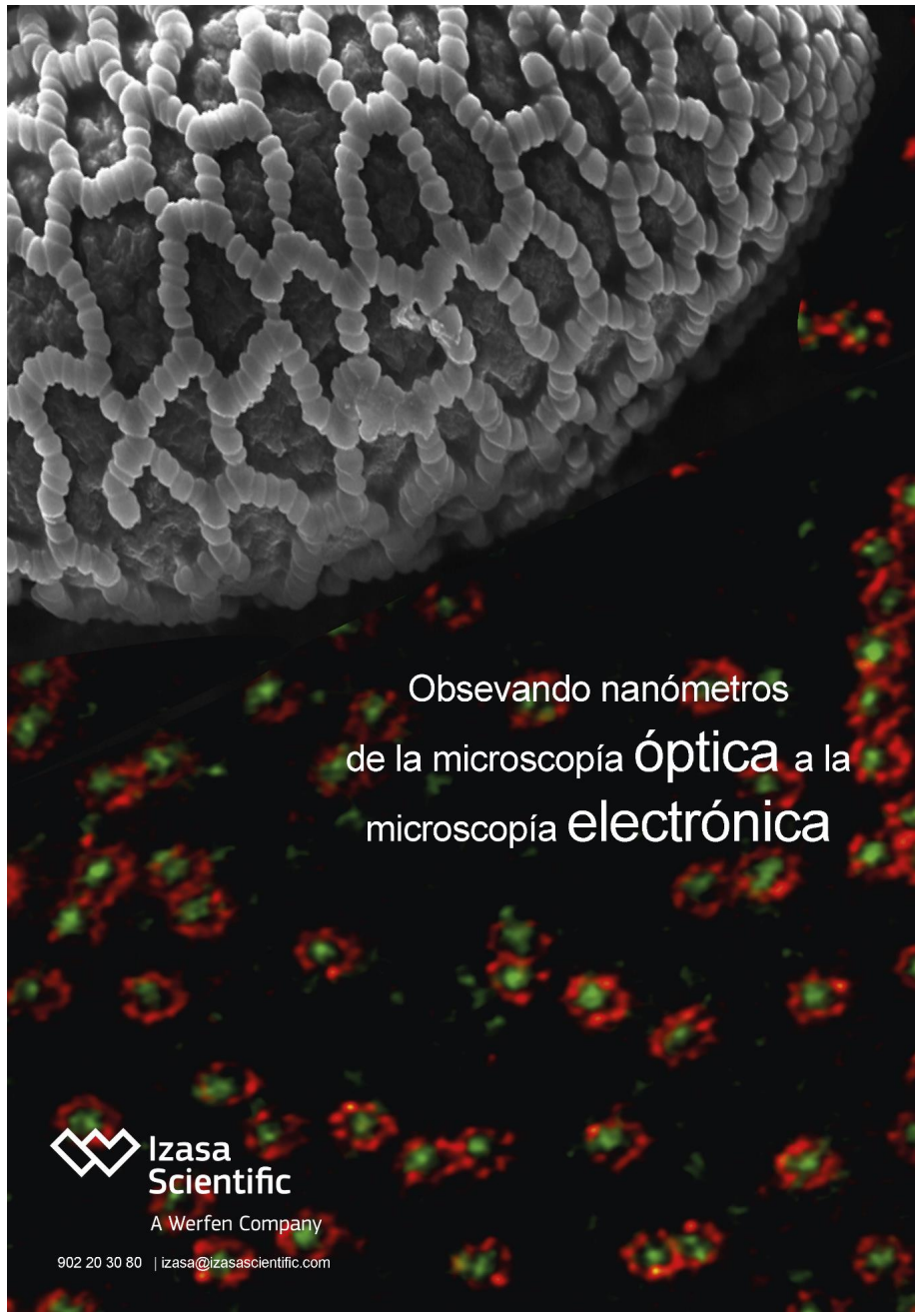

Gold Sponsor

Bronze Sponsor

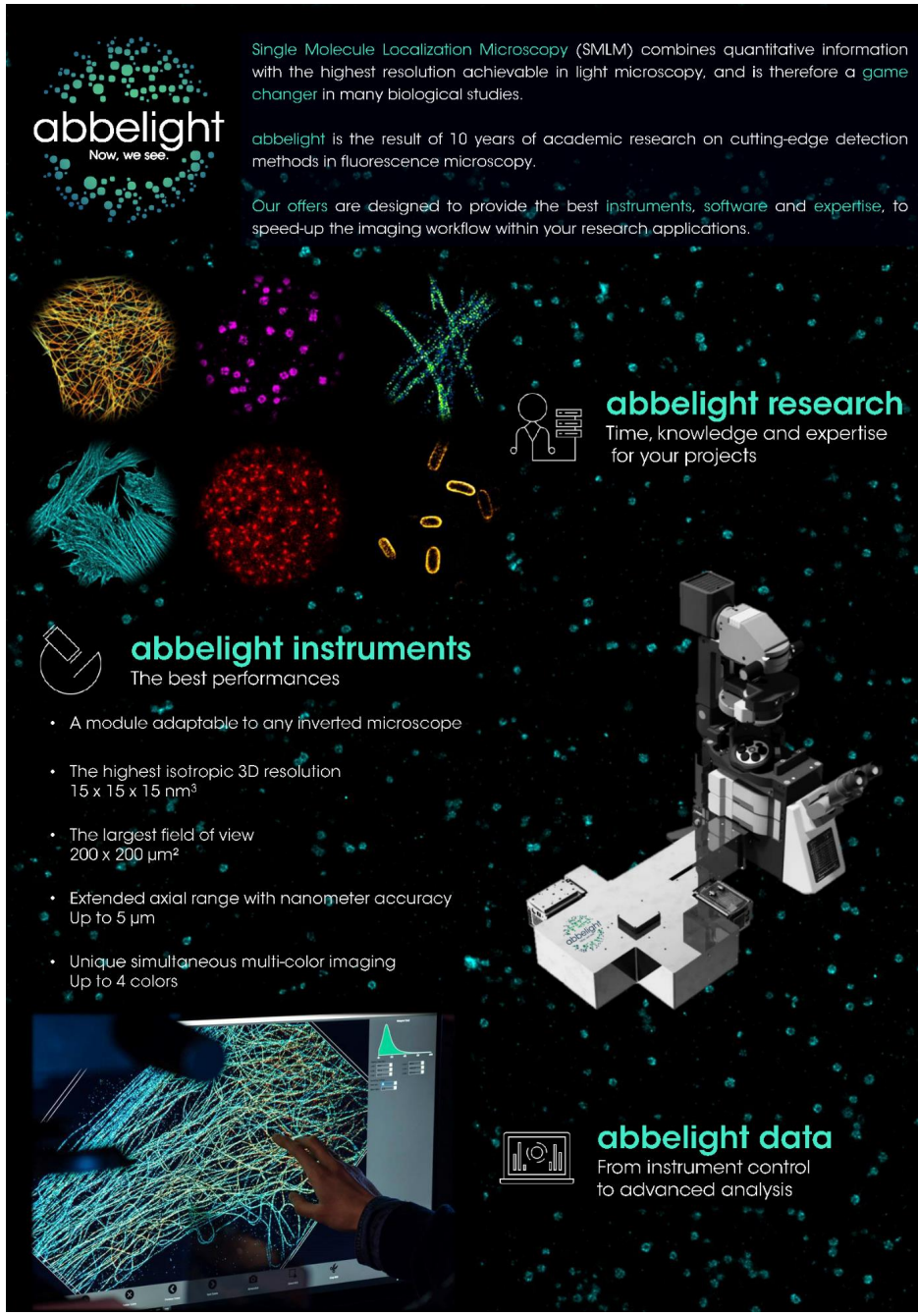

Other Sponsors

Institutional Sponsor

List of authors (by alphabetical order)

D

E

F

M

N

Z